Ph.D. Thesis
in Mathematics

On Periodic Stationary and Axisymmetric Black Hole Configurations

Javier Peraza

Supervisor: Martín Reiris

Facultad de Ciencias
Universidad de la República

Thesis submitted in fulfillment of the requirements of the Ph.D. Degree in Mathematics, PEDECIBA

Title of the thesis:

On Periodic Stationary and Axisymmetric Black Hole Configurations

Student: Javier Peraza

Supervisor: Martín Reiris

Thesis Jury:

Juan Alonso (*Universidad de la República*)
Florencia Benítez (*Universidad de la República*)
Juan Pablo Borthagaray (*Universidad de la República*)
Dmitry Korotkin (*University of Concordia*)
Gustavo Dotti (*Universidad Nacional de Córdoba*)

Acknowledgements

First and foremost, I would like to thank my advisor, Martin Reiris, for his patience, guidance and constant encouragement throughout this project. His commitment, contributions and discussions will have a lasting effect in my scientific career.

I would like to thank Juan Alonso, Ernesto Blanco, Miguel Campiglia, Walter Ferrer, Rodolfo Gambini, Jorge Griego, Mariana Haim, Ernesto Mordecki, Carlos Negreira, Iván Pan, Alejandro Passeggi, Miguel Paternain, Rafael Potrie, Álvaro Rittatore, and Michael Reisenberger for their excellent courses and their passion when imparting their knowledge. It has been a privilege to research, discuss and talk about physics, mathematics and life with them. Thanks to them, I went from being a student to a researcher.

Special thanks to Omar Ortiz, for all these years of collaboration and for teaching me how to implement and understand numerical analysis. To Dmitry Korotkin, for making the visit to Concordia University possible, for all the discussions and for reviewing this thesis. To Lars Andersson, for inviting me to speak at the Max Planck Institute Geometry and Gravitation seminar. To Hermann Nicolai, for valuable discussions. To Nacho Bustamante, for his support, the interesting discussions and for his comments on the first versions of this thesis. To Juan Pablo Borthagaray, for the suggestions and questions after the revision of this thesis.

To my friends: Yamil Abraham, Ramón Arbelo, León Carvajales, Maxi Escayola, Rodrigo Eyerhalde, Matías Fernández, Alejo García and Julio Vera, for all the good times during courses, exams and in general.

Thanks to CMAT, IFFC, IMERL and IFFI, for all the seminars, courses, lectures and the excellent human environment. Thanks to CMAT for allowing me to take a sabbatical year to travel to collaboration visits, and for always trying to help graduate students pursue their academic achievements. Special thanks to the CMAT and IFFC secretaries, Claudia, Lydia and Jimena, for all their help with administrative logistics.

I thank the ANII, CAP and CSIC for the financial support.

I conclude by expressing my gratitude to my family: my parents, Mónica and Eduardo, for their unwavering support, and my wife, Karen, for all her constant support, cheerful encouragement and immeasurable patience throughout these years, during which time was usually the hardest resource to manage. Without their presence, this journey would have remained ashore. They have been, are, and will continue to be the calming sea, the pushing wind, and the guiding stars that make my endeavors not only possible but achievable.

ñ-.

Oh, pilot of the storm who leaves no trace
Like thoughts inside a dream
Hid the path that led me to that place
Yellow desert stream...

—Led Zeppelin, *Kashmir*

Abstract

In this thesis, we study the problem of finding periodic coaxial configurations of co-rotating 3+1 vacuum black holes, for which existence and uniqueness have not yet been theoretically proven. The existence of such configurations would extend Myers/Korotkin-Nicolai's family of non-rotating (static) coaxial arrays of black holes [1, 2], and would significantly contribute to our understanding of black hole solutions with no restriction in their topology and asymptotic behavior. We study the problem numerically and analytically.

On the numerical side, in Python, we developed and implemented the necessary numerical methods to solve the reduced Einstein Equations in the periodic setup. After an exhaustive numerical investigation, we provide strong numerical evidence of their existence for a wide range of natural parameters. We found that numerical solutions, with a given value for the area A and angular momentum J of the horizons, appear to exist only when the (coordinate) separation between two consecutive horizons is larger than certain critical value L_c that depends only on A and $|J|$. We also observed that the solutions have the same Lewis' cylindrical asymptotic behavior as van Stockum's infinite rotating cylinders. Below L_c, the rotational energy appears too big to sustain a global equilibrium, and a singularity shows up at a finite distance from the axis.

On the analytic side, we first proved a non-existence result on a specific range of parameters characterizing the co-rotating solutions. It provides a lower bound for the critical value L_c, showing that no solution can be complete at infinity if the parametric distance between the rotating horizons (in terms of the Weyl-Papapetrou coordinates) is below that value. Then, we proved the existence of a lower bound of the distance between consecutive horizons below which the Myers/Korotkin-Nicolai family of solutions can not be put into rotation, given in terms of their area and L_c. To our knowledge, this result constitutes the first example in the literature of a family of regular, static black hole vacuum solutions that are highly constrained by their geometry to undergo deformations into stationary solutions. Finally, assuming the existence of solutions, we construct a candidate of Lewis' kind for the asymptotic behavior.

Resumen

En esta tesis estudiamos configuraciones periódicas de agujeros negros estacionarios y axisimétricos en el vacío, co-axiales e idénticos, en 3+1 dimensiones, para las cuales la existencia y unicidad aún no han sido demostradas teóricamente. Estas configuraciones extenderían la familia de soluciones de infinitos agujeros negros estáticos y co-axiales de Myers/Korotkin-Nicolai [1, 2], y contribuiría significativamente a nuestra comprensión de soluciones de agujeros negros en topologías arbitrarias y comportamientos asintóticos no planos. Estudiamos el problema numérica y analíticamente.

Del lado numérico, en Python, desarrollamos e implementamos los métodos numéricos necesarios para resolver las Ecuaciones de Einstein reducidas en la configuración periódica. Tras una exhaustiva investigación numérica, proporcionamos evidencia numérica sólida de su existencia para una amplia gama de parámetros naturales. Vemos que las soluciones numéricas, dados el área A y el momento angular J de los horizontes, parecen existir solo cuando la separación (en coordenadas) entre dos horizontes consecutivos es mayor que cierto valor crítico

L_c que depende solo de A y $|J|$. Las soluciones presentan el mismo comportamiento asintótico cilíndricamente simétrico de tipo Lewis que los cilindros rotantes infinitos de van Stockum. Por debajo de L_c, la energía rotacional es demasiado grande para mantener un equilibrio global, y aparece una singularidad a una distancia finita del eje.

Del lado analítico, demostramos la no existencia en un rango específico de parámetros que caracterizan las soluciones co-rotantes. Esto proporciona una cota inferior para el valor crítico L_c, mostrando que ninguna solución puede ser completa en infinito si la distancia paramétrica entre los horizontes rotativos (en términos de las coordenadas de Weyl-Papapetrou) es inferior a la cota hallada. Luego, demostramos la existencia de una cota inferior para la distancia entre horizontes consecutivos (en términos del área y L_c) por debajo de la cual la familia de soluciones de Myers/Korotkin-Nicolai no puede ponerse en rotación. Hasta donde sabemos, este resultado constituye el primer ejemplo en la literatura de una familia de soluciones de agujero negro regulares y estáticas en el vacío que está fuertemente limitada por su geometría al momento de admitir deformaciones estacionarias. Finalmente, asumiendo existencia de soluciones, construimos un candidato de tipo Lewis para el comportamiento asintótico de las soluciones.

Contents

1 Introduction **1**

1.1 Motivation and overview . . . 1
1.2 Preliminaries . . . 3
1.2.1 Stationary and axisymmetric black hole solutions . . . 3
1.2.2 Weyl-Papapetrou coordinates . . . 4
1.2.3 Schwarzschild and Kerr solutions in Weyl-Papapetrou coordinates . . . 6
1.2.4 Gauge freedom and surface gravity fixing . . . 7
1.3 Periodic analogs of asymptotically flat spacetimes . . . 8
1.3.1 MKN solutions . . . 8
1.3.2 Stationary generalizations of static periodic solutions . . . 9
1.3.3 The existence problem of periodic analogs of Kerr . . . 11
1.4 Results . . . 13
1.4.1 Numerical results . . . 13
1.4.2 Analytic results . . . 15
1.5 Open problems and further questions . . . 16
1.6 Structure of this thesis . . . 18
1.7 Notation . . . 18

2 Stationary axisymmetric solutions in General Relativity **20**

2.1 Introduction . . . 20
2.1.1 Killing fields and Killing horizons . . . 21
2.2 Reduction by symmetries and harmonic maps . . . 22
2.3 Stationary and axisymmetric spacetimes . . . 24
2.4 Weyl-Papapetrou coordinates . . . 26
2.4.1 Exact stationary axisymmetric solutions . . . 29
2.4.2 Behavior near the axis and horizon . . . 32
2.4.3 Periodic analogs . . . 34
2.4.4 The coordinate ρ . . . 35
2.4.5 Residual Gauge Freedom . . . 37

2.5 Stationary and axisymmetric data on the cylinder . . . 38
2.5.1 Change of variables to (σ, ω) and reconstruction of the metric . . . 38
2.5.2 Periodic stationary and axisymmetric data . . . 38
2.5.3 Angle defects: struts . . . 41
2.6 Komar integrals and Smarr Formula . . . 42
2.6.1 Mass and Angular Momentum . . . 42
2.6.2 Area and surface gravity of the horizon . . . 43
2.6.3 Smarr formula . . . 44
2.7 Mass functional and regularization of the energy . . . 45

3 A priori estimates in the asymptotic region **46**
3.1 Anderson's and Reiris' estimates . . . 46
3.1.1 Curvature estimate . . . 46
3.1.2 Backry-Émery-Ricci tensor and its properties . . . 48
3.1.3 Estimates for stationary axisymmetric data . . . 49
3.2 ρ: the good, the bad *or* the ugly coordinate . . . 52
3.3 T^2-symmetric solutions . . . 57
3.3.1 Solving $z-$independent equations . . . 57
3.3.2 Lewis' families of solutions . . . 60
3.3.3 Smarr formula for Lewis models . . . 62

4 Non-existence theorems **64**
4.1 Preliminary results . . . 64
4.1.1 Scaled diameter decay . . . 64
4.1.2 A monotonic quantity . . . 68
4.2 A non-existence theorem when $m/L > 1/4$ . . . 70
4.3 Distance-Area bound for MKN Solutions . . . 74

5 Asymptotic behavior **77**
5.1 Approach to the asymptotic study: an overview . . . 77
5.2 Curvature decay and collapse . . . 79
5.3 Lewis-like asymptotic behavior . . . 81
5.3.1 Scaling of transverse tori . . . 82
5.3.2 Asymptotic geometry of the periodic Kerr analogs . . . 82
5.3.3 Proof of the asymptotic behavior theorem . . . 87
5.3.4 Discussion and further work . . . 88

6 Numerical results **89**
6.1 Overview of results . . . 89
6.2 Boundary conditions for the harmonic map heat flow . . . 91
6.2.1 Boundary conditions for the fields . . . 91
6.2.2 Initial data for the harmonic map heat flow . . . 94

6.2.3 Some comments on the seed . . . 96
6.3 Numerical Implementation . . . 98
6.4 Results . . . 101
6.4.1 First series: $J = 1/4$ . . . 102
6.4.2 Second series: $J = 1/2$ . . . 111
6.5 Multi-horizon set ups . . . 111
6.5.1 Construction of the seed . . . 113
6.5.2 Two counter-rotating black holes . . . 114

A Formulas and distorted Black Holes **119**
A.1 Functions for Kerr solution on Weyl-Papapetrou coordinates . . . 119
A.1.1 Prolate spheroidal coordinates . . . 119
A.1.2 Kerr metric . . . 120
A.1.3 Algebraic comparison between stationary axisymmetric metric forms . . . 121
A.2 Distorted black holes and area formula . . . 122

B Preliminary results concerning the Inverse Scattering Method **124**
B.1 Numerical implementation . . . 125
B.2 Results . . . 126
B.3 Comparison with the harmonic map heat flow method . . . 127

Bibliography **128**

Chapter 1

Introduction

1.1 Motivation and overview

Since the early days of General Relativity, black holes have been fundamental objects in our understanding of the mathematics and physics of the theory. Already in 1916, Schwarzschild found the first explicit solution to Einstein's equations. At first, this solution was thought of as the simple analogy of the Newtonian gravitational potential of a point-like particle in general relativity. However, it contains a new, unique, distinctive feature: a black hole horizon. Nowadays, we call it a static black hole solution and know how to characterize it in many different ways. In particular, thanks to the works of Israel [3], Zum Hagen, Robinson and Seifert [4] and Bunting and Masood-ul Alam [5], it is known that the Schwarzschild solution is the only asymptotically flat static vacuum solution in 3+1 dimensions having a compact albeit not necessarily connected horizon. Even though the Schwarzschild solution was found in 1916, it took the effort of many mathematicians and physicists (including Einstein) over decades to reveal its real nature, and it took almost five decades until the rotating, non-static generalization was found by Kerr in 1963 [6]. We now call these rotating solutions the Kerr family of black holes, a fundamental family of the theory. This difference between the time when the Schwarzschild and the Kerr solutions were found tells, in fact, how difficult it is to deal with stationary solutions in comparison to static ones and how difficult it could be to find a rotating analog of a non-rotating solution.

Soon after Schwarzschild, a systematic investigation of the static vacuum solution began. In [7], Weyl found a remarkable reduction of the static axisymmetric vacuum equations that systematized the construction of solutions. In Weyl's reduction, Einstein's equations reduce to a linear equation for a potential and a quadrature. In [8], Weyl and Bach proved that when one uses Weyl's method to align two or more Schwarzschild black holes (by linearly adding their potentials), the result is a new static and axisymmetric solution that, however, has an angle defect or strut, on each of the axis components between two consecutive horizons, and that is therefore non-smooth. This angle defect acts as a repulsive force between the holes to balance against their gravitational attraction. Thus, there are no configurations of aligned horizons in static equilibrium. However, thanks to the uniqueness theorem of the Schwarzschild solution

mentioned earlier, we know that this impossibility is indeed general. In [9], Myers showed that an infinite, periodic number of coaxial horizons does not give rise to struts. Thus, infinitely many aligned black holes can indeed be in static equilibrium. This solution was found independently by Korotkin and Nicolai in [2].

Vacuum black hole configurations with nonstandard topology or with nonstandard asymptotic behavior have gained considerable attention in recent years. In the late '80s and '90s, the research in string theory and supergravity led to the exploration of black hole solutions in high dimensional compactified or semi-compactified spacetimes (e.g. [9–16]). The higher the dimension of the manifold, the more exotic the objects can be. In four dimensions, we can take the quotient by translations (isometries) of the Myers/Korotkin-Nicolai solutions (from now on, denoted as MKN solutions) along the axis direction, obtaining one or several black holes in gravitational equilibrium inside an open solid 3-torus. This is in sharp contrast to the uniqueness theorem of the Schwarzschild solution and shows that the topology of the manifold critically frames the properties of the solutions that it can hold. In five dimensions, Emparan and Reall [17] found asymptotically flat stationary solutions with ring-like $S^1 \times S^2$ horizon and Elvang and Figueras [18] found asymptotically flat black Saturns, where a black ring $S^1 \times S^2$ rotates around a black sphere S^3. Recently, Khuri, Weinstein and Yamada [19, 20] found periodic static coaxial arrays of horizons in five dimensions either with spherical S^3 or ring-like $S^1 \times S^2$ topology. Rather than being asymptotically flat, these latter configurations are asymptotically Kasner [21] (Kasner solutions are exact solutions to the vacuum Einstein Equations, although the specific form of these solutions was independently found by Levi-Civita [22]) and generalize the already mentioned MKN family.

After presenting the periodic static solution, Korotkin and Nicolai proposed the following general conjecture for the existence of periodic analogs of stationary solutions [23, p. 245].

Conjecture 1.1. *Every stationary and axisymmetric asymptotically flat solution must have its periodic analog. The leading order of the asymptotic behavior should be that of a Kasner solution.*

A natural approach to this conjecture is to ask if the MKN periodic Schwarzschild solutions accept rotating analogs, i.e., stationary axisymmetric solutions with the same horizon area but arbitrary angular momentum. Nevertheless, the existence of stationary generalizations of static solutions remains an open problem in most situations, either in four or higher dimensions.

In this thesis, we study periodic, coaxial configurations of rotating, equidistant identical black holes. Such configurations allow us to step on a common ground between the conjecture and stationary generalizations. Indeed, these *periodic Kerr analogs* generalize the MKN family in 3+1 dimensions. With this particular construction, we provide (numerically) a positive answer to Conjecture 1.1 and show (analytically) a first example in which the geometry of the static black hole solutions highly constrains the existence of stationary generalizations.

1.2 Preliminaries

1.2.1 Stationary and axisymmetric black hole solutions

A Lorentzian metric g on a 4-manifold $\mathcal{M}$ satisfies the vacuum Einstein's Equation if

$$\mathrm{Ric}(g) = 0. \tag{1.1}$$

Solutions with symmetries play a central role in the study of General Relativity, as in any geometric theory. In this thesis, we consider *stationary* and *axisymmetric* black hole solutions.

Stationary spacetimes are in the interface between Riemannian Geometry and General Relativity. Over the last decades, construction methods of exact solutions have been implemented, and techniques from comparison geometry and analysis have been introduced to understand their moduli spaces of solutions, reinvigorating the analytical study.

In its original form, the definition of black hole solutions requires an asymptotically flat spacetime having a well-defined and complete future null infinity $\mathscr{I}^+$ and a non-empty event horizon, i.e., such that the casual past of $\mathscr{I}^+$ has a smooth non-empty boundary, $\mathcal{H} := \partial J^-(\mathscr{I}^+)$ (see [24, Chp. 9] and [25, Chp. 12] for a thorough exposition of the topic). On the same lines, a stationary black hole solution was initially meant as a black hole solution having a Killing field χ that is timelike sufficiently near infinity. Such a Killing field must leave the event horizon, which is a null surface, invariant.

By now, the definition of stationary black hole solutions has been considerably relaxed so that researchers speak of them without requiring a null infinity or the notion of an event horizon. In the following lines, we will clarify the definition we took in this thesis for a *generalized* stationary black hole solution.

Definition 1.1. *A generalized stationary black hole solution is an $3+1-$dimensional, globally hyperbolic, spacetime $(\mathcal{M}, g)$, having a Killing field χ, such that*

1. *$\partial\mathcal{M} = \mathcal{N} \cup \mathcal{H}$, where $\mathcal{N}$ is a metrically complete Cauchy hypersurface with compact boundary and $\mathcal{H}$ is a future complete, future null hypersurface*[1].

2. *χ is non-zero at $\mathcal{H}$, tangent to $\mathcal{H}$ and is timelike outside a compact set of $\mathcal{N}$.*

The Killing field ∂_χ generates the stationary symmetry.

We say that a generalized stationary black hole solution is *axisymmetric* if its group of isometries has a subgroup isomorphic to $SO(2)$. Let ξ be the generator of the axisymmetry. The orbits are either circles or points. The set of point orbits is called *axis of symmetry* and is denoted by $\mathcal{A}$.

In this case, ξ is *also* tangent to the null hypersurface $\mathcal{H}$. It can be shown (see [24, 25]) that a linear combination of χ and ξ,

$$\ell = \chi - \Omega_{\mathcal{H}}\xi,$$

[1] A future null hypersurface is a null hypersurface such that future timelike vectors point outside the manifold. We say the null hypersurface is future complete if the affine parameter of its null generators is defined in $\mathbb{R}^+$.

is a Killing field that is tangent to the null generators of $\mathcal{H}$ and therefore is the generator of the null hypersurface. The property of a Killing field being nonzero and normal to the null generators of a null hypersurface is the definition of a Killing horizon. It plays a fundamental role in General Relativity: by Carter-Robinson-Hawking rigidity theorem, the event horizon of a stationary, asymptotically flat black hole solution (supplemented by certain additional assumptions, see [26, Theorem 1.1] and references therein for a review) is a Killing horizon. The area of the spatial two-surface $H := \mathcal{H} \cap \mathcal{N}$ is denoted by A and called the *area of the horizon*.

Given a Killing horizon generated by a Killing field ℓ, the *surface gravity* κ is defined as (see [25,27,28] for other equivalent definitions)

$$\kappa^2 := -\frac{1}{2} \langle \nabla \ell, \nabla \ell \rangle . \tag{1.2}$$

Unless stated otherwise, we will always assume the solutions to be a generalized stationary and axisymmetric black hole solution.

1.2.2 Weyl-Papapetrou coordinates

Stationary axisymmetric black hole solutions are usually studied on the *Weyl-Papapetrou coordinates*. These coordinates were originally introduced by Weyl [7] in the static case and later generalized to the stationary case by Papapetrou [29,30]. Although very distorted, these coordinates simplify the treatment when multiple horizons are present and give a clear reduction from (1.1) to an elliptic system of two non-linear PDEs along with two quadratures (see below and section 2.4). In these coordinates, a stationary axisymmetric metric takes the form (see [25,31] and references therein)

$$g = -V dt^2 + 2W dt d\phi + \eta d\phi^2 + \frac{e^{2\gamma}}{\eta}(d\rho^2 + dz^2), \tag{1.3}$$

where $(t, \rho, z, \phi) \in \mathbb{R} \times (\mathbb{R}_0^+ \times \mathbb{R}) \times S^1 =: \mathcal{M}$[2] and the components V, W, η and γ depend only on (ρ, z). The metric coefficients W and V are not independent,

$$W = \eta\Omega, \quad V = \frac{\rho^2 - W^2}{\eta}, \tag{1.4}$$

with Ω called the *angular velocity function*.

The vector field ∂_t is the stationary Killing vector, and ∂_ϕ is the Killing vector field generating axial rotations. The surfaces of transitivity of the abelian group of isometries generated by these Killing fields are orthogonal to spacelike surfaces. Let $(\theta^\phi)_d = \epsilon_{abcd}(\partial_\phi)^a \nabla^b (\partial_\phi)^c$ be the twist form of $(\partial_\phi)^a$, where ϵ_{abcd} is the volume element of g. It can be shown that $d\theta^\phi = 0$, so locally it can be defined a *twist potential*, ω, such that $d\omega = \theta^\phi$.

The elliptic system satisfied by $\eta(\rho, z)$ and $\omega(\rho, z)$ constitutes the following harmonic map

[2] By abuse of notation, the Cauchy hypersurface $\mathcal{N} \simeq (\mathbb{R}_0^+ \times \mathbb{R}) \times S^1$ is not on the boundary of $\mathcal{M}$, since $t \in \mathbb{R}$. Formally, one should take a fixed time t_0 and consider $[t_0, +\infty)$ as the factor parametrized by the time. This technical issue will not be important in this work.

equations (known as Ernst equations, [32]),

$$\Delta\eta = \frac{|\nabla\eta|^2 - |\nabla\omega|^2}{\eta}, \tag{1.5}$$

$$\Delta\omega = 2\langle\nabla\omega, \frac{\nabla\eta}{\eta}\rangle, \tag{1.6}$$

where $\nabla f := (\partial_\rho f, \partial_z f)$, the 2-gradient, $\langle\ ,\ \rangle$ is the flat space inner product in the (ρ, z) embedded space, and $\Delta := \partial_\rho^2 + \frac{1}{\rho}\partial_\rho + \partial_z^2$ is the $3D$ axisymmetric flat-space Laplacian operator in cylindrical coordinates (ρ, z, ϕ). Once these equations have been solved, the exponent γ and the angular velocity function Ω are found by direct integration,

$$\partial_z\gamma = \frac{\rho}{2\eta^2}(\partial_\rho\eta\partial_z\eta + \partial_\rho\omega\partial_z\omega), \quad \partial_\rho\gamma = \frac{\rho}{4\eta^2}((\partial_\rho\eta)^2 - (\partial_z\eta)^2 + (\partial_\rho\omega)^2 - (\partial_z\omega)^2), \tag{1.7}$$

$$\partial_z\Omega = \rho\frac{\partial_\rho\omega}{\eta^2}, \quad \partial_\rho\Omega = -\rho\frac{\partial_z\omega}{\eta^2}. \tag{1.8}$$

Thus, the stationary axisymmetric Einstein equations are solved in a ladder-like fashion: first solve the harmonic map equations (1.5)-(1.6), then solve the quadratures (1.7) and (1.8), and finally get the coefficients V and W from (1.4).

The described ladder-like way of solving the equations does not guarantee the regularity of the final metric. This is a rather inconvenient phenomenon of the Weyl-Papapetrou reduction: solving the reduced equations is not enough, and one has to check the regularity of the final metric. Generically, there are angle deficits around the axis that can be easily computed via a quadrature (they can also be derived from the function γ) and give rise to the well-known *struts*. As it was first shown by Bach and Weyl [8] in the static case, a singular string-like matter distribution can be associated with the strut along the axis where angle deficits are present. Therefore, on physical grounds, the struts represent the impossibility of the solution being at equilibrium: if, say, two horizons are linked by a strut, there exists a string connecting the black holes such that they are at equilibrium. Such strings can be compact (between horizons) or non-compact (from a horizon to infinity on the axis).

Let us now consider Weyl-Papapetrou reduction in the context of Definition 1.1. The manifold $\mathcal{N} := (\mathbb{R}_0^+ \times \mathbb{R}) \times S^1$ serves as the Cauchy hypersurface where the initial data can be put after solving (1.5), (1.6), (1.7) and (1.8). The axis of axisymmetry is given by the set $\mathcal{A} := \{\eta = 0\} \subset N$. Since ρ^2 is the area density on the orbits generated by ∂_t and ∂_ϕ, the set $\{\rho = 0, \eta > 0\} \subset \mathcal{M}$ is a 3-dimensional null hypersurface. A straightforward computation shows that the following null vector generates $\mathcal{H}$,

$$\chi = \partial_t - \Omega_{\mathcal{H}}\partial_\phi, \tag{1.9}$$

where $\Omega_{\mathcal{H}}$ is the value of Ω at $\mathcal{H}$ [33] (see also section 2.4 for a derivation). On the transverse surface of coordinates (ρ, z), denoted by $\mathcal{S}$, $H := \mathcal{H} \cap \mathcal{S}$ is represented by disjoint segments on

$\{\rho = 0\} \cap \mathcal{S}$ (those on which $\eta > 0$). Suitable boundary conditions at $\mathcal{A}$ and $\mathcal{H}$ for η, ω, γ and Ω can be straightforwardly computed to characterize a black hole solution [31][3].

Static metrics, i.e., non-rotating solutions with $\omega \equiv 0$, admit a nice characterization in Weyl-Papapetrou reduction. Via the change of variables $\eta = \rho^2 e^{\sigma}$, equation (1.5) becomes linear,

$$\Delta\sigma = 0, \tag{1.10}$$

which is known as the Lapse equation for static solutions [25, 34].

1.2.3 Schwarzschild and Kerr solutions in Weyl-Papapetrou coordinates

Discovered by Karl Schwarzschild in 1916 [35], just a few months after Einstein published the field equations for General Relativity [36], the Schwarzschild metric in Weyl-Papapetrou form reads

$$g_{Sch} = -e^{-\sigma_{Sch}} dt^2 + e^{\sigma_{Sch}}(e^{2k}(d\rho^2 + dz^2) + \rho^2 d\phi^2),$$

where,

$$\sigma_{Sch} = \ln\left(\frac{\sqrt{(z-m)^2+\rho^2} + \sqrt{(z+m)^2+\rho^2} + 2m}{\sqrt{(z-m)^2+\rho^2} + \sqrt{(z+m)^2+\rho^2} - 2m}\right), \quad m > 0, \tag{1.11}$$

and e^{2k} is given by

$$e^{2k} = \frac{\left(\sqrt{(z-m)^2+\rho^2} + \sqrt{(z+m)^2+\rho^2}\right)^2 - 4m^2}{4\sqrt{(z-m)^2+\rho^2}\sqrt{(z+m)^2+\rho^2}}.$$

Schwarzschild's solutions represent a family of static, spherically symmetric, asymptotically flat and *vacuum* spacetimes [25], diffeomorphic to $\mathbb{R} \times (\mathbb{R}^3 \setminus B)$, where B is an open ball. The boundary of the manifold is the set $\mathcal{H} = \{\rho = 0, |z| < m\}$, which is a Killing horizon with Killing field ∂_t. It can be shown that the parameter $m > 0$ is the ADM mass of the solution [25]; thus, we say that it is the *mass*.

In a general astrophysical situation, bodies are rotating, and the metric outside them is not expected to be static. As mentioned before, the first family of stationary (non-static) solutions was found by Kerr [6], and they are so far the only known solution that could represent the stationary axisymmetric asymptotically flat gravitational field in the exterior of a black hole[4]. In Weyl-Papapetrou coordinates, the metric components are more convoluted than those of Schwarzschild (see subsection 2.4.1) and are given in an algebraically closed form.

Two parameters are needed to determine the solution, $m > 0$ and $J \in \mathbb{R}$. Here, J corresponds to the angular momentum of the solution. The horizon is given by the set $\mathcal{H} = \{\rho = 0, |z| < m\}$,

[3] As we will discuss in detail in chapter 2 and chapter 4, the boundary conditions that will be imposed for the elliptic system (1.5)-(1.6) and the quadratures (1.7)-(1.8) will be both a consequence of the topology of $\mathcal{M}$ and the presence of a Killing horizon.

[4] The Kerr solution is the exterior solution of an axisymmetric rotating body only if the body possesses a particular combination of multipole moments. This phenomenon occurs since there are no matching inner and outer solutions, in contrast to the spherical symmetric Schwarzschild case. In a general situation, a different solution must be considered, e.g., [37].

which is the Killing horizon associated to the vector field $\partial_t - \Omega_{\mathcal{H}}\partial_\phi$ (remember that $\Omega_{\mathcal{H}}$ is constant on the horizon). The parameter m is usually called *horizon semi-length*. The ADM mass of the solution is $M = \sqrt{m^2 + \sqrt{m^2 + 4J^2}}/\sqrt{2}$.

When expressed in Weyl-Papapetrou coordinates, both the Schwarzschild and the Kerr families present a highly distorted geometry near the horizons. The horizons H are topologically spheres, whereas they are represented as segments on the line $\rho = 0$. This shows one of the many subtleties of this coordinate choice.

1.2.4 Gauge freedom and surface gravity fixing

Consider a solution in Weyl-Papapetrou coordinates, such that the horizon semi-length is m, the area of $H = \mathcal{H} \cap \mathcal{N}$ is A and the total angular momentum is J. Observe that A and J are physical parameters, while m is a *coordinate* parameter, with no a priori physical meaning.

The transformation generated by the scaling $\chi \to \lambda^{-1}\chi$, with $\lambda > 0$, leaves the metric (1.3) invariant. Due to the intricacies of the Weyl coordinates (section 2.4), this transformation implies the following scalings,

$$m \to \lambda m, \quad A \to A, \quad \kappa \to \lambda\kappa, \quad J \to J, \tag{1.12}$$

recall that κ is the surface gravity of the horizon. This transformation is what we call a *residual gauge*, meaning that it is a diffeomorphism leaving the metric invariant after fixing the Weyl-Papapetrou coordinates. Observe that the quantities m/κ, A and J are gauge invariant.

In the case of black holes in asymptotically flat spacetimes, the boundary condition $g(\chi,\chi) \to -1$ for the Killing field χ allows us to fix λ, i.e., to fix the residual gauge. Then, a closed relation between A, κ and J can be established via Smarr's identity, using the Komar integral for the total mass, denoted by M [25, 38–40],

$$M = \frac{\kappa A}{4\pi} + 2J\Omega_{\mathcal{H}}, \tag{1.13}$$

where $\Omega_{\mathcal{H}}$ is the angular velocity of the horizon. First, both the Komar mass and the ADM mass coincide in stationary spacetimes (e.g., [41]). Second, it can be shown that in Weyl-Papapetrou coordinates $\frac{\kappa A}{4\pi} = m$ (see section 2.6), establishing a relation between the physical parameters with the coordinate parameter[5]. Finally, since a gauge fixing of the Killing field at infinity is equivalent to a gauge fixing of the surface gravity κ (cf. (1.2)) and the angular velocity $\Omega_{\mathcal{H}}$ (1.9), we conclude that the area A, angular momentum J and ADM mass M are not independent.

Thus, the Schwarzschild family is parametrized by the area A of the black hole (with mass $M^2 = A/16\pi$), and the Kerr family is parametrized by (A, J) (with mass $M^2 = \frac{A}{16\pi} + \frac{4\pi J^2}{A}$).

[5] Although this is a remarkable feature of these coordinates, the *mixing* between physical and coordinate parameters is often taken for granted in the literature and can lead to misunderstandings. Here, we clarify this point since it will be important to understand the difference between physical and coordinate parameters in the periodic solutions.

1.3 Periodic analogs of asymptotically flat spacetimes

Given the representation in Weyl-Papapetrou coordinates, (1.3), we say that a solution is *periodic* if it is $z-$periodic, i.e., if for some $L > 0$ the map $z \mapsto z + L$ is an isometry. In this case, $\mathcal{N}$ will be homeomorphic to $\mathbb{R}^3$ minus an infinite number of disconnected balls and $\mathcal{H}$ will be a Killing horizon.

A *periodic analog* of an asymptotically flat solution is a periodic solution with the same horizon properties. That is, a periodic black hole solution with the same area, angular momentum, charge, etc.

As an example, a periodic analog of the Schwarzschild solution would consist of infinitely many Schwarzschild black holes, distributed co-axially along the axis, equidistant and with the same area. In principle, there is no reason to assume such solutions can exist. Surprisingly, they do exist, and we review their construction below.

1.3.1 MKN solutions

Myers [1] and independently Korotkin and Nicolai [2] used Weyl-Papapetrou reduction to align infinitely many static Schwarzschild black holes of (ADM) mass M along the symmetry axis. The linearity of equation (1.10) in the static reduction implies that the superposition of solutions produces new solutions. Appropriate constant counter-terms should be added when considering infinitely many horizons to renormalize the series. The result is a static solution with infinitely many coaxial equidistant horizons and is referred to sometimes as *periodic analog of Schwarzschild solution*, or periodic Schwarzschild for short. Surprisingly, it is a regular solution that does not possess a strut in any axis component.

The construction of the solution is straightforward. Consider $\sigma_0(\rho, z)$ to be the Schwarzschild solution (1.11) with mass M and $L > 2M$, then define the periodic solution $\sigma_{MKN}(\rho, z)$ as

$$\sigma_{MKN}(\rho, z) = c + \sigma_0(\rho, z) + \sum_{n=1}^{\infty} \left(\sigma_0(\rho, z - nL) + \sigma_0(\rho, z + nL) - \frac{4M}{nL} \right), \tag{1.14}$$

where $\{\frac{4M}{nL}\}_{n\geq 1}$ are the counter-terms that renormalize the series, and c is a constant such that the horizon gauge is satisfied (i.e., $\kappa_{MKN} = \kappa_0$, the surface gravity for the Schwarzschild black hole). Observe that σ_{MKN} is periodic in z with period L, and therefore V, η and γ in (1.3) are also z-periodic with period L. The solution is symmetric with respect to the reflection $z \to -z$, and the horizon is $\mathcal{H} = \bigcup_{n\in\mathbb{Z}} \{|z - Ln| < M\}$ (recall that m is equal to the ADM mass M in the Schwarzschild solution).

An important feature of these periodic analogs of Schwarzschild is that the asymptotic behavior is no longer asymptotically flat. The metric approaches asymptotically a Kasner solution depending on M and L as follows,

$$g \approx -C\rho^{\alpha} dt^2 + \tilde{C}\rho^{\alpha^2/2-\alpha}(dx^2 - d\rho^2) + C^{-1}\rho^{2-\alpha} d\phi^2, \quad \alpha = \frac{4M}{L}. \tag{1.15}$$

The parameter α is known as the *Kasner exponent* and is a gauge invariant quantity.

Heuristically, as we go far away from the details near the axis, a cylindrical symmetry should emerge (an abelian subgroup of isometries generated by ∂_z and ∂_ϕ). The leading asymptotic behavior of the solution is thus independent of z and ϕ. Therefore, if we consider the quotient of the solution by the translation $z \mapsto z + L$, the further we go away from the horizon, the closer to a manifold that has a *free isometric* T^2-*action* we are. The only family of *exact* solutions, other than the Minkowski solution, that contains a free isometric T^2-action is the Kasner family [21].

There is no preferred way to fix the residual gauge in the periodic case. The coordinate period transforms as $L \to \lambda L$ under the scaling $\chi \to \lambda^{-1}\chi$, and thus $\frac{m}{L}$ is a new gauge invariant quantity (see (1.12)) related to the distance between consecutive horizons. This implies that the degrees of freedom in a periodic analog should be one more than in its asymptotically flat counterpart. Since $\frac{\kappa A}{4\pi} = m$ is still valid, by fixing κ we fix the value of m in terms of the area, and therefore we can parametrize the new degree of freedom by L. A practical prescription for the gauge fixing in periodic analogs, that we will call *horizon gauge*, consists in defining κ as the surface gravity of its asymptotically flat counterpart. Other gauges may be chosen differently (e.g., [42]).

The parametrization of the solution space is achieved via two gauge-independent parameters: M/L and A. Although M and L are coordinate distances (the first being the horizon semi-length and the second being the period), the quotient M/L is related to the *physical distance* of two consecutive horizons (see chapter 4). The area A of the black hole is related to the constant c in (1.14), via the gauge fixing and (1.13). Both parameters are also related to the asymptotic behavior, as can be seen in the Kasner representation (1.15). The Kasner exponent depends on M/L and the constants C and $\tilde{C}$ depend on both M/L and A.

1.3.2 Stationary generalizations of static periodic solutions

In recent years, generalized static black hole solutions in arbitrary topology in 3+1 dimensions have been well understood ([43–48]). The next natural step (as historically was the case of the Kerr solution with respect to the Schwarzschild solution) is to understand the stationary black hole solutions on a manifold $\mathcal{M}$ with nonstandard topology.

We reformulate Conjecture 1.1 as follows:

Conjecture 1.2. *Every stationary and axisymmetric asymptotically flat solution must have its periodic analog. The leading order of the asymptotic behavior should be that of a Kasner solution, (1.15), with its exponent given as a function of the total horizon area, the total angular momentum and the distances between consecutive horizons.*

The study of this conjecture faces many challenges on both analytical and numerical sides. The usual methods in exact solutions have failed so far to provide a formula or proof of existence or at least to give a convergent recursive construction algorithm. Equations (1.5)-(1.6) are non-linear, and superposition is no longer an option to construct a solution candidate. It is not known whether the proposed method in [23] to prove the existence of the periodic Kerr solution, known as the Inverse Scattering Method (see e.g. [49]), provides a uniform convergence

of the superposition of infinitely many solitons in a recursive approach. Harmonic map tools, such as in [31], rely heavily on the barrier method (e.g., [50]), but such methods diverge in the periodic scenario.

Although the existence problem proposed in Conjecture 1.2 remains elusive, certain progress can be made regarding the possible models for the a priori unknown asymptotic behavior.

Assuming that the stationary periodic analogs are *asymptotically* independent of z (as in the static case), the possible asymptotic behaviors correspond to stationary cylindrically symmetric solutions, first studied by Lewis [51]. These solutions were later used by van Stockum [52] for constructing solutions with thin rotating cylindrical rods, gluing different Lewis' models through the cylinder wall.

Lewis' models constitute the stationary generalization of the Kasner solution. In Weyl-Papapetrou coordinates, the possible forms for η^L are the following[6],

$$(\mathrm{I}\pm) : \eta^L = \rho\frac{|w|}{a}\sin(\pm a\ln(\rho/\rho_*)),\ a>0,\ \rho_*\in\mathbb{R}^+, \tag{1.16}$$

$$(\mathrm{II}\pm) : \eta^L = \rho|w|(\pm\ln(\rho/\rho_*)),\ \rho_*\in\mathbb{R}^+, \tag{1.17}$$

$$(\mathrm{III}\pm) : \eta^L = \rho\frac{|w|}{a}\sinh(\pm a\ln(\rho/\rho_*)),\ a>0,\ \rho_*\in\mathbb{R}^+, \tag{1.18}$$

where a and ρ_* are free parameters and w is related to the twist potential by

$$\omega^L = wz, \quad w\neq 0.$$

The manifold is $\mathcal{M} = \mathbb{R}_t\times\Sigma^L$, where $\Sigma^L\simeq\mathbb{R}_z\times I_\rho\times S^1_\phi$, where $I_\rho\subset\mathbb{R}$ is some connected interval. The solutions extending to infinity, i.e., admitting $I_\rho=[\rho^*,\infty)$, are (II+) and (III+). They are positive only after ρ_*, where the singularity is located.

In section 3.3, we show a rederivation of Lewis' models in Weyl-Papapetrou coordinates, where they can be classified naturally into three families[7]. The family of models that present a single singularity (at finite distance from $\partial\mathcal{N}$) and are complete at infinity is characterized by three parameters. These parameters are related to the Kasner exponent, the total angular momentum and the location of the singularity (in Weyl coordinates).

The natural definition for Lewis' asymptotic behavior (inspired by the definitions of asymptotically flat and Kasner, cf. [46]) is as follows.

Definition 1.2. *Consider a periodic generalized stationary and axisymmetric black hole solution $(\mathcal{M},g)$ in Weyl-Papapetrou form, with $\mathcal{N}$ a metrically complete Cauchy surface of $\mathcal{M}$ and let h be the metric on $\mathcal{N}$. We say it is asymptotically Lewis if there exists a Lewis' model $(\Sigma^L;g^L,\eta^L,\omega^L)$, $\Sigma^L=(0,\infty)\times T^2$,*

[6] We use the superscript L to indicate that it is a Lewis solution.

[7] Through a different approach, Mavrin in [53] obtained a different, though equivalent, representation of the solutions given in (1.16), (1.17) and (1.18).

such that for any $m \geq 1$ and $n \geq 0$ there is $C > 0$ and a bounded set $K \subset N$ that satisfy,

$$\begin{aligned} |\partial_I (h)_{ij} - \partial_I g^L_{ij}| &\leq \frac{C}{\rho^m}, \\ |\partial_I (\eta)_{ij} - \partial_I \eta^L| &\leq \frac{C}{\rho^m}, \\ |\partial_I (\omega)_{ij} - \partial_I \omega^L| &\leq \frac{C}{\rho^m}, \end{aligned}$$

for any multi-index I with $|I| \leq m$, where ρ, z, ϕ are the coordinates in Σ^L.

1.3.3 The existence problem of periodic analogs of Kerr

Conjecture 1.2 remains an open problem. Moreover, it is still unknown whether an example of a periodic analog of asymptotically flat black hole solutions can be explicitly constructed. This is where the main objects of our study enter the scene: the *periodic analog of Kerr*. That is, periodic solutions where the horizon has area A and angular momentum J.

Problem 1.1. *Given three parameters $(m/L, A, J)$, study the existence of a periodic generalized stationary and axisymmetric black hole solution $(\mathcal{M}, g)$ with one horizon per period (i.e., a periodic analog of Kerr) such that each connected component of the horizon has area A and angular momentum J. We take Weyl-Papapetrou coordinates (t, z, ρ, ϕ) on $\mathcal{M} \simeq \mathbb{R}_t \times (\mathbb{R}^+_{0,\rho} \times \mathbb{R}_z) \times S^1_\phi$ and the metric g as in (1.3).*

We approach our study by focusing on three lines.

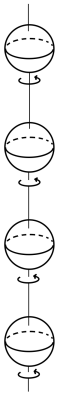

Figure 1.1: Periodic configuration for identical and coaxial black holes. The horizons are equally spaced and have the same area A and angular momentum J.

Finding a solution: numerical analysis

We study the existence part of the problem by using numerical methods. Due to the singular nature of the equations, we need appropriate variables to solve the problem. Consider the

following heat flow on Weyl-Papapetrou coordinates,

$$\dot{\sigma} = -\Delta\sigma - \frac{e^{2\sigma}}{\rho^4}|\nabla\omega|^2, \tag{1.19}$$

$$\dot{\omega} = -\Delta\omega + 2\langle\nabla\omega, \nabla(\sigma + 2\ln\rho)\rangle, \tag{1.20}$$

where $\sigma = \ln\eta - 2\ln\rho$ and the dot indicates the derivative with respect to the heat flow time, which we call τ. This heat flow is equivalent to the harmonic map heat flow for (η, ω), in the sense that the final equilibrium solution of (1.19)-(1.20) corresponds to a solution of (1.5) and (1.6). Without the risk of confusion, we will also call equations (1.19)-(1.20) a harmonic map heat flow.

Although numerical implementations of parabolic flows in General Relativity are pretty standard in the literature (see, e.g., [54]), the study of black hole solutions with non-flat asymptotic behaviors is not standard. Part of the exploratory nature of our project was establishing suitable boundary conditions in the numerical domain, particularly the asymptotic region.

Since the coordinate domain is a rectangle of height L where the upper strip is identified with the lower strip, we used a spectral method on a uniformly spaced grid for z. We used a pseudo-spectral method for ρ (specifically, a Chebyshev grid) to have a good resolution near the axis. The three input parameters are $(m/L, A, J)$. The parameter m/L provides the width of the horizon relative to the periodic length, the area is related to σ at the poles of $H = \mathcal{H} \cap \mathcal{N}$, and the angular momentum is related to the values of ω at the axis. Therefore, Dirichlet or Neumann conditions are sufficient for σ and ω at the axis and the horizon.

We use the horizon gauge, identifying the surface gravity of the horizon with κ_{Kerr}, the value of the surface gravity for the (asymptotically flat) Kerr solution with parameters (A, J). This allows us to leave L as the free parameter, which is helpful for numerical computations. See Figure 1.1 for a schematic reference of the configuration.

The main difficulty of the numerical implementation is finding the appropriate boundary conditions for σ and ω at the asymptotic region. By assuming that the asymptotic regime is dominated by a T^2-symmetry (proved in chapter 5), Lewis' models are the clear asymptotic candidates. This reduces the complexity in the study of the asymptotic behavior since the possible Lewis' models that are complete at infinity form a three-parameter family. One of the parameters is directly related to J and thus fixes the asymptotic boundary condition for ω. There are still two parameters to fix with no a priori relation with $(m/L, A, J)$, and one of them is the Kasner exponent, which is related to the Komar mass (see subsection 3.3.3).

The non-existence condition

The second problem we are interested in was motivated by the numerical analysis.

Problem 1.2. *Show that there is a value $L_c < 1/2$, such that for any $m/L < L_c$ there are no solutions to Problem 1.1.*

The following definition establishes the link between periodic analogs and stationary, axisymmetric perturbations to the MKN solutions.

Definition 1.3. *An MKN solution with parameters $(m/L, A)$ can be put into rotation if there exists a periodic analog of Kerr with parameters $(m/L, A, J)$ for some $J \neq 0$.*

In view of Problem 1.2, the natural problem to consider is stated as follows.

Problem 1.3. *Given an MKN solution, under which conditions can it be put into rotation? Can the bound L_c be written in terms of the distance between the horizons and their area?*

Problems 1.2 and 1.3 were studied using various tools from geometric analysis.

The study of perturbations of MKN solutions is related to the study of the asymptotic behavior, although indirectly. By inspecting the Lewis' models in families III+ and II+, observe that the quotient η grows at least linearly in ρ. Surprisingly, this is an obstruction to the existence of solutions!

The asymptotic behavior

Assuming we have a solution, the emergence of the $z-$symmetry is clearly the expected behavior in the asymptotic region. Such emergence should result in the solution decaying into one of the Lewis' models. In the final problem we studied, we focused on the possible asymptotic behaviors of the solutions.

Problem 1.4. *Given periodic analogs of Kerr, which asymptotic properties do they possess?*

1.4 Results

Here, we present the results obtained in our study of Conjecture 1.2.

1.4.1 Numerical results

In collaboration with O. Ortiz (FAMAF, Córdoba) and M. Reiris (FCien, Montevideo), we developed and implemented a code in `Python` that numerically solves Problem 1.1 given $(m/L, A, J)$ as input parameters and specific boundary conditions. In particular, the code finds a solution for the harmonic map equations ((1.5) and (1.6)) on a finite rectangle in two dimensions, corresponding to a domain on the surface parametrized by (z, ρ) (see section 6.2).

We developed a way to drive the flow to the right asymptotic behavior by defining a dynamical Neumann condition on σ using Smarr identity (see subsection 6.2.1). Specifically, the derivative of σ far away from the axis is given by

$$\rho_{\text{MAX}} \partial_\rho \sigma \big|_{\rho_{\text{MAX}}} = -\frac{4\overline{M}(\tau)}{L}, \tag{1.21}$$

where ρ_{MAX} is the maximum value of ρ in the grid and $\overline{M}(\tau)$ is the *average* of the Mass Komar integrals $M(\rho)$ for all the ρ's on the grid. Since we are evolving the heat flow starting on some seed (σ_0, ω_0), on each $(\sigma_\tau, \omega_\tau)$ the function $M(\rho)$ is not necessarily constant. At equilibrium, one expects a solution to be attained and $M(\rho)$ should be constant. The function $M(\rho)$ then gives us a simple test to know whether we are close to a solution. Heuristically, the right-hand side of (1.21) is the Kasner exponent at time τ (cf. (1.15)), given by certain smearing of the evolved (σ, ω), and actualizes the derivative of σ.

To understand the nature of the boundary condition (1.21), we did many runs with different parameter values, grid sizes, and different definitions of averages for $\overline{M}$. Because of this, we decided to keep the code as simple as possible. Using Euler's method to solve the parabolic PDEs (1.19)-(1.20) was the simplest possibility since it is an explicit, conditionally stable method with accuracy at linear order in the time step for τ. An implicit, more stable method, like Crank-Nicholson, requires solving a large algebraic system of equations at every time step, which would have been too time-consuming and thus limiting our exploration possibilities.

As a result of the numerical studies, we obtain strong numerical evidence of the existence of solutions on a wide range of the parameter space $(m/L, A, J)$. This indicates a positive answer to Conjecture 1.2. We establish that the asymptotic behavior of the numerical solutions is the same as Lewis' cylindrical asymptotic behavior for van Stockum's infinite rotating cylinders [52]. Below a certain critical value ($L \approx 4m$), we show that the rotational energy appears too big to sustain a global equilibrium, and a singularity shows up at a finite distance from the bulk, in agreement with Theorem 1.1. This phenomenon is also akin to van Stockum's asymptotic collapse when the angular momentum per unit of axial length reaches a critical value compared to the mass per unit of axial length. These results have been published recently [55], and are presented in chapter 6.

We also show that the Komar mass M per black hole satisfies the relevant inequality

$$M \geq \sqrt{\frac{A}{16\pi} + \frac{4\pi J^2}{A}},$$

and equality is approached as the separation between the black holes grows unbounded and the geometry near the horizons approaches that of Kerr.

The boundary condition (1.21) has a remarkable universal appearance, connecting the Kasner exponent with the dissipation produced by the heat flow in the interior of the domain. It seems suitable for a numerical study of the periodic analogs on a more general scope, not just in the context of Problem 1.1. With this in mind, we wrote a code that admits several horizons on each period and provides further evidence of the existence of solutions in the multi-horizon case. This will be discussed in detail also in chapter 6.

1.4.2 Analytic results

The first result concerns a lower bound for L_c in Problem 1.2. It is a non-existence theorem for periodic analogs of Kerr, and provides bounds for m/L in Conjecture 1.2.

Theorem 1.1. *Consider an asymptotically flat Kerr black hole with area A, angular momentum J and horizon semi-length m (in Weyl-Papapetrou coordinates). If the following inequality holds for $L > 0$,*

$$\frac{m}{L} > \frac{1}{4}, \tag{1.22}$$

then the solution does not admit a periodic analog with period L.

Inequality (1.22) is written in terms of the parameters m and L, which depend on the Weyl-Papapetrou coordinates. Using the gauge fixing by the horizon gauge, $\kappa = \kappa_{Kerr}$, the inequality reads

$$\sqrt{\frac{A}{\pi}}\frac{1-(8\pi J/A)^2}{\sqrt{1+(8\pi J/A)^2}} > L,$$

which contains the physical parameters on the left-hand side. This constitutes a lower bound for L_c (cf. Problem 1.2).

By a careful analysis of the decays of the fields and using Anderson's and Reiris' estimates in stationary spacetimes (e.g., [46,56,57]), we show that a solution cannot have sublinear growth of η with respect to ρ. The final step, via a monotonically decreasing quantity bounded from above by $4m - L$, is to relate the monotonic quantity with the growth of η.

For values of m/L above $1/4$, the value of the density of rotational energy decays slower than quadratically with the distance (section 4.2), which implies that the total energy diverges. Then, it can not sustain a global equilibrium and a singularity shows up at a finite distance from the axis. This phenomenon is akin to van Stockum's asymptotic collapse ([52]), manifest when the angular momentum (per unit of axial length) reaches a critical value compared to the mass (per unit of axial length) of the cylinder, and that results from a transition in the Lewis' class of the cylindrical exterior solution.

As a direct consequence of Theorem 1.1, we can show that a certain subfamily of MKN solutions *can not* be put into rotation (cf. Definition 1.3 and Problem 1.3). Remarkably, we could relate the parameters $(m/L, A)$ with the *physical* distance between the horizons in the MKN solutions.

Theorem 1.2. *Given a MKN solution with parameters $(m/L, A)$ (such that $2m < L$), the distance D between the horizons is bounded by*

$$D^2 \geq A\frac{\pi^2}{36}\Gamma_{\min}^2\frac{L}{2m}\left(1-\frac{2m}{L}\right)^2,$$

where $\Gamma_{\min}$ is the minimum of the gamma function in $\mathbb{R}^+$. Therefore, in view of Theorem 1.1, no MKN solution with $D < \frac{\pi\Gamma_{\min}}{6\sqrt{2}}\sqrt{A}$ can be put into rotation. As a reference, $\frac{\pi\Gamma_{\min}}{6\sqrt{2}} \approx 0.3279...$.

This result is interesting in itself for two reasons. First, it provides a bound for the distance between horizons in terms of the Weyl-Papapetrou coordinates. Second, to our knowledge, this result constitutes the first example in the literature where the existence of stationary deformations of a family of static vacuum solutions is highly constrained by their geometry.

The third result answers Problem 1.4.

Theorem 1.3. *Assume the existence of a periodic analog of a Kerr solution with parameters $(m/L, A, J)$ and $m/L \leq 1/4$. Consider Weyl-Papapetrou coordinates and let $(\mathcal{S}, \mathfrak{q})$ be the Riemannian surface parametrized by (z, ρ) and metric $\mathfrak{q} = e^{\gamma - \ln\rho - \sigma}(d\rho^2 + dz^2)$. Then there is a divergent sequence of points $\{p_i\}_{i\geq 0} \subset \mathcal{S}$ and a sequence of rescaled annuli $\{(\mathcal{A}_{r_i}(p_i; 1/2, 2), \mathfrak{q}_{r_i})\}$ on $\mathcal{S}$ such that $\mathfrak{q}_{r_i} \to C\bar{\rho}^{\alpha}(d\bar{\rho}^2 + d\bar{z}^2)$. The parameters C, α and J determine a unique Lewis' model that matches the asymptotic behavior of the solution.*

We obtain a sequence of diverging points such that certain annuli based on them converge to a fixed Lewis' model. This result leave us close to prove that the solutions, if exist, are asymptotically a Lewis' model (recall Definition 1.2) We need an extra technical step to connect our result with the definition, going from a behavior of the solution on a sequence of annuli to a *global* behavior in the asymptotic region. The technical details and proof will appear in a future work. We discuss this in subsection 5.3.4.

1.5 Open problems and further questions

Our work has left us with several open problems requiring further exploration. From analytical questions to more numerical constructions, here we mention, in our view, some of the most interesting ones.

Open Problem 1: Existence

Prove the existence of periodic analogs of Kerr solutions or provide further conditions on which non-existence holds.

The existence of solutions when $m/L \leq 1/4$ remains an open problem. Given the solid numerical evidence obtained for a wide range of parameters and the analysis of the asymptotic behavior, we conjecture that the problem has a positive answer, given that $L \geq L^*$, for certain critical value L^* related to m, A and J. Observe that Theorem 1.1 gives $L^* = 4m$, but it does not seem to be a sharp result.

Numerical heuristics help to understand certain aspects of the asymptotic behavior, particularly the decay of the rotational energy relative to the gravitational energy. As we prove in chapter 4, if a solution exists, then the decay of the rotational energy is sub-quadratic in the distance from the axis. A better upper bound for this term, relating the rate of decay with the horizon parameters, can lead to new insights into the existence problem. Indeed, due to its relation with the harmonic map energy [31], the decay rate for the rotational energy can be used to control stationary perturbations around MKN solutions.

Related to the study of a priori estimates for the rotational energy, it would be interesting to compare the MKN solutions with the stationary perturbation (if it exists). In this direction, a generalization of Theorem 1.2 with a bound for the distance between the black holes in terms of the mass, the angular momentum and other parameters (such as in the asymptotically flat case done in [58]) could be an interesting result. Some marginal results can be obtained (see chapter 6), but they do not represent an improvement in the bounds. In particular, it would be interesting to obtain a lower bound independent of m/L.

Open Problem 2: Bound for the distance between horizons

Given a periodic analog of the Kerr solution, show that the distance between two consecutive horizons is bounded from below by a function $D(A, J) > 0$.

Multi-horizon solutions are essential for the classification problem. They could provide counter-examples of uniqueness (once existence has been established).

Open Problem 3: Multi-horizon problem

Determine under which hypothesis a periodic analog of a multi-horizon asymptotically flat solution exists.

As we prove in subsection 2.5.3, the absence of struts can be generalized to multiple horizons, and thus *if* a solution to the equations is shown to exist, then it is regular. Also, the proof of Theorem 1.3 can be immediately adapted to the multi-horizon case (see chapter 5).

In this line, it would be interesting to study the case of two horizons with zero total angular momentum. The non-existence theorem (Theorem 1.1) is not necessarily valid, and the asymptotic behavior should be Kasner. It would be possible, in principle, to take the black holes arbitrarily close one from another.

Open Problem 4: Periodic analog of the Kerr binary solution

1. *Determine under which hypothesis a periodic analog of a Kerr binary solution with zero total angular momentum exists.*

2. *Given a periodic analog of a Kerr binary solution with zero total angular momentum, show that the asymptotic behavior is that of Kasner solutions.*

3. *Describe the moduli space of these solutions.*

We have made some progress regarding the numerical analysis of the first part of the above problem, and the second part is a straightforward application of the arguments provided in chapter 5. The last part is still in the numerical stage.

Finally, extending the results of stationary analog of static solutions in periodic setups remains an open problem in higher dimensions.

Open Problem 5: Periodic analogs in other contexts

Study stationary periodic configurations in dimensions $n + 1$, with $n \geq 4$.

This problem is already in its beginnings for static solutions, [59], and it would be interesting to study the asymptotic behavior of such solutions and a priori bounds for the rotational energy. Some progress for multi-horizon solutions in higher dimensions has been recently made, [60].

1.6 Structure of this thesis

The thesis is organized as follows.

In chapter 2, we present the background material of our work. We define the periodic generalized stationary and axisymmetric black hole solutions. We then review the Weyl-Papapetrou reduction of the Einstein equations using two commuting Killing fields. We outline some techniques for analyzing stationary solutions, e.g., their link with harmonic maps and the Komar integrals.

In chapter 3, we study the well-posedness of the Weyl-Papapetrou coordinates in the periodic context and present the T^2-symmetric Lewis' models. After a review of the a priori estimates given by Anderson and Reiris, we prove that ρ is unbounded and has no critical points. We then find a divergent sequence of points $\{p_i\}_{i\geq 0}$ on which the decay of $|\nabla \ln \rho|$ is bounded from below. Then, we show a new, updated derivation of Lewis' models and classify them in terms of a natural phase space.

In chapter 4, we prove the main analytic result, Theorem 1.1. First, we establish a central result on the decays of the scaled diameter of the loops $\{\rho = cnt\}$. Then, we provide several properties of the decay of the fields, using the sequence $\{p_i\}_{i\geq 0}$. We define a monotonic quantity, whose geometric meaning allows us to relate the initial data m/L with the Kasner exponent. Finally, we prove Theorem 1.2.

In chapter 5, *assuming* existence of solutions, we proceed to show that the curvature decays quadratically with the distance. Then, via the decays found in the previous chapter and results from Cheeger-Gromov theory, we prove Theorem 1.3.

In chapter 6, we present our numerical analysis (expanding the contents of [55]). First, we define the problem over a finite domain and impose suitable boundary conditions. Then, we discuss the numerical methods involved, with particular emphasis on the criteria by which the convergence of the algorithm is studied. In section 6.4, we present the results obtained for several values of J and L. A thorough analysis is shown, especially in the asymptotic region. Ergospheres and other global properties are also studied in detail. Finally, we present the numerical analysis in multi-horizon setups and show preliminary results.

1.7 Notation

The main objects of our work are 4-dimensional Lorentzian manifolds $(\mathcal{M}, g)$, with signature $(-+++)$. We interchangeably call *metric* or *line element*.

We use the following notation for intervals of the real line:

$$\mathbb{R}^+ := (0, +\infty), \quad \mathbb{R}^+_0 := [0, +\infty).$$

Whenever we have certain global coordinates on a manifold written as the product of one-dimensional manifolds, we use the notation

$$\mathcal{M} \simeq N^1_{x_1} \times ... \times N^n_{x_n},$$

to indicate that the domain of the *coordinate* x_i is N^i.

Throughout the text, we use abstract index notation, although we mix with the usual mathematical notation for geometrical objects (e.g., [61]) when there is no risk of confusion:

- Identify any $(j,k)-$tensor T with its abstract index notation, $T^{b_1 \ldots b_j}_{a_1 \ldots a_k}$.
- The metric tensor is denoted by
$$g \quad \text{or} \quad g_{ab}.$$
- The covariant derivative by
$$\nabla_a \quad \text{or} \quad \nabla.$$
- The curvature tensor as
$$R_{abc}{}^d \quad \text{or} \quad \text{Rm}.$$
- The Ricci curvature tensor as
$$R_{ab} \quad \text{or} \quad \text{Ric}.$$

We will also use the notation,

$$\langle \cdot, \cdot \rangle_g \equiv g(\cdot, \cdot)$$

to facilitate reading.

Given $(\mathcal{M}, g)$ an $n-$dimensional Riemanninan manifold, we define the following objects:

- At a point $p \in \mathcal{M}$, we called the rescaled metric, g_r, the new metric tensor scaled by $\text{dist}^2(p, X)$, for $X \subset \mathcal{M}$ some reference subset and $r = \text{dist}(p, X)$,
$$g_r := \frac{1}{\text{dist}^2(p, X)} g$$
- $(\mathcal{A}(p; a, b), g)$ is the annulus centered at $p \in \mathcal{M}$,
$$\mathcal{A}(p; a, b) = \{q \in M : a < \text{dist}(q, p) < b\}.$$
- $(\mathcal{A}_r(p; a, b), g_r)$ is the rescaled annulus centered at $p \in \mathcal{M}$,
$$\mathcal{A}(p; a, b) = \{q \in M : a < \text{dist}_{g_r}(q, p) < b\}.$$

We use the geometric system of units, $G = c = 1$.

Chapter 2

Stationary axisymmetric solutions in General Relativity

In this chapter, we introduce the stationary and axisymmetric spacetimes and present the Weyl-Papapetrou coordinates, our primary tool in their analysis. First, we review the well-known reduction of equation (1.1) using two Killing fields which are commuting and orthogonal to hypersurfaces. Then, we review the definition of the Weyl-Papapetrou coordinates for stationary and axisymmetric solutions. In terms of these coordinates, we define the periodic stationary data with suitable boundary conditions on the horizon and the axis. We prove the regularity of the reconstructed solutions from the Weyl-Papapetrou method for a specific set of stationary data. Finally, we review the properties of the Komar integrals and define the mass functional.

2.1 Introduction

Given a 4−dimensional manifold $\mathcal{M}$ with a Lorentzian metric g_{ab}[1] and a matter distribution given by a stress-energy tensor T_{ab}, the Einstein equation is

$$R_{ab} - \frac{1}{2} R g_{ab} = T_{ab},$$

where R_{ab} is the Ricci tensor associated to g_{ab}, and $R := R_{ab} g^{ab}$ the scalar curvature.

We are interested in the four-dimensional vacuum case, in which all matter content vanishes, $T_{ab} = 0$. The resulting equation, after a simple manipulation, is

$$R_{ab} = 0, \tag{2.1}$$

which asserts that any Ricci-flat Lorentzian metric is a solution to the vacuum Einstein equation. In this thesis, all the solutions to (2.1) that we will consider are assumed to be globally hyperbolic[2].

[1] Although Einstein equations can be defined in arbitrary dimension $n \geq 2$, our main discussion is in 4 dimensions and therefore we will always assume $n = 4$.

[2] The reader can check the definition of globally hyperbolic spacetimes given in [24], Chapter 6, Section 6.

When solving (2.1), one usually first imposes the topology of $\mathcal{M}$ and then some constraints on the possible admissible metrics based on physical grounds. While the first condition is an *a priori* condition, the second one is usually more delicate to define and work with since it needs a global understanding of the solutions and their properties.

On the other hand, the presence of symmetries allows for a systematic approach to the analysis of the equations. Certain symmetries on $(\mathcal{M}, g)$ simplify considerably equation (2.1) while at the same time maintaining a rich structure on the solutions moduli space. Such symmetries play a central role in the study of General Relativity. In this thesis, we consider *stationary* symmetry and *axisymmetry*.

2.1.1 Killing fields and Killing horizons

Given a Lorentzian manifold $(\mathcal{M}, g)$, a *symmetry* is an element of $\mathrm{Iso}(\mathcal{M}, g)$. Certain families of symmetries were historically named after their Euclidean analogs, such as the axial symmetry (invariance under rotation around certain spacelike axis) or translation symmetries, both spacelike and timelike.

A one-parameter group of isometries $\phi_t : \mathcal{M} \to \mathcal{M}$, $t \in \mathbb{R}$ is generated by a vector field V if

$$\dot{\phi}_t(x) = V(\phi_t(x)), \quad \forall t \in \mathbb{R}, x \in \mathcal{M}.$$

Definition 2.1. *Consider $(\mathcal{M}, g)$ a 4-dimensional Lorenzian manifold, and let ξ^a be a vector field.*

- *We say that ξ^a is a Killing field if*

$$\nabla_{(a}\xi_{b)} = 0,$$

  i.e., if it generates a subgroup of symmetries ($\mathcal{L}_\xi g = 0$).

- *We define the twist 1-form associated with ξ^a as*

$$\theta^\xi_a = \epsilon_{abcd}\xi^b\nabla^c\xi^d,$$

  where ϵ_{abcd} is the volume form associated to the metric g. Observe that this is the 1-form given by the dual formulation of Frobenius Theorem [25, p. 436], such that $\theta^\xi = 0$ if and only if ξ is hypersurface orthogonal.

- *Given a Killing field ξ^a and g a solution to (2.1), it can be shown [31, p. 906]*

$$d\theta^\xi = 0,$$

  so locally, and up to a constant, there is a potential ω which satisfies $d\omega = \theta^\xi$. The function ω is called the twist potential associated to ξ.

As we mentioned earlier, we are interested in stationary and axisymmetric spacetimes. We first define each concept separately.

Definition 2.2. *Let $(\mathcal{M}, g)$ be a globally hyperbolic spacetime.*

- *$(\mathcal{M}, g)$ is called stationary if there exists a Killing field χ which is timelike at infinity, i.e., such that for any Cauchy hypersurface there is a compact set outside which χ is timelike.*
- *$(\mathcal{M}, g)$ is called axisymmetric if $SO(2) < Iso(\mathcal{M}, g)$. We call ξ the associated Killing vector field that generates this symmetry.*

In an axisymmetric spacetime, the orbits of ξ are either points or circles since $SO(2) \simeq S^1$. We call $\mathcal{A} \subset \mathcal{M}$ the set of orbits consisting of one point. By the globally hyperbolic property of spacetime, ξ is spacelike[3].

Definition 2.3. *Let $(\mathcal{M}, g)$ be a Lorentzian manifold, ℓ a Killing field, and $\mathcal{H} \subset \mathcal{M}$ a smooth null hypersurface. If ℓ is nonzero on $\mathcal{H}$, null on $\mathcal{H}$, and tangent to the null generators of $\mathcal{H}$, we say that $\mathcal{H}$ is a Killing Horizon of ℓ.*

Killing horizons can have either one or several connected components, in the latter case, we require that the interior of its closure is a smooth connected hypersurface (see [62] for a detailed study). Killing horizons play a fundamental role in General Relativity since they can be used to define a black hole in equilibrium without the casual structure at infinity (Carter-Hawking-Robinson Theorem, [24]).

Definition 2.4. *A generalized stationary black hole solution is a $4-$dimensional, globally hyperbolic, spacetime $(\mathcal{M}, g)$, having a Killing field ℓ, such that*

1. *$\partial\mathcal{M} = \mathcal{N} \cup \mathcal{H}$, where $\mathcal{N}$ is a metrically complete Cauchy hypersurface with compact boundary and $\mathcal{H}$ is a future complete, future null hypersurface* [4].
2. *ℓ is non-zero at $\mathcal{H}$, tangent to the null generators of $\mathcal{H}$ and is timelike outside a compact set of $\mathcal{N}$.*

The set $H := \mathcal{H} \cap \mathcal{N}$ is a spatial 2-surface with a certain area, A. This quantity is called the *area of the horizon*.

Definition 2.5. *Given a Killing horizon of a Killing field ℓ, the surface gravity κ is defined as follows (see [25, 28], and we refer to [27] for a comparison between the different definitions),*

$$\kappa^2 := -\frac{1}{2}|\nabla \ell|^2\Big|_{\mathcal{H}}.$$

2.2 Reduction by symmetries and harmonic maps

In what follows, we review a standard procedure by which we reduce equations (2.1) via a 1-parameter group of symmetries generated by a Killing field ξ. The nature of the reduced equations depends on the character of the Killing field ξ. However, generically, they consist of Einstein equations in a reduced (Lorentzian of Riemannian) manifold coupled to matter,

[3] Recall that the property of being spacelike, null or timelike does not change along the orbit of the Killing field, due to $\mathcal{L}_\xi(g(\xi,\xi)) = 2\xi^a\xi^b\nabla_{(a}\xi_{b)} = 0$

[4] A future null hypersurface is a null hypersurface such that future timelike vectors point outside the manifold. We say the null hypersurface is future complete if the affine parameter of its null generators is defined in $\mathbb{R}^+$.

sourced from the norm and the twist of the Killing field. In particular, when ξ is spacelike, the reduced equations are the Einstein equations on a $2+1$-manifold, and a wave map into the hyperbolic plane models the matter.

Here, it is essential to note that if $\mathcal{M}$ is simply connected, then we can define *globally* ω by Poincaré lemma. Generally, a solution can only have ω defined locally and globally in the cover map $\tilde{\mathcal{M}}$.

A Killing field ξ with a non-vanishing norm on $\mathcal{M}$ allows a decomposition of the metric in the following form, assuming a well-defined quotient of $\mathcal{M}$ by its orbits,

$$g = \eta(dx^4 + A)^2 + \frac{1}{\eta}h, \tag{2.2}$$

where $\xi = \partial_{x^4}$, $\eta(x^1, x^2, x^3)$ is a function, $A(x^1, x^2, x^3)$ is a one-form and $h(x^1, x^2, x^3)$ is a 3-dimensional metric with Lorentzian or Riemannian signature (depending on the type of ξ) on the quotient of $\mathcal{M}$ by the orbits of ξ with Levi-Civita connection ∇. We will call such quotient $\mathcal{N}$ and assume $\mathcal{M} \simeq I \times \mathcal{N}$, where I is either $\mathbb{R}$ or S^1 (to simplify the discussion, we are not considering any other case). Then, the twist of the Killing field is given by

$$\theta^{\xi} = *dA.$$

The scalar curvature of the metric (2.2) is given by

$$R(g) = \frac{|\nabla\eta|^2 + |\nabla\omega|^2}{2\eta^2} - R(h),$$

which can be used as the Lagrangian in the *reduced* action,

$$S_{red} = C\int_{\mathcal{N}} \left(\frac{|\nabla\eta|^2 + |\nabla\omega|^2}{2\eta^2} - R(h) \right) dv_h,$$

where C is a constant related to the integration along I. By computing the variation with respect to η, ω and the metric h, we obtain

$$\Delta_h\eta = \frac{1}{\eta}(|\nabla\eta|^2 - |\nabla\omega|^2), \tag{2.3}$$

$$\Delta_h\omega = \frac{2}{\eta}\langle\nabla\eta, \nabla\omega\rangle_h, \tag{2.4}$$

$$\mathrm{Ric}(h) = \frac{1}{2\eta^2}(\nabla\eta\nabla\eta + \nabla\omega\nabla\omega), \tag{2.5}$$

where Δ_h denotes the Laplacian (or D'Alemberian) operator associated with the metric h. Equation (2.5) states that the Ricci tensor of $\mathcal{N}$ can be decomposed in terms of gradients of η and ω, and, more importantly, that the scalar curvature is non-negative. Equations (2.3),(2.4) and (2.5) are thus equivalent to $\mathrm{Ric}(g) = 0$[5].

[5]By writing $\mathrm{Ric}(g) = 0$ and manipulating the equations, one also arrive at (2.3),(2.4) and (2.5).

Equations (2.3) and (2.4) can be understood in terms of the harmonic/wave map formalism.

Definition 2.6. *Let $\mathcal{H}$ be the hyperbolic plane, $\mathcal{H} = \{(\eta, \omega) : \eta > 0\}$, with metric $ds^2 = \frac{1}{\eta^2}\left(d\eta^2 + d\omega^2\right)$. A function $f : \mathcal{N} \to \mathcal{H}$ that is a critical point of the energy integral*

$$E(f) = \int_{\mathcal{N}} \frac{|\nabla\eta|^2 + |\nabla\omega|^2}{\eta^2} dv_N, \tag{2.6}$$

is said to be a harmonic map if $\mathcal{N}$ is Riemannian or a wave map if $\mathcal{N}$ is Lorentzian.

Observe that the Euler-Lagrange equations for the harmonic (wave) map are exactly (2.3) and (2.4). The following proposition can be found in [31, p. 908].

Proposition 2.1. *Let $(\mathcal{M}, g)$ be a Lorentzian connected manifold, with g a solution to Einstein equations in vacuum, and ξ a Killing vector field, with norm $\eta = \xi_a\xi^a$, and twist potential ω. Then the pair (η, ω) defines, wherever ξ is not null, a harmonic (wave) map from $\mathcal{M}$ to the hyperbolic plane*

$$(\mathcal{H}, q_{\mathcal{H}}) = \left(\{(\eta, \omega) : \eta > 0, \}, \frac{d\eta^2 + d\omega^2}{\eta^2}\right).$$

2.3 Stationary and axisymmetric spacetimes

When considering two Killing vector fields, the reduction from a 4-dimensional problem to a 2-dimensional one is analogous to the previous section by doing the reduction twice. The structure of the final equations depends on the group structure formed by the particular Killing fields (i.e., if they are both spacelike or one timelike and one spacelike and if they commute with each other). The transverse two-manifolds to the orbits also depend on the specific orbits taken from the Killing fields. This is a subtle point, which we will explain below.

Definition 2.7. *A spacetime $(\mathcal{M}, g)$ is called a stationary and axisymmetric spacetime if it is axisymmetric, stationary, with Killing fields ξ and χ respectively, and such that the following conditions hold,*

$$\begin{aligned} [\chi, \xi] &= 0, \\ \theta^{\chi}(\xi) &= 0, \\ \theta^{\xi}(\chi) &= 0. \end{aligned}$$

The first condition establishes that the subgroup of isometries generated by these Killing vector fields is abelian. The second and third conditions imply, via the Frobenius theorem, that the surfaces spanned by χ, ξ are integrable and orthogonal to spacelike surfaces.

Consider a generalized stationary black hole solution $(\mathcal{M}, g)$ with horizon $\mathcal{H}$. By definition, it has a Killing field χ that generates the stationary symmetry. Now, if, in addition, it is axisymmetric (generated by ξ), then both χ and ξ are tangent to the horizon $\mathcal{H}$, but they are not null on $\mathcal{H}$. It can be proven [25] that there is, however, a linear combination of χ and ξ,

$$\ell = \chi - \Omega_{\mathcal{H}}\xi, \tag{2.7}$$

such that ℓ is null on $\mathcal{H}$, non-vanishing on $\mathcal{H}$ and tangent to the null generators of $\mathcal{H}$. Therefore, $\mathcal{H}$ is a Killing horizon of ℓ.

Let us now consider the quotient of $\mathcal{M}$ by the orbits of ξ and χ. The subgroups of isometries generated by the flows of ξ and χ are isomorphic to $SO(2)$ and $\mathbb{R}$, respectively. The quotient manifold,

$$\mathcal{S} := (M \setminus \mathcal{A})/(\mathbb{R} \times SO(2)), \tag{2.8}$$

is a two-dimensional connected manifold, generically with nontrivial topology. When $\mathcal{M}$ is asymptotically flat, $\mathcal{S}$ is considered to be simply connected. In the periodic analogs mentioned in the Introduction, $\mathcal{S}$ is topologically a cylinder. Let ϕ be the coordinate associated with the $SO(2)$ action (labeling elements on the axisymmetry orbits), and t be the coordinate associated with the $\mathbb{R}$ action (labeling elements on the stationary orbits).

The quotient $\mathcal{N} = (M \setminus \mathcal{A})/(SO(2))$ is a well-defined Lorentzian manifold with metric h written as (cf. (2.2))

$$h_{ab} = g_{ab} - \frac{1}{\eta}\xi_a\xi_b =: \frac{1}{\eta}\left(-\rho^2 dt^2 + \mathfrak{q}\right) \tag{2.9}$$

where we use that the metric is stationary, the quantity ρ^2 is defined as $\eta h_{ab}\chi^a\chi^b$ and $\mathfrak{q}$ is the lift of a Riemannian metric on $\mathcal{S}$. Since we can extend the orbits of χ to all $\mathbb{R}$, in Definition 2.4 we should take any $t_0 \in \mathbb{R}$ as the initial value of the flow and take the hypersurface $\{t = t_0\} \simeq \mathcal{S} \times \mathbb{R}$ as the boundary of the manifold. In the rest of the work, we will not consider this technical issue, assuming such t_0 if needed.

Because of the previous observations, we have the following definition.

Definition 2.8. *A generalized stationary and axisymmetric black hole solution is a generalized stationary black hole solution $(\mathcal{M}, g)$, with two commuting Killing fields ξ and χ, generating the axisymmetry and the time-translation respectively, satisfying Definition 2.7.*

Integrability of the spatial surfaces orthogonal to ξ and χ implies that the one form A can be written as

$$A = \Omega dt,$$

where Ω is the *angular velocity function*. The value of Ω at the horizon is $\Omega_{\mathcal{H}}$, which plays an important role in the linear combination (2.7).

By defining $W = \xi^\mu\chi_\mu$ and $V = -\chi^\mu\chi_\mu$ all the functions depends only on (x^2, x^3), we can rewrite the double reduction of the metric (2.2) as follows,

$$g = -Vdt^2 + 2Wdtd\phi + \eta d\phi^2 + \frac{1}{\eta}\mathfrak{q},$$

where the function ρ is given by $\rho = \sqrt{\eta V + W^2}$. Observe that a similar approach is done in the Kaluza-Klein reductions of high dimensional gravity ([63,64]), where the dilaton takes the role of ρ as the volume density of the transverse hypersurfaces.

Since we have the decomposition (2.9), equations (2.3) and (2.4) now read,

$$\hat{\nabla}^A(\rho\hat{\nabla}_A\eta) = \frac{\rho}{\eta}(|\hat{\nabla}\eta|^2 - |\hat{\nabla}\omega|^2), \tag{2.10}$$

$$\hat{\nabla}^A(\rho\hat{\nabla}_A\omega) = 2\frac{\rho}{\eta}\left\langle\hat{\nabla}\eta, \hat{\nabla}\omega\right\rangle_{\mathfrak{q}}, \tag{2.11}$$

where $\hat{\nabla}$ is the covariant derivative compatible with $\mathfrak{q}$. Equation (2.11) is the integrability condition for the equation

$$d\omega = \frac{\eta^2}{\rho} * d\Omega, \tag{2.12}$$

where $*$ is the Hodge dual operator in $\mathfrak{q}$. Since $\mathcal{S}$ is a Riemannian surface, equations (2.11) and (2.10) are the *harmonic map* equations corresponding to the energy

$$E(\omega,\eta) = \int_{\mathcal{S}} \rho\frac{|\hat{\nabla}\eta|^2 + |\hat{\nabla}\omega|^2}{\eta^2}\epsilon_{\mathfrak{q}},$$

where $\epsilon_{\mathfrak{q}}$ is the area element of $\mathcal{S}$ associated to $\mathfrak{q}$.

Next, we discuss equation (2.5). By definition, fields are independent of t, so (2.5) implies that $\mathrm{Ric}(h)$ is purely tangential to $\mathcal{S}$. Using the co-area formula (from the $t-$derivative of the second fundamental form of the slices $t = cnt$, see [31] for a derivation), we have that equation (2.5) is equivalent to the following couple of equations,

$$\hat{\Delta}\rho = 0, \quad \hat{\nabla}\hat{\nabla}\rho = -\rho(\pi_{\mathfrak{q}}(\mathrm{Ric}(h)) - \frac{1}{2}R(h)\mathfrak{q}), \tag{2.13}$$

where $\pi_{\mathfrak{q}}$ is the projection to the tensor fields on $(\mathcal{S},\mathfrak{q})$ from (N,h).

Finally, we use that (2.10) and (2.11) satisfy the conformal invariance property. The metric $\mathfrak{q}$ is 2-dimensional, thus by the Uniformization Theorem we can consider a function γ on $\mathcal{S}$ such that

$$\mathfrak{q} = e^{2\gamma}\delta, \tag{2.14}$$

where δ is a flat metric on $\mathcal{S}$. Then, equations (2.13) decouple from the equations (2.10) and (2.11).

That is the main point of this section: our original system of coupled equations with unknowns η, ω and h can be reduced to a system of coupled equations for η, ω and a decoupled pair of equations for ρ, γ and Ω. Further simplification of the equations can be done via the Weyl-Papapetrou coordinates, defined by Weyl in the static case ([7]) and later Papapetrou in the stationary axisymmetric case [29,30] (see also [25] for a historical account). We will review this construction in the next section.

2.4 Weyl-Papapetrou coordinates

If we assume that the function ρ has no critical points (i.e. $\hat{\nabla}\rho \neq 0$ on $\mathcal{S}$), then we can consider the set of coordinates (ρ, z), with z the harmonic conjugate of ρ, and write the flat metric δ on

(2.14) as

$$\delta = d\rho^2 + dz^2.$$

The first equation in (2.13) is trivially satisfied. For the second equation, we can use the formula of conformal change in the curvature $\mathrm{Ric}(\mathfrak{q})$,

$$e^{2\gamma}\hat{\nabla}\gamma = -\hat{\nabla}_{\hat{\nabla}\rho}\hat{\nabla}\rho,$$

and therefore, it reduces to a set of first-order equations, using (2.5),

$$d\gamma = \left(\frac{\rho}{4\eta^2}((\partial_\rho\eta)^2 - (\partial_z\eta)^2 + (\partial_\rho\omega)^2 - (\partial_z\omega)^2)\right)d\rho + \left(\frac{\rho}{2\eta^2}(\partial_\rho\eta\partial_z\eta + \partial_\rho\omega\partial_z\omega)\right)dz. \quad (2.15)$$

The coordinates (t, ρ, z, ϕ) are known as *Weyl-Papapetrou* coordinates, and allow to simplify equations (2.10), (2.11) and (2.13). They are also suitable for numerical implementations. In these coordinates, the metric has the following form,

$$g = -Vdt^2 + 2Wdtd\phi + \eta d\phi^2 + \frac{e^{2\gamma}}{\eta}(d\rho^2 + dz^2). \quad (2.16)$$

The metric coefficients are found from η and the twist potential ω satisfying the harmonic map equations on $\mathcal{S}$. Equations (2.10) and (2.11) reduce to

$$\Delta_\rho\eta = \frac{|\nabla\eta|^2 - |\nabla\omega|^2}{\eta}, \quad (2.17)$$

$$\Delta_\rho\omega = \frac{2}{\eta}\langle\nabla\omega, \nabla\eta\rangle, \quad (2.18)$$

where the inner product is with respect to the flat metric $d\rho^2 + dz^2$, and the Laplacian is the $\mathbb{R}^3$ Laplacian in cylindrical coordinates (ρ, z, ϕ) under axial symmetry:

$$\Delta_\rho = \partial_\rho^2 + \frac{1}{\rho}\partial_\rho + \partial_z^2$$

Once η and ω are found, the metric (2.16) is recovered by

$$W = \eta\Omega, \quad V = \frac{\rho^2 - W^2}{\eta}, \quad (2.19)$$

where Ω and γ are given by the following quadratures (from (2.12) and (2.15)),

$$\partial_z\Omega = \rho\frac{\partial_\rho\omega}{\eta^2}, \qquad \partial_\rho\Omega = -\rho\frac{\partial_z\omega}{\eta^2}, \quad (2.20)$$

$$\partial_z\gamma = \frac{\rho}{2\eta^2}(\partial_\rho\eta\partial_z\eta + \partial_\rho\omega\partial_z\omega), \qquad \partial_\rho\gamma = \frac{\rho}{4\eta^2}((\partial_\rho\eta)^2 - (\partial_z\eta)^2 + (\partial_\rho\omega)^2 - (\partial_z\omega)^2). \quad (2.21)$$

The described ladder-like way of solving the equations does not guarantee the regularity of the final metric. This is a rather inconvenient phenomenon of the Weyl-Papapetrou reduction:

solving the reduced equations is not enough to guarantee a regular metric, and one has to check the regularity *after* a solution has been found. The problematic behavior is at the axis. Note that the points at the axis $\mathcal{A}$ are those where the norm of ∂_ϕ vanishes, and therefore $\rho = 0$ there. Then, by removing the set $\mathcal{A}$ in the quotient (2.8), we have to check if the metric is indeed regular at $\mathcal{A}$.

The circumference of a circle at constant ρ and z near the axis can be computed using η, and it gives

$$c(z,\rho) := 2\pi\sqrt{\eta}(z,\rho),$$

while the radius of such a circle is given by

$$r(z,\rho) := \int_0^\rho \frac{e^{\gamma(z,\mathfrak{r})}}{\sqrt{\eta}} d\mathfrak{r}.$$

The limit when $\rho \to 0$ of the quotient of both quantities gives the regularity of the metric at the axis: if

$$\lim_{\rho\to 0} \frac{c(z,\rho)}{2\pi r(z,\rho)} = 1,$$

then the metric is regular. Otherwise, there is an *angle deficit* at the axis, given by

$$\beta = 2\pi\left(1 - \lim_{\rho\to 0} \frac{c(z,\rho)}{2\pi r(z,\rho)}\right),$$

which can be associated with a singular matter distribution (e.g., [8,31]). The regularity of the metric naturally leads to the condition

$$\gamma - \ln\eta + \ln\rho \to 0 \quad (\rho \to 0).$$

In our case, having η and ω, this defect can be better computed with the help of the auxiliary function $q := \gamma - \sigma - \ln\rho$ as $\delta(z_0) = 2\pi - \pi e^{-q(0,z_0)}$. This function can be easily computed (once we have a solution for the harmonic map) from the quadratures,

$$\partial_\rho q = \frac{\rho}{4}((\partial_\rho\sigma)^2 - (\partial_z\sigma)^2) + \frac{\rho}{4\eta^2}((\partial_\rho\omega)^2 - (\partial_z\omega)^2), \quad \partial_z q = \frac{\rho}{2}\left(\partial_z\sigma\partial_\rho\sigma + \frac{1}{\eta^2}\partial_z\omega\partial_\rho\omega\right). \quad (2.22)$$

These quadratures determine q up to a constant, which can be fixed at some point $p \in \mathcal{A}$ as $\lim_{x\to p} q(x) = 0$. After we compute a solution to the harmonic map equations, we must verify that $q \to 0$ at each axis point. As we mentioned in the Introduction, generically, there are angle defects around the axis that give rise to the well-known *struts*. We will further discuss this point in subsection 2.4.2.

Another feature of the Weyl-Papapetrou coordinates is the high level of distortion near the axis and horizons relative to the usual Boyer-Lindquist coordinates. This is because ρ is an area density and, therefore, can be zero on the points where the surfaces spanned by ∂_t and ∂_ϕ contain a null direction. To see these subtleties, we first review some classic examples of exact solutions written in these coordinates and then comment on the behavior of Weyl-Papapetrou

coordinates near the axis, the horizon, and the asymptotic region.

Remark on alternative reduction. A different reduction can be made by taking the Killing vectors ℓ and ξ. In that case, the transverse three-manifolds will not be orthogonal to the orbits of the time-transnational Killing vector. The resulting metric is of the form

$$g = -f(dt + Ad\phi)^2 + f^{-1}(\mathfrak{q}_W + \rho^2 d\phi^2),$$

where f, A are functions depending on (ρ, z) and $\mathfrak{q}_W = e^{2k}(d\rho^2 + dz^2)$. This is a well known reduction when working in the Inverse Scattering Method (see Appendix B). We present some formulas relating the coefficients V, W and X in (2.16) with f, A and ρ in Appendix A.

2.4.1 Exact stationary axisymmetric solutions

In this subsection, we provide several examples of exact solutions to the system of equations (2.17) and (2.18), written in Weyl-Papapetrou form (2.16). They are also historically relevant in the development of the theory of General Relativity and will serve as primary examples to illustrate the properties of stationary and axisymmetric solutions.

Minkowski spacetime

The first known solution for General Relativity was Minkowski spacetime $\mathbb{M}^4$. It is a flat, maximally symmetric spacetime, with 10 independent symmetries: four translations, three rotations and three boosts, with the structure of $\mathbb{R}^{1,3} \rtimes O(1,3)$ and product $(T, f) \cdot (S, g) = (T + f \cdot S, f \cdot g)$[6]. The metric is given by

$$g_{Minkowski} = -dt^2 + d\rho^2 + dz^2 + \rho^2 d\phi^2.$$

Observe that ρ plays the role of the radial polar coordinate.

Schwarzschild family

The first nontrivial solution with a non-vanishing Riemann tensor was derived by Karl Schwarzschild [35], and it has a four-dimensional symmetry group, $\mathbb{R} \times O(3)$. The manifold is $\mathbb{R} \times (\mathbb{R}^3 \setminus B)$, where B is an open ball, and the metric is usually presented as

$$g_{Sch} = -\left(1 - \frac{R}{r}\right) dt^2 + \left(1 - \frac{R}{r}\right)^{-1} dr^2 + r^2 d\Omega_{S^2},$$

where R is the radius of B. The coordinates are (t, r, θ, ψ), where (θ, ψ) are the usual sphere coordinates. The spheres of constant r have area $4\pi r^2$. In Weyl-Papapetrou form, the manifold on which the metric is defined is $\mathcal{M} = \mathbb{R}_t \times \mathbb{R}^+_{0,\rho} \times \mathbb{R}_z \times S^1_\phi$, and the metric given by

$$g_{Sch} = -e^{-\sigma_{Sch}} dt^2 + e^{\sigma_{Sch}}(e^{2k}(d\rho^2 + dz^2) + \rho^2 d\phi^2),$$

[6] Famously called Poincaré group.

where

$$\sigma_{Sch} = \ln\left(\frac{\sqrt{(z-m)^2+\rho^2}+\sqrt{(z+m)^2+\rho^2}+2m}{\sqrt{(z-m)^2+\rho^2}+\sqrt{(z+m)^2+\rho^2}-2m}\right), \quad m>0,$$

and e^{2k} is given by

$$e^{2k} = \frac{\left(\sqrt{(z-m)^2+\rho^2}+\sqrt{(z+m)^2+\rho^2}\right)^2-4m^2}{4\sqrt{(z-m)^2+\rho^2}\sqrt{(z+m)^2+\rho^2}}.$$

The coordinate transformation from the usual spherical coordinates (r,θ,ϕ) to the Weyl-Papapetrou coordinates is given by

$$\rho = r\left(1-\frac{2m}{r}\right)^{1/2}\sin\theta,$$
$$z = (r-m)\cos\theta.$$

The radius of B satisfies $R = 2m$, and the ADM mass is m. Observe that the set $\{\rho = 0\}$ contains the axis and the boundary of B. Therefore, the topologically spherical set ∂B is *represented* by a segment in these coordinates. There is no inconsistency in this: the axisymmetry implies that we can quotient the sphere (minus both poles) by the action of the rotations, and the result is a segment. The poles are points where the coordinates are singular. This shows the distortion produced by the coordinate transformation.

The boundary of the manifold is thus the set $\mathcal{H} = \{\rho = 0, |z| < m\}$. A direct computation shows that $\mathcal{H}$ is the Killing horizon associated with ∂_t.

Kasner family

In 1921, Kasner presented [21] a new set of solutions, now known as the *cosmological Kasner family*, which was originally derived looking for algebraic relations between the metric coefficients. In Cartesian coordinates, the base manifold is $(0,+\infty)\times\mathbb{R}^3$ and the metric is given by

$$g_K = -dt^2 + t^{2p_x}dx^2 + t^{2p_y}dy^2 + t^{2p_z}dz^2,$$

where p_x, p_y, p_z are parameters satisfying the following constraints,

$$p_x^2+p_y^2+p_z^2 = 1, \quad p_x+p_y+p_z = 1.$$

These solutions have a transitive action of its abelian isometry group, $\mathbb{R}^3$. Their static counterpart, which will be useful later in the work when studying asymptotic behavior, is given in Weyl-Papapetrou coordinates by

$$g_K = -\rho^{2p_t}dt^2 + \rho^{2p_\rho}d\rho^2 + \rho^{2p_z}dz^2 + \rho^{2p_\phi+2}d\phi^2,$$

with

$$p_t + p_z + p_\phi = p_\rho, \quad p_t^2 + p_z^2 + (p_\phi + 1)^2 = (p_t + p_z + p_\phi + 1)(1 + p_\rho).$$

In our axisymmetric context, $p_\rho = p_z$, due to the factorization in $\mathcal{S}$ (in fact, it can be shown that it is a necessary condition for this metrics to be axisymmetric), and therefore,

$$g_K = -\rho^\alpha dt^2 + \rho^{\alpha^2/2-\alpha}(d\rho^2 + dz^2) + \rho^{2-\alpha} d\phi^2, \tag{2.23}$$

for certain $\alpha \in \mathbb{R}$.

A particular solution of the Kasner family is given by the Boost (also known as Rindler wedge)

$$g_{Boost} = -\tilde{\rho}^2 dt^2 + (d\tilde{\rho}^2 + d\tilde{z}^2) + \tilde{\rho}^2 d\phi^2,$$

for $\tilde{\rho}, \tilde{z}$ reparametrizations of the coordinates ρ, z.

Kerr family

In 1963, Kerr discovered a two-parameter family of stationary and axisymmetric solutions, called the *Kerr family*, with isometry group $Iso(M, g_{Kerr}) = \mathbb{R} \times SO(2)$. The base manifold is the same as Schwarzschild solution, $\mathbb{R} \times (\mathbb{R}^3 \setminus B)$, with the metric written in Boyer-Lindquist coordinates,

$$g_{Kerr} = -\left(1 - \frac{Rr}{\Sigma}\right) dt^2 + \frac{\Sigma}{\Delta} dr^2 + \Sigma d\theta^2 + \left(r^2 + a^2 + \frac{Rra^2}{\Sigma} \sin^2\theta\right) \sin^2\theta \, d\phi^2 - \frac{2Rra \sin^2\theta}{\Sigma} dt \, d\phi,$$

where R is the radius of B, $\Sigma = r^2 + a^2 \cos^2\theta$ and $\Delta = r^2 - Rr + a^2$. The parameters R and a characterize each solution within the family, the former related to the mass of the solution and the latter to the angular momentum.

In Weyl-Papapetrou coordinates, the functional expressions are more convoluted than that of Schwarzschild (see section 2.3), although they have a closed algebraic form,

$$V = \frac{p^2x^2 + q^2y^2 - 1}{(px+1)^2 + q^2y^2}, \quad A = \frac{2mq}{p} \frac{(1-y^2)(px+1)}{p^2x^2 + q^2y^2 - 1},$$
$$e^{2\gamma} = \frac{\eta}{V} \frac{p^2x^2 + q^2y^2 - 1}{p^2(x^2 - y^2)}, \quad \eta = \frac{\rho^2 - V^2A^2}{V}, \quad W = VA,$$

where

$$x = \frac{1}{2m}\left(\sqrt{(z+m)^2 + \rho^2} + \sqrt{(z-m)^2 + \rho^2}\right),$$
$$y = \frac{1}{2m}\left(\sqrt{(z+m)^2 + \rho^2} - \sqrt{(z-m)^2 + \rho^2}\right),$$
$$p = \frac{m}{M}, \quad q = \frac{J}{M^2}, \quad M = \sqrt{m^2 + \sqrt{m^2 + 4J^2}}/\sqrt{2}.$$

The parameter M is the ADM mass of the solution.

As is well-known, the Kerr family has a Killing horizon at $r = R$, which in Weyl-Papapetrou

coordinates corresponds to the set $\mathcal{H} = \{\rho = 0, |z| < m\}$. The generator is not ∂_t, but a linear combination of ∂_t and ∂_ϕ,

$$\ell = \partial_t - \Omega_{\mathcal{H}} \partial_\phi,$$

where $\Omega_{\mathcal{H}}$ is the value of Ω at $\mathcal{H}$ (see next section for a proof of the constancy of Ω at the Killing horizon). A region of the spacetime, known as the *ergo-region*, is determined by the set of points $p \in \mathcal{M}$ where $V < 0$. Its boundary is the Killing horizon associated with ∂_t, commonly referred to as *ergosphere*[7]. See Figure 2.1 for a schematic comparison between Schwarzschild and Kerr solutions.

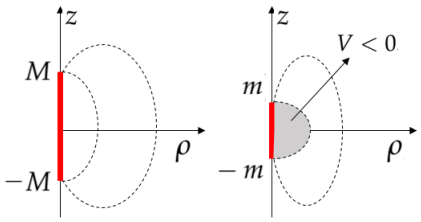

Figure 2.1: Representation of a Schwarzschild solution and a Kerr solution with the same ADM mass M, in Weyl-Papapetrou coordinates. The dashed lines represent level sets of V. Observe the reduction in the horizon coordinate length ($m < M$) and the position of the ergo-region.

2.4.2 Behavior near the axis and horizon

As stated in Definition 2.4, horizons are defined as future null, future complete Killing horizon. In the case of Weyl-Papapetrou coordinates, we are considering coaxial horizons, as in Schwarzschild and Kerr solutions. Since the surfaces spanned by $\{\partial_t, \partial_\phi\}$ are tangent to the horizon, and it is a null hypersurface, it will be located at the set $\{\rho = 0\}$. Moreover, $\{\partial_\phi\}$ cannot vanish at the horizon. Then, the set

$$\mathcal{H} := \{\rho = 0, \quad \eta > 0\},$$

is a future null, future complete Killing horizon. At each connected component of $\mathcal{H}$, consider the null vector field $\zeta = \partial_t + \Omega \partial_\phi$. Abusing nomenclature, we will call $H := \mathcal{H} \cap \mathcal{N}$ the horizon, and it will be clear from the context if we are referring to H or $\mathcal{H}$.

In Figure 2.2 we show a typical situation where some connected components of the horizon are located along $\{\rho = 0\}$, and the axis has several connected components.

As it is well known (e.g., [31,33]), when we restrict $\zeta \mid_{\mathcal{H}}$ we obtain the null Killing generator of the Killing horizon, extendible to all spacetime simply as

$$\partial_t + \Omega_{\mathcal{H}} \partial_\phi,$$

where $\Omega_{\mathcal{H}}$ is the *angular velocity* at the connected component of the horizon.

[7]The boundary of the ergo-region for an asymptotically flat black hole solution is topologically a sphere, hence the name.

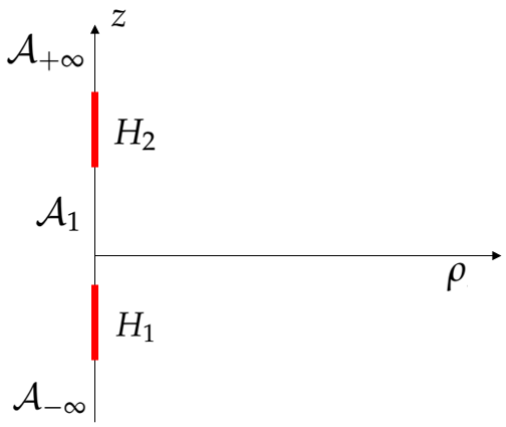

Figure 2.2: Example showing the case where $H := \mathcal{H} \cap \mathcal{N}$ has two connected components, H_1 and H_2, and the axis has three connected components: $\mathcal{A}_{-\infty}$ and $\mathcal{A}_{+\infty}$ are unbounded, while $\mathcal{A}_1$ is bounded.

The presence of horizons implies certain boundary conditions for η and ω needed to characterize a black hole solution.

Definition 2.9. *Consider a generalized stationary and axisymmetric black hole solution $(\mathcal{M}, g)$, and take the Weyl-Papapetrou coordinates. Let $H = \mathcal{N} \cap \mathcal{H}$, i.e., $\partial\mathcal{N} = H$. Each connected component of the horizon is denoted as H_i, with $i = 1, ..., N$ in the case of finitely many horizons or $i \in \mathbb{Z}$ in the case of infinitely many. Each connected component of the axis $\mathcal{A}$ is denoted by $\mathcal{A}_{i-1}$, with $\mathcal{A}_0 := \mathcal{A}_{-\infty}$ and $\mathcal{A}_N := \mathcal{A}_{+\infty}$, the unbounded components reaching $z = -\infty$ and $z = +\infty$ respectively. Then,*

$$\partial_\rho \eta \mid_{\mathcal{A}_i} (0, z) = 0, \quad \omega \mid_{\mathcal{A}_i} = c_i \in \mathbb{R},$$

and

$$\eta \mid_{H_i \setminus \{S_i, N_i\}} (0, z) > 0, \quad \partial_\rho \omega \mid_{H_i} = 0,$$

where $\{S_i, N_i\} := H_i \cap \mathcal{A}$ are the "south" and "north" poles of each H_i. The constants c_i are such that the angular momentum at each H_i is given by

$$J_i = \frac{1}{8}(c_i - c_{i-1})$$

In the stationary axisymmetric case, we can give a straightforward proof that Ω and γ are constants at the horizon, using the quadrature equations (2.21), (2.20) and the previous definition.

Proposition 2.2. *Consider a generalized stationary and axisymmetric black hole solution $(\mathcal{M}, g)$ with horizon $\mathcal{H}$. The function Ω is constant on each connected component of the horizon.*

Proof. From (2.20), we have $\partial_z \Omega = \frac{\rho \partial_\rho \omega}{\eta^2}$. From the Definition 2.9 we have $\partial_z \Omega = 0$ at $H_j \setminus \{S_j, N_j\}$. Consider one H_j, and let z_- and z_+ be the Weyl-Papapetrou coordinates of S_j, N_j,

respectively. Then, for $z \in (z_-, z_+)$,

$$\Omega(z,0) = \int_{z_-}^{z} \partial_z \Omega dz + \Omega(z_-,0) =: \Omega_{H_j}.$$

□

Analogously, we can prove that γ is also constant at $\mathcal{H}$.

Proposition 2.3. *Consider a generalized stationary and axisymmetric black hole solution $(\mathcal{M}, g)$ with horizon $\mathcal{H}$. The function γ is constant at each connected component of the horizon.*

Proof. Observe that $\partial_\rho \eta, \partial_z \eta, \partial_\rho \omega$ and $\partial_z \omega$ are bounded at $H_j \setminus \{S_j, N_j\}$. Then, by the quadrature (2.21) and the condition $\eta > 0$, we obtain that $\partial_z \gamma = 0$ at the interior of the horizon. Then, using the same notation as in the previous proof, for each H_j and $z \in (z_-, z_+)$,

$$\gamma(z,0) =: \gamma_{H_j}.$$

□

2.4.3 Periodic analogs

This subsection defines periodic solutions and periodic analogs of asymptotically flat solutions, as discussed in the Introduction. For completeness purposes, we also give below the definitions of asymptotically flat and asymptotically Kasner solutions.

Definition 2.10. *A stationary data set is given by $(\mathcal{N}; h, \eta, \omega)$ such that N is a 3-manifold, h a Riemannian metric on $\mathcal{N}$, and together with η and ω they satisfy (2.3), (2.4) and (2.5).*

The quotient manifold, $\mathcal{N}$, is a Riemannian 3-manifold. Since $\mathcal{M} \simeq \mathbb{R} \times \mathcal{N}$, this splitting allows us to precisely define the asymptotic behavior from the *physical conceptualization* of an isolated system. The starting point is the Schwarzschild solution, which, written in terms of Definition 2.10, is given by $(\Sigma^{Sch}; h^{Sch}, \eta^{Sch}, 0)$.

Definition 2.11. *A stationary data set $(\mathcal{N}; h, \eta, \omega)$ is asymptotically flat*[8] *if there is a compact set $K \subset \mathcal{N}$ and a diffeomorphism into the image $\phi : \mathcal{N} \setminus K \to \Sigma^{Sch}$ such that*

$$\begin{aligned}(\phi_* h)_{ij} &= \left(1 + \frac{2M}{r}\right)\delta_{ij} + o_2(r^{-1}),\\ \phi_* \eta &= r^2 \cos^2\theta + o_2(r^{-1}),\\ \phi_* \omega &= O(\theta) + o_2(r^{-1}),\end{aligned}$$

where $r = \sqrt{\sum x_i^2}$, $O(\theta)$ is some regular angular function and the notation $o_2(r^{-p})$ means that a function is $o(r^{-p})$, its first derivative is $o(r^{-p-1})$ and its second derivative $o(r^{-p-2})$. The parameter M is called the mass of N.

[8] This definition is often called *strongly asymptotically flat*, cf. [31].

Another notion of asymptotic behavior comes from the Kasner family of static solutions, given by the following definition.

Definition 2.12. *A stationary data set $(\mathcal{N}; h, \eta, \omega)$ is asymptotically a Kasner solution $(\Sigma^K; g^K, \eta^K)$, $\Sigma^K = (0,\infty) \times T^2$, if for any $m \geq 1$ and $n \geq 0$ there is $C > 0$, a bounded set $K \subset \mathcal{N}$ and a diffeomorphism into the image $\phi : \mathcal{N} \setminus K \to \Sigma^K$ such that*

$$|\partial_I(\phi_* h)_{ij} - \partial_I g^K_{ij}| \leq \frac{C}{x^m},$$
$$|\partial_I(\phi_* \eta) - \partial_I \eta^K| \leq \frac{C}{x^m},$$
$$|\partial_I(\phi_* \omega)| \leq \frac{C}{x^m},$$

for any multi-index I with $|I| \leq n$, where x, y, z are the coordinates in Σ^K.

Definition 2.13. *Periodic solutions and periodic analogs.*

- *Given the representation in Weyl-Papapetrou coordinates, (1.3), a periodic solution is a generalized stationary and axisymmetric black hole solution such that it is $z-$periodic, in the sense that $z \mapsto z + L$ is an isometry for some $L > 0$. In this case, $\mathcal{N}$ will be homeomorphic to $\mathbb{R}^3$ minus an infinite number of disconnected balls and $\mathcal{H}$ will be a Killing horizon.*
- *Given an asymptotically flat stationary and axisymmetric black hole solution, we say that a periodic generalized stationary and axisymmetric black hole solution is its periodic analog if the local properties of the horizon can be described by the same parameters used in the asymptotically flat case.*

As shown in [23], the periodic Schwarzschild solution (1.14) is asymptotically Kasner-like. More recently, in [48] it was shown that an axisymmetric solution which is asymptotically Kasner-like and has the topology of an MKN solution, *is* an MKN solution. In the next chapter, we define a solution that is *asymptotically a Lewis model* after reviewing the derivation of those models. These models will characterize the asymptotic behavior of the periodic Kerr analogs.

2.4.4 The coordinate ρ

The Weyl-Papapetrou method relies on taking the function ρ, which is a density (recall it is the "area" density of the transverse surfaces spanned by $\{\partial_t, \partial_\phi\}$), as a coordinate. This implies, in particular, that the first hypothesis on ρ is the absence of critical points. Besides the absence of critical points, one also expects that the limit

$$\lim_{d(p,\partial\mathcal{S})\to+\infty} \rho(p) = +\infty,$$

should be satisfied, where d is the metric distance from an interior point p to the boundary $\partial\mathcal{S}$. In the first equation in (2.13) we see that ρ is a harmonic function on $\mathcal{N}$, and therefore one has to consider the possible topological obstructions for the desired properties for ρ. Below, we discuss the differences that arise when considering asymptotically flat and periodic cases.

Asymptotically flat case

When $(\mathcal{M}, g)$ is an asymptotically flat solution(2.11), we are imposing asymptotic boundary conditions on the decay of the fields,

$$\eta d\phi^2 + \frac{1}{\eta}\mathfrak{q} \to (1 + \frac{2m}{r})\delta, \quad (r \to \infty),$$

where r is the Euclidean distance and δ is the Euclidean metric for some coordinates on each connected component outside a compact set on $\mathcal{N}$. In particular, we can rescale the modulus of the stationary Killing field χ such that $V \to 1$ as $r \to \infty$. The asymptotically flat condition imposes a topological condition on the manifold $(\mathcal{N} \setminus \mathcal{A})/SO(2)$, i.e., that it is simply connected outside $\{\rho = 0\}$. Therefore it is diffeomorphic to $((0, +\infty) \times \mathbb{R})$.

By inspecting (2.21), we obtain that ρ is asymptotically equal to the distance between $\mathcal{A}$ and a point $(\rho, z) \in \mathcal{S}$, as can be seen directly from

$$\int_l e^{\gamma} dl \approx \rho(x^2, x^3) + O(1),$$

for $r \to \infty$, where l is a path along $\hat{\nabla}\rho$, joining $(x_0^2, x_0^3) \in \mathcal{A}$ with (x^2, x^3). This means that we can take a (simply connected) region $R = \{0 < \rho < \rho_0\}$, with ρ_0 large enough, such that ∂R consists of two nonclosed curves. The distance between the curves is approximately ρ_0. By Riemann's Mapping Theorem, there exists a conformal map from R to the strip $0 < Re(x + iy)) < \rho_0$, where $x = x(x^2, x^3)$ and $y = y(x^2, x^3)$. By the conformal invariance of the Laplacian in two dimensions, we obtain that $\rho(x + iy)$ is also harmonic. Therefore, $x \equiv \rho$, and ρ has no critical points for all values $\rho > 0$.

This guarantees that (ρ, z) can be taken as coordinates for the metric, allowing the Weyl-Papapetrou method to work.

Periodic case

In the periodic solutions, Definition 2.13, the surface $(\mathcal{N} \setminus \mathcal{A})/SO(2)$ is still a simply connected manifold. Nevertheless, the previous analysis fails to provide a clear relation between ρ and the distance to the axis computed from γ. As we will see, the periodic setup introduces several subtleties that make the analysis challenging.

Taking the quotient by the discrete symmetry $z \mapsto z + L$, we obtain a *new* manifold that is not simply connected and has the topology of a cylinder. Since ρ is a harmonic function, there are general techniques on stationary spacetimes that we can use from [48] to show that the function is unbounded and does not have any critical points (see section 3.2 for detailed proof).

Moreover, once we have a well-suited coordinate, there is no guarantee to have a *solution* complete at infinity! This also has to be considered when studying the possible asymptotic models. Some Lewis' models cannot be extended to infinity (see section 5.3) in the case of stationary solutions in periodic topology.

2.4.5 Residual Gauge Freedom

The choice of Weyl-Papapetrou coordinates has a residual gauge freedom, usually fixed by the boundary conditions when solving (2.10) and (2.11). This residual gauge is also related to a scale transformation of the coordinates that preserves the form of (2.16). We explain both below.

- First, equations (2.17) and (2.18) contain an arbitrary scale to fix. Given $\lambda \in \mathbb{R}$, the scaling

$$\eta \to \lambda^2 \eta, \quad \omega \to \lambda \omega, \tag{2.24}$$

  leaves invariant the equations. Going back to the relations (2.19), we have that

$$\rho \to \lambda \rho, \quad z \to \lambda z, \quad W \to \lambda W, \quad V \to V,$$

  and therefore $t \to \lambda t$ and $\gamma \to \gamma + 2 \ln \lambda$. These transformations imply a rescaling of the metric

$$g \to g = \lambda^2 \left(-V dt^2 + 2W dt d\phi + \eta d\phi^2 + \frac{e^{2\gamma}}{\eta} (d\rho^2 + dz^2) \right)$$

  Observe that this is an actual rescaling of the metric: we are changing the physical metric.

- Second, given $\lambda > 0$ and a solution (η, ω), the coordinate transformation

$$\bar{t} = t/\lambda, \quad \bar{\rho} = \lambda \rho, \quad \bar{z} = \lambda z, \tag{2.25}$$

  allows to define $(\bar{\eta}, \bar{\omega})$ as

$$\bar{\eta}(\rho, z) = \eta(\bar{\rho}, \bar{z}), \quad \bar{\omega}(\rho, z) = \omega(\bar{\rho}, \bar{z})$$

  where $(\bar{\eta}, \bar{\omega})$ are solutions to (2.17) and (2.18) with respect to the coordinates $(\bar{\rho}, \bar{z})$. Then,

$$\Omega \to \lambda W, \quad V \to \lambda^2 V, \quad \gamma \to \gamma - 2 \ln \lambda,$$

  and the form of the metric does not change,

$$g \to g.$$

  Then, the transformation (2.25) is a residual gauge in the sense that it does not change the solution.

In the next section, we define the periodic stationary and axisymmetric black hole data. They will be characterized with four parameters, relying on Weyl-Papapetrou coordinates. We will show how the residual gauge affects those quantities and construct *gauge invariant* parameters based on the transformation laws for the residual gauge (2.25).

2.5 Stationary and axisymmetric data on the cylinder

In order to have a well-posed problem, in this section we present the periodic stationary and axisymmetric data that we are using in the rest of the work.

2.5.1 Change of variables to (σ, ω) and reconstruction of the metric

Consider $(\mathcal{M}, g)$ a periodic stationary and axisymmetric black hole solution. Let $\mathcal{S} = (\mathcal{M} \setminus \mathcal{A})/(\mathbb{R} \times SO(2))$ be the quotient manifold of $\mathcal{M}$ by the orbits of both the stationary and the axisymmetric Killing vectors.

Let $\sigma := \ln \eta - 2 \ln \rho$. Then, in view of (2.10) and (2.11), $\sigma, \omega : \mathcal{S} \to \mathbb{R}$ satisfy the following equations,

$$\Delta_\rho \sigma = -\frac{e^{-2\sigma}}{\rho^4} |\nabla \omega|^2, \tag{2.26}$$

$$\Delta_\rho \omega = 2 \langle \nabla \omega, \nabla(\sigma + 2 \ln \rho) \rangle , \tag{2.27}$$

where ω is not actually defined in $\mathcal{S}$ but in its universal cover. Observe that the metric on $\mathcal{N}$ can be written as,

$$h = e^{\sigma} \left(\rho^2 d\phi^2 + e^{2q} \left(d\rho^2 + dz^2 \right) \right),$$

where,

$$q = \gamma - \ln \rho - \sigma,$$

is the solution to the quadratures (2.22). By a conformal change in the two-dimensional metric in $\mathcal{S}$, by the coefficient e^{σ}, the new metric on $\mathcal{S}$ is given by

$$\mathfrak{q}_W = e^{2q}(d\rho^2 + dz^2).$$

Both metrics $\mathfrak{q}_W$ and $\mathfrak{q}$ are useful in distinct contexts. For example, $\mathfrak{q}_W$ contains the information about the struts at the axisymmetry axis, while $\mathfrak{q}$ contains the information regarding the horizon area. For our purposes, $\mathfrak{q}$ is more suitable since it comes from the axisymmetric decomposition.

2.5.2 Periodic stationary and axisymmetric data

Unless mentioned otherwise, we work in Weyl-Papapetrou coordinates. First, we need to define the position of the horizons and the parameters that define them.

Definition 2.14. *On the surface $\mathcal{S} = \mathbb{R}^+_{0,\rho} \times S^1_z$, given the parameters $(\{m_i\}_{i=1}^N, \{z_i\}_{i=1}^N)$, with $m_i > 0$, a horizon is the union of the sets,*

$$H_i := \{\rho = 0, -m_i \leq z - z_i \leq m_i\},$$

and we call it an admissible horizon if

$$H_i \cap H_j = \emptyset \quad \forall i \neq j.$$

The axis $\mathcal{A}$ is the following set

$$\mathcal{A} = \bigcup \mathcal{A}_i, \quad \mathcal{A}_i = \{\rho = 0, z_i + m_i \leq z \leq z_{i+1} - m_{i+1}\}.$$

The poles of each connected component are $\{S_i := z_i - m, N_i := z_i + m_i\} (= H \cap \mathcal{A})$.

The parameter L will denote the coordinate length of the factor S^1_z, i.e.,

$$L = \int_{S^1_z} 1 dz.$$

The boundary conditions presented in the following definition are a direct consequence of Definition 2.9.

Definition 2.15. *We call $(\mathcal{S}, \mathfrak{q}, \sigma, \omega)$ a periodic stationary and axisymmetric black hole data with parameters $(\{m_i\}_{i=1}^N, \{z_i\}_{i=1}^N, L, \{A_i\}_{i=1}^N, \{J_i\}_{i=1}^N)$, provided the following conditions hold:*

- *$H = \bigcup_i \{\rho = 0, -m_i \leq z - z_i \leq m_i\}$ is an admissible horizon.*
- *The boundary conditions at $H \setminus (H \cap \mathcal{A})$ are*

$$\rho \partial_\rho \sigma \to 2, \quad \partial_\rho \omega = 0,$$

- *Regularity at the axis and angular momentum of each horizon,*

$$\text{at } \mathcal{A}: \quad \partial_\rho \sigma = 0, \quad \omega = c_i,$$

  where j labels each connected component of $\mathcal{A}$ and $\frac{1}{8}(c_i - c_{i-1}) = J_i$.

- *The metric $\mathfrak{q}$ is given by*

$$\mathfrak{q} = e^{2\gamma}(d\rho^2 + dz^2),$$

  with $\gamma = q + \ln \rho + \frac{1}{2}\sigma$, and q satisfying (2.22) and boundary condition $q\,|_{A_1} = 0$.

- *Area at each connected component of the horizon,*

$$Area(H_i) := 2\pi \int_{H_i} e^\gamma dz = A_i.$$

From the periodic stationary and axisymmetric black hole data, we can construct a periodic stationary and axisymmetric black hole solution, as presented in Definition 2.4 as follows,

- Consider the manifold

$$\mathcal{N} = \mathcal{A} \cup (S^1 \times (\mathcal{S} \setminus \mathcal{A})),$$

  with the metric $h = \eta d\rho^2 + \frac{1}{\eta}\mathfrak{q}$, with $\eta = \rho^2 e^\sigma$.

- Let $\Omega : \mathcal{S} \to \mathbb{R}$ be a solution to(2.20). We define the *angular velocity* of the horizon as $\Omega\,|_{\mathcal{H}_i}$, and denote is as $\Omega_{\mathcal{H}_i}$,
$$\Omega_{\mathcal{H}_i} := \Omega\,|_{\mathcal{H}_i}\,.$$
- Let $\mathcal{M} = \mathcal{N} \times \mathbb{R}_t$ and g as in (2.16).
- Then, by the definition of the periodic stationary and axisymmetric black hole data,
$$\partial\mathcal{N} = H,$$
and $\chi = \partial_t + \Omega_H \partial_\phi$ is a null generator of the horizon. The temperature at each horizon will be denoted κ_i.

We can construct a periodic stationary and axisymmetric black hole solution from the 2-dimensional data by this procedure. Observe that the prescribed singular behavior of σ at the horizons H_i arises by imposing that the lapse function N for the metric (2.16) vanishes on the horizon,
$$\begin{cases} 0 = N\,|_{\partial\mathcal{N}} & = & e^{-\sigma/2}\,|_{\partial\mathcal{N}} \\ \eta\,|_{\partial\mathcal{N}^\circ} & > & 0 \end{cases} \quad \Rightarrow \quad \rho\partial_\rho\sigma\,|_{\partial\mathcal{N}} \to 2.$$

We will consider reflection symmetries on the data, allowing us to show the regularity of the metric at the axis.

Definition 2.16. *Given a periodic stationary and axisymmetric black hole data $(\mathcal{S}, \mathfrak{q}, \sigma, \omega)$ with parameters $(\{m_i\}_{i=1}^N, \{z_i\}_{i=1}^N, L, \{A_i\}_{i=1}^N, \{J_i\}_{i=1}^N)$, we call it $z-$even if*
$$\sigma(z) = \sigma(-z), \quad \omega(z) = -\omega(-z),$$
and $z-$odd if
$$\sigma(z) = \sigma(-z), \quad \omega(z) = \omega(-z),$$

When we have an even number of black holes, a $z-$even data imposes certain constraints on the parameters,
$$m_i = m_{N-i+1}, \quad z_i = L - z_{N-i+1}, \quad A_i = A_{N-i+1}, \quad J_i = J_{N-i+1},$$
while $z-$odd data impose the other sign constraint on the J's,
$$m_i = m_{N-i+1}, \quad z_i = L - z_{N-i+1}, \quad A_i = A_{N-i+1}, \quad J_i = -J_{N-i+1}.$$
When the number of horizons is odd, only $z-$even data for non-vanishing J's can be defined since $z-$odd would imply $J = 0$ for the central horizon.

The previous definitions are in terms of *gauge-dependent* parameters. To see this, recall definition (2.25). Under such a transformation, observe that
$$m_i \to \lambda m_i, \quad L \to \lambda L, \quad A \to A, \quad \kappa_i \to \lambda\kappa_i, \quad J \to J.$$

Therefore, while A and J are invariant under the residual gauge transformation, m_i, L, κ_i are not invariant. Nevertheless, the quotients m_i/L and κ_i/L are invariant. With this in mind, we will denote the parameters $(\{m_i\}_{i=1}^N, \{z_i\}_{i=1}^N, L)$ simply as

$$(\{m_i/L\}_{i=1}^N, \{z_i/L\}_{i=1}^N)$$

which are gauge-independent. Of course, the physical meaning of these parameters is hidden within the distorted Weyl-Papapetrou coordinates.

We are interested in the case of one horizon, $N = 1$. All we need are three parameters, $(m/L, A, J)$ (taking $z_1 = 0$), to define the data. The statement of Problem 1.1 can be rewritten as follows.

Problem 2.1. *Prove that there is a $z-$even periodic stationary and axisymmetric black hole data $(\mathcal{S}, \mathfrak{q}, \sigma, \omega)$ with parameters $(m/L, A, J)$, where σ and ω satisfy equations (2.26) and (2.27), $\mathfrak{q}$ is given by*

$$\mathfrak{q} = e^{2\gamma}(d\rho^2 + dz^2),$$

with γ given by the quadratures (2.21), the area of the horizon is A and the angular momentum of the solution is J.

Remark 2.1. *As the Introduction discusses, the gauge freedom can be fixed by fixing κ to some arbitrary value. In order to compare with the asymptotically flat Kerr solution, we chose $\kappa = \kappa_{Kerr}$, with κ_{Kerr} the surface gravity of a Kerr black hole with parameters (A, J). This is what we call horizon gauge.*

2.5.3 Angle defects: struts

Proposition 2.4. *Given a periodic stationary and axisymmetric black hole data $(\mathcal{S}, \mathfrak{q}, \sigma, \omega)$ with parameters $(\{m_i/L\}_{i=1}^N, \{z_i/L\}_{i^1}^N, \{A_i\}_{i=1}^N, \{J_i\}_{i=1}^N)$ such that*

- *is $z-$even or $z-$odd,*
- *$m_i/L = m/L$ for all i,*
- *$A_i = A$ for all i,*
- *the horizons are equidistant: $(z_{i+1} - z_i)/L = 1/N$,*
- *$|J_i| = J$ for all i,*

then $q = 0$ at the axis.

Proof. The quadratures for q are (2.22), and a simple inspection of these equations shows that q is constant on each axis component. We will show below that if $q(0, L/2) = 0$ then $q(0, -L/2) =$

0. By periodicity q would be 0 on $\mathcal{A}_+$ and $\mathcal{A}_-$. Adding $-\ln 2$, we obtain angle defect 0 everywhere. Now, the integral of the closed 1-form

$$\left(\frac{\rho}{4}((\partial_\rho\sigma)^2-(\partial_z\sigma)^2)+\frac{\rho}{4\eta^2}((\partial_\rho\omega)^2-(\partial_z\omega)^2)\right)d\rho+\frac{\rho}{2}(\partial_z\sigma\partial_\rho\sigma+\frac{1}{\eta^2}\partial_z\omega\partial_\rho\omega)dz$$

on the segment from $(1, L/2)$ to $(1, -L/2)$ is zero by the symmetries of σ and ω. Also by these symmetries, the integral on the segments $[0,1]\times\{L/2\}$ and $[0,1]\times\{-L/2\}$, oriented in the same direction are equal. Therefore, the integral on the three consecutive intervals is zero, so $0 = q(L/2) = q(-L/2)$.

On the other hand, we can go from $q(0, L/2) = 0$ to $q(0, -L/2) = 0$ via a path with contributions surrounding the poles of each horizon at $z_i \pm m$. These contributions cancel in pairs of consecutive poles by virtue of the symmetries on σ and ω. □

2.6 Komar integrals and Smarr Formula

In this section, we review the Komar integrals (e.g., [25,40]). These integrals are related to the concept of *charge* in a pure gauge theory, [65], which is the case of gravitation in general relativity. When considering families of solutions with symmetries, such as in the case of stationary axisymmetric spacetimes, these charges simplify and give an expression on a codimension two spacelike surface.

Consider $(\mathcal{M}, g)$ a stationary and axisymmetric solution. Given a 2-dimensional surface $\Sigma \subset \mathcal{M}$ and a Killing vector ξ, we can define a conserved quantity, called the *Komar integral* associated to Σ and ξ, as follows,

$$Q_\xi(\Sigma) = \frac{1}{16\pi}\int_\Sigma *d\xi,$$

where we are taking the Hodge dual operator associated with the metric g on M. We say that $Q_\xi(\Sigma)$ is conserved in the following sense. By the Killing vector equation, one can show that any two surfaces Σ, Σ' forming the boundary of a region $\Omega \subset \mathcal{N} \subset \mathcal{M}$ satisfy

$$Q_\xi(\Sigma) = Q_\xi(\Sigma').$$

2.6.1 Mass and Angular Momentum

The *mass* of the solution, which we will denote by M, is the Komar integral for the stationary Killing vector,

$$M := \frac{1}{4\pi}\int_\Sigma \epsilon_{\mu\nu\alpha\beta}\nabla^\alpha(\partial_t)^\beta. \tag{2.28}$$

In Weyl-Papapetrou coordinates, this expression results in,

$$M = -\frac{1}{4}\int_\ell \left(\rho\partial_\rho\sigma - \Omega\partial_z\omega\right)d\ell, \tag{2.29}$$

where $\ell \subset \mathcal{S}$ is some path on the surface $\mathcal{S}$ which is either closed or has its endpoints on the set $\{\rho = 0\}$. As an example, for the Schwarschild solution,

$$M = m,$$

and for Kerr solutions, it results in

$$M = \sqrt{m^2 + \sqrt{m^4 + 4J^2}}/\sqrt{2}.$$

In the periodic setup, we can take the quotient by $z \mapsto z + L$. Then, when computed on this quotient manifold, the Komar mass is a finite conserved quantity. For example, for the MKN solution,

$$M = \frac{\alpha L}{4},$$

where L is the coordinate periodic length and α is the Kasner exponent, cf. (1.15). We establish, therefore, the relation between M/L and the Kasner asymptotic.

The Komar integral for the rotational Killing vector, ∂_ϕ in our case, gives the total angular momentum associated to the selected surface,

$$Q_{\partial_\phi}(\Sigma) = \frac{1}{16\pi}\int_\Sigma \epsilon_{\mu\nu\alpha\beta}\nabla^\alpha(\partial_\phi)^\beta.$$

Let us compute this quantity in Weyl-Papapetrou coordinates for one horizon. By the Stokes Theorem, on a curve $\mathcal{C}$, generating a surface of revolution Σ that intersects the axis twice at $(0, z_1)$ and $(0, z_2)$, we obtain

$$Q_{\partial_\phi}(\Sigma) = \frac{1}{8}(\omega(0, z_2) - \omega(0, z_1)).$$

Then, the total angular momentum on Σ is given by $J = \frac{1}{8}(\omega(0, z_2) - \omega(0, z_1))$. This is consistent with our definition of boundary conditions for ω, Definition 2.15.

2.6.2 Area and surface gravity of the horizon

The area and the surface gravity of a horizon are subtly related to the Weyl-Papapetrou coordinates. In physical terms, the surface gravity of a horizon is conjugated to the definition of time scale (via the transformation $\chi \to \lambda^{-1}\chi$ and (1.12)), and therefore makes sense *globally* only when fixing the residual gauge. The usual case is in asymptotically flat spacetimes, where one can impose that the stationary Killing vector field has asymptotically norm -1 (see discussion in chapter 1). In the case of a stationary axisymmetric solution admitting the Weyl-Papapetrou form, (2.16), we have (cf. (2.5))

$$|\nabla\ell|^2_{\mathcal{H}} = \left.\frac{e^{\sigma-2\gamma}\left(-4\rho^2\eta^2 + \rho\eta^4\rho|\nabla\Omega|^2 - \rho^4|\nabla\eta|^2 + 4\rho^3\eta\partial_\rho\eta\right)}{2\eta^3}\right|_{\mathcal{H}}.$$

Since $|\nabla\Omega|^2 = \frac{\rho^2}{\eta^4}|\nabla\omega|^2$, and $\nabla\eta = 2\rho e^{\sigma}\nabla\rho + \rho^2 e^{\sigma}\nabla\sigma$, the expression for the horizon temperature is ,

$$\kappa^2 = \left(e^{-2\gamma}\rho^2\left(\frac{1}{2}\frac{|\nabla\omega|^2}{\eta^2} - |\nabla\sigma|^2\right)\right)\Big|_{\mathcal{H}}. \tag{2.30}$$

By the boundary conditions at the horizon for σ and ω from Definition 2.15, and from Proposition 2.3, we have,

$$\kappa = e^{-\gamma_{\mathcal{H}}}. \tag{2.31}$$

This is inversely proportional to the area of the horizon in Weyl-Papapetrou coordinates: consider the area element from (2.16), for the ϕ, z surface resulting from the horizon. Then,

$$A = \int_{-m}^{m}\int_{0}^{2\pi} e^{\gamma_{\mathcal{H}}} dz d\phi = 4\pi m e^{\gamma_{\mathcal{H}}} = \frac{4\pi m}{\kappa}, \tag{2.32}$$

which is a nontrivial consequence of the coordinate choice.

Remark 2.2. *One of the advantages of Weyl-Papapetrou coordinates is that the product of κA is exactly $4\pi m$, simplifying the implementations of the numerical methods. If we fix κ via the horizon gauge, then $\gamma_{\mathcal{H}}$ is fixed. This, in turn, fixes the area via the relation (2.32) between A and m.*

2.6.3 Smarr formula

For stationary and axisymmetric spacetimes, the Smarr formula relates the evaluation of the Komar mass integral at two different surfaces: one in the asymptotic limit $\rho \to +\infty$ and the other in the limit approaching the horizon. Famously, [40], this formula was introduced in the context of black hole thermodynamics.

Here, we show a more straightforward derivation on Weyl-Papapetrou coordinates for a periodic stationary and axisymmetric solution. Staring in (2.29), consider the limit $\ell \to \{\rho = 0\}$

$$M = -\frac{1}{4}\lim_{\rho^*\to 0}\int_{\mathcal{C}_{\rho^*}} \left(\rho\partial_\rho\sigma - \Omega\partial_z\omega\right) d\ell,$$

where $\mathcal{C}_{\rho^*} = \{\rho = \rho^*\}$. Then, by the boundary conditions in Definition 2.15,

$$M = \sum_i m_i + 2J_i\Omega_{\mathcal{H}_i}.$$

This equation is the periodic analog to the so-called *Smarr formula* in the case of asymptotically flat spacetimes. By equation (2.32), we can give a gauge-independent meaning to the terms m_i,

$$M = \sum_i \frac{\kappa_i A_i}{4\pi} + 2J_i\Omega_{\mathcal{H}_i}. \tag{2.33}$$

2.7 Mass functional and regularization of the energy

In this section, we review the definition of *mass functional*. This integral is related to the Komar mass and the ADM mass in the asymptotically flat case and, in general, to the energy of the harmonic map. The mass functional integral is given by (see, e.g., [66, 67]),

$$\mathcal{M}_{\mathcal{D}}(\sigma,\omega)=\frac{1}{32\pi}\int_{\mathcal{D}}|\nabla\sigma|^2+\frac{1}{\eta^2}|\nabla\omega|^2dS$$

where $\mathcal{D}\subset\mathbb{R}^3$ is some domain. Observe that this function is proportional to the energy of the harmonic map (2.6) up to a boundary term. Indeed, we have that

$$\begin{aligned}E(\eta,\omega) &= \int_{\mathcal{D}}(|\nabla\sigma|^2+|\nabla\ln\rho|^2+2\langle\nabla\sigma,\nabla\ln\rho\rangle)+\frac{1}{\eta^2}|\nabla\omega|^2dvol\\ &= \mathcal{M}_{\mathcal{D}}(\sigma,\omega)-\oint_{\partial\mathcal{D}}(2\sigma+\ln\rho)\nabla_n\ln\rho dS.\end{aligned}$$

The Euler-Lagrange equations are the same since the difference is a boundary term. The main point of this procedure is that it can be done with any harmonic function, as in the deduction of the Smarr formula. The following lemma can be found in [66], Section 3.

Lemma 2.1. *Let $h:\mathcal{D}\to\mathbb{R}$ be a harmonic function. Then, if $\eta=e^{x+h}$,*

$$E(\eta,\omega)=\mathcal{M}_{\mathcal{D}}(x,\omega)-\oint_{\partial\mathcal{D}}(2x+h)\nabla_n h dS.$$

The previous lemma allows us to take any harmonic function at our disposal and relate it to the energy of the harmonic map.

Chapter 3

A priori estimates in the asymptotic region

This chapter studies the asymptotic behavior of the possible solutions to Problem 1.1. First, in section 3.1, we review the curvature estimates in Anderson's and Reiris' works [56,57]. These estimates translate to bounds for the decay of the main functions that we are interested in, namely, η, σ and ω. In section 3.2, we show that the Weyl-Papapetrou coordinate ρ can be considered a global coordinate because it is unbounded and does not possess critical points. Similar to those obtained in [47,48], these results are shown here in the context of stationary solutions. We also construct a divergent sequence of points, which will be important in the next chapter. Finally, in section 3.3, we review Lewis' models for the T^2-symmetric asymptotic behaviors by assuming $z-$independence of the stationary axisymmetric solutions. By computing the Smarr formula for such models, we obtain a heuristic idea of the non-existence result that will be proven in the next chapter.

3.1 Anderson's and Reiris' estimates

In this section, we give a short review of the curvature estimates given by Anderson [56] and Reiris [57]. We start with the classic estimates for the Riemann and Ricci tensors, deduced for a broad family of stationary solutions of the vacuum Einstein Equations. Then we move to the *Backry-Émery Ricci tensor*, a generalization of the Ricci tensor that shares many of its properties when dealing with non-negative curvature manifolds [68]. These results can be used to deduce an a priori estimate for the Weyl-Papapetrou coordinate ρ in many contexts (e.g., in electrostatic and axisymmetric solutions [69]).

3.1.1 Curvature estimate

Consider the metric (2.2), and take $x^4 \equiv t$, $\chi \equiv \partial_t$. The norm of χ will be denoted as $-u^2$. Then

$$g = -u^2(dt + \Phi)^2 + \frac{1}{u^2}h. \tag{3.1}$$

By comparing the metric coefficients of g with the metric coefficients of the metric in (2.16), observe that the function u^2 is exactly V. The 1-form dual to χ is given by

$$\underline{\chi} = -u^2(dt + \Phi),$$

where we use $\underline{\cdot}$ as a symbol of 1-form associated with a vector via the metric g. The twist of χ is given by

$$\theta^{\chi} = \frac{1}{2} * (\underline{\chi} \wedge d\underline{\chi}).$$

Let ϕ be the twist potential associated with θ^{χ}. The reduction of (2.1) to equations in u, the twist and the 3-dimensional Ricci tensor of $\mathcal{N}$ can be done straightforwardly. The resulting equations are

$$\Delta_h u = -\frac{2}{u^3}|\nabla\phi|^2 \tag{3.2}$$

$$\Delta_h \phi = 3\langle \nabla\phi, \nabla \ln u\rangle \tag{3.3}$$

$$\mathrm{Ric}(h) = \frac{1}{u}\nabla\nabla u + \frac{2}{u^4}(\nabla\phi\nabla\phi - |\nabla\phi|^2 h) \tag{3.4}$$

We remark that if we restrict to axisymmetric solutions, the existence of a transverse Riemannian 2-surface allows for a simplification of the equations for (u, ϕ), which are equivalent to those for (η, ω), (2.3), (2.4) and (2.5).

Here we briefly comment on this equivalence. First, having a harmonic function, ρ, present in the axisymmetric case is vital for implementing the Weyl-Papapetrou method. Second, the quotient manifold of $\mathcal{M}$ by the orbits of the axisymmetry generator (i.e., by S^1) is diffeomorphic to $\mathbb{R}^+ \times \mathbb{R} \cup \mathcal{A}$ or $\mathbb{R}^+ \times S^1 \cup \mathcal{A}$, depending on the topology chosen. The periodic topology stated in 1.1 is the latter in our particular case. Third, the relation between the twists θ^{ξ} and θ^{χ} can be directly obtained in Weyl-Papapetrou coordinates from the relation between $\Phi = Ad\phi$ and Ω, see Appendix A,

$$A = \frac{\eta^2\Omega}{\eta^2\Omega^2 - \rho^2}.$$

Anderson's estimates are written in terms of u and the twist potential ϕ for θ^{χ}, instead of η and ω. The validity of those estimates is whenever $u > 0$, which is the region outside the ergo-region (recall that the ergo-region is where $V \leq 0$). Next, we define orbit data for stationary solutions. We use Definition 2.15 given in chapter 2.

Definition 3.1. *Stationary orbit data.*

We say that (N, h, u, ϕ) is a stationary orbit data for a stationary solution (M, g) if they satisfy $u > 0$, (3.2), (3.3) and (3.4).

The following result can be found in [56], and states a general bound for the curvature tensor of the manifold (M, g).

Theorem 3.1. *Anderson Estimates I*

There is a constant $K < \infty$ such that if (M, g) is any chronological stationary vacuum solution (not necessarily geometrically complete), then

$$|Rm|[p] \leq \frac{K}{dist_N^2([p], \partial N)},$$

where $K > 0$ a constant, Rm is the curvature tensor of g, $[p]$ is the Killing orbit through $p \in M$ and $dist_N$ is the distance in the quotient manifold. The constant K is independent of the data (M, g).

A stronger result, given in section 3 of the same work [56], states a bound for the Ricci curvature.

Theorem 3.2. *Anderson Estimates II*

Let (M, g) be a stationary vacuum solution, with orbit data (N, h, u, ϕ), and $U \subset\subset N$ a domain with smooth boundary, so that $u > 0$ on $\bar{U}$. Then there is an (absolute) constant $K < \infty$, independent of (M, g) and U, such that for all $p \in U$

$$|Ric|(p) \leq \frac{K}{dist^2(p, \partial N)},$$

where Ric is the Ricci tensor of g_N, the constant K is independent of the data (M, g).

The previous result is particularly useful when the structure of the Ricci tensor is like the one we are interested in, (3.4). In that sense, we can immediately obtain a priori estimates for u and ϕ.

Corollary 3.1. *Let (M, g) be a stationary vacuum solution, with orbit data (N, h, u, ϕ), on the same hypothesis as in the previous theorem,*

$$|\nabla \ln u|(p) \leq \frac{K}{dist(p, \partial N)}, \qquad \frac{|\nabla \phi|}{u^2}(p) \leq \frac{K}{dist_N(p, \partial N)}$$

3.1.2 Backry-Émery-Ricci tensor and its properties

We want to translate the bounds in Corollary 3.1 to the variables (η, ω). Observe that the 2-dimensional Ricci tensor $\mathrm{Ric}(\mathfrak{q})$ is given by (2.13)

$$\mathrm{Ric}(\mathfrak{q}) = \frac{1}{2\eta^2}(\nabla\eta\nabla\eta + \nabla\omega\nabla\omega) + \frac{\nabla\nabla\rho}{\rho},$$

where recall that the first term is $\mathrm{Ric}(h)$ (equation (2.5)). Upon defining $f = \ln \rho$, we obtain

$$\mathrm{Ric}(\mathfrak{q}) = \frac{1}{2\eta^2}(\nabla\eta\nabla\eta + \nabla\omega\nabla\omega) + \nabla\nabla f + \nabla f \nabla f, \tag{3.5}$$

Here, observe that f is a harmonic function. This form of the Ricci tensor is known as the *Backry-Émery Ricci tensor*. It plays a crucial role in relating the variables in the usual stationary reduction with the ones arising in the Weyl-Papapetrou reduction.

Definition 3.2. *Given a manifold (N, g_N), if Ric denotes the Ricci tensor associated to g_N,*

- *The β-Backry-Émery Ricci tensor is defined as*

$$Ric_f^\beta := Ric - \nabla\nabla f + \beta\nabla f\nabla f.$$

- *The $f-$Laplacian, denoted by Δ_f, acting on a function r is defined as*

$$\Delta_f r := \Delta r + \langle \nabla f, \nabla r\rangle_{g_N},$$

where Δ is the usual Laplacian with respect to g_N.

As we can see from equation (3.5), the Ricci tensor in $(\mathcal{S}, \mathfrak{q})$ adopts the form of a Backry-Émery-Ricci tensor with $f = \ln\rho$ and $\beta = 0$,

$$\mathrm{Ric}_f(\mathfrak{q}) = \frac{1}{2\eta^2}(\nabla\eta\nabla\eta + \nabla\omega\nabla\omega) + \nabla f\nabla f (= \mathrm{Ric}(\mathfrak{q}) - \nabla\nabla f).$$

Observe that $\mathrm{Ric}_f(\mathfrak{q}) \geq 0$. The following result, which the reader can find as Lemma 3.2.3 in [46] (first presented in [57], although it has been previously known in a different form in [70]) states one of the principal properties of manifolds with positive Ric_f tensor.

Lemma 3.1. *Reiris Estimate*

Given (N, g_N) be a metrically complete Riemannian 3-manifold with $Ric_f^\beta \geq 0$ for some function f and a constant $\beta > 0$. Let ϕ be a non-negative function such that

$$\Delta_f\phi \geq c\phi^2,$$

for some constant $c > 0$. Then, for any $p \in N^\circ$ we have

$$\phi(p) \leq \frac{(36 + 4/\beta)/c}{dist^2(p, \partial N)},$$

3.1.3 Estimates for stationary axisymmetric data

Rewriting equations (2.10), (2.11) and (2.13) in terms of definition 3.2, we have

$$\Delta_f\eta = \frac{1}{\eta}(|\hat{\nabla}\eta|^2 - |\hat{\nabla}\omega|^2) \tag{3.6}$$

$$\Delta_f\omega = \frac{2}{\eta}\langle\hat{\nabla}\omega, \hat{\nabla}\eta\rangle \tag{3.7}$$

$$\Delta\rho = 0$$

$$\mathrm{Ric}_f(\mathfrak{q}) = \frac{1}{2\eta^2}(\nabla\eta\nabla\eta + \nabla\omega\nabla\omega) + \nabla f\nabla f,$$

where $f = \ln\rho$. First, we define the stationary and axisymmetric orbit data. We also define the periodic case using the definition of 2.15 given in chapter 2. Recall that we are not assuming

ρ can be taken as a coordinate. In the next section, we will prove that ρ can be taken as the Weyl-Papapetrou coordinate by showing that it is unbounded and has no critical points.

Definition 3.3. *Stationary and axisymmetric orbit data.*

- *We say that* $(N, h, \eta, \omega, \rho)$ *is a stationary and axisymmetric orbit data for a stationary solution* (M, g) *if they satisfy* (2.10), (2.11) *and* (2.13), *with* $\rho \geq 0$.

- *We say that* $(\tilde{\mathcal{S}}, \mathfrak{q}, \eta, \omega, \rho)$ *is a periodic stationary and axisymmetric orbit data for a stationary solution* (M, g) *if* $(N = (\tilde{\mathcal{S}} \setminus \mathcal{A}) \times S^1 \cup \mathcal{A}, \rho^2 d\phi^2 + \mathfrak{q}, \eta, \omega, \rho)$ *is a stationary axisymmetric orbit data and if there exists* $L > 0$ *such that* $z \mapsto z + L$ *is an isometry of* $\tilde{\mathcal{S}}$. *We usually take the quotient of* $\tilde{\mathcal{S}}$ *by such isometry and denote it as* $\mathcal{S} (= \mathbb{R}^+_0 \times S^1)$, *simply saying that* $(\mathcal{S}, \mathfrak{q}, \eta, \omega, \rho)$ *is a periodic stationary and axisymmetric orbit data.*

- *Finally, we say that* $(\mathcal{S}, \mathfrak{q}, \eta, \omega, \rho)$ *is a* $z-$*even periodic stationary and axisymmetric black hole orbit data if it is a periodic stationary and axisymmetric orbit data, and there is also a compact connected Killing horizon* $H \subset \partial\mathcal{S}$ *such that* $\eta \mid_H > 0$ *and*

$$\begin{aligned} \int_{\partial\mathcal{S}} \rho \nabla_n (\ln \eta) - 2\nabla\rho dl &= \beta' < 0, \quad \liminf_{dist(x,\partial\mathcal{S}) \to +\infty} \left| \int_{\mathcal{C}_{\rho(x)}} 2\rho \nabla_n \ln \eta dl \right| \geq \beta > 0, \\ \omega \mid_{\mathcal{A} \cap \mathcal{H}} = \pm 4J &> 0, \quad \frac{\omega \nabla_n \omega}{\eta^2} \mid_H \geq 0, \quad \int_{\partial\mathcal{S}} \nabla_n \rho dl = \beta'' > 0. \end{aligned}$$

Recall that although ω *is a function on the universal cover* $\tilde{\mathcal{S}}$ *of* $\mathcal{S}$, *we can think of it as a local function in* $\mathcal{S}$.

A straightforward computation shows that the first condition implies that the horizon is non-empty (if one *assumes* that we can proceed with the Weyl-Papapetrou method, it gives $-\beta' = 4m > 0$).

It can be easily checked that the map in the second condition, namely

$$\rho \mapsto \int_{\mathcal{C}_\rho} 2\rho \nabla_n \ln \eta dl, \tag{3.8}$$

is monotonically decreasing (see proof of Lemma 3.2). When evaluating the right-hand side of (3.8) in the limit $\rho \to 0$, it implies non-overlapping horizons (in Weyl-Papapetrou coordinates it is equal to $2L - 4m > 0$).

The third and fourth conditions imply that ω is odd and Ω periodic. The fourth condition also fixes the angular momentum as a non-zero value, $J > 0$. The final condition is rather technical, asserting that χ, ξ are non-vanishing at the horizon (recall that ρ is the transverse area of the orbits generated by $\{\chi, \xi\}$).

Following Reiris in [69], we can extract information from Ric_f such that an a priori estimate for ∇f can be obtained. The following proposition is in the context of stationary and axisymmetric orbit data, a proof of which can be found directly by the Böchner formula, see, e.g., [68].

Proposition 3.1. *Let $(\mathcal{S}, \mathfrak{q}, \eta, \omega, \rho)$ be a periodic stationary and axisymmetric orbit data, where $Ric_f(\mathfrak{q}) \geq 0$, $f = \ln \rho$. Let K be the Gaussian curvature of $\mathfrak{q}$. Then*

$$\Delta_f K \geq K^2,$$
$$\Delta_f |\nabla f|^2 \geq 2|\nabla f|^2.$$

From Proposition 3.1 and Lemma 3.1, we obtain the following estimate for ρ, η and ω.

Proposition 3.2. *There is a constant $C > 0$ such that for any stationary data $(\mathcal{S}, \mathfrak{q}, \eta, \omega, \rho)$ and $p \in \mathcal{S}$, we have*

$$\frac{|\nabla \rho|}{\rho}, \frac{|\nabla \eta|}{\eta}, \frac{|\nabla \omega|}{\eta} \leq \frac{C}{dist(p, \partial \mathcal{N})}.$$

Proof. We follow [69], although the variables here are η and ω. Consider the Bochner formula adapted to the Ric_f. Then, for a function $g : \mathcal{S} \to \mathbb{R}$,

$$\frac{1}{2}\Delta |\nabla g|^2 = |\nabla \nabla g|^2 + \langle \nabla g, \nabla \Delta_f g \rangle + \mathrm{Ric}_f(\nabla g, \nabla g).$$

The first term is always positive. Take $g = f$. Since f is $f-$harmonic, we have

$$\Delta_f \left(|\nabla f|^2 \right) \geq 2|\nabla f|^4,$$

which implies the bound for ρ. Next, we use the harmonic map property of equations (3.6) and (3.7). Consider the map $(\eta, \omega) : \mathcal{S} \to \mathcal{H}$, with energy density

$$\varepsilon = \frac{1}{\eta^2}(|\hat{\nabla} \eta|^2 + |\hat{\nabla} \omega|^2) = 2\mathrm{Ric}_f(\mathfrak{q}) - \nabla f \nabla f.$$

The Bochner formula for such a map is given by (see [68])

$$\frac{1}{2}\Delta_f e = |\nabla dh|^2 + \sum_i (\langle dh(\mathrm{Ric}_f(e_i)), dh(e_i) \rangle) - \sum_{i,j} \mathrm{Rm}^{\mathcal{H}}(dh(e_i), dh(e_j), dh(e_i), dh(e_j)).$$

The last term is non-negative since $\mathcal{H}$ has negative curvature. The second term can be computed directly as

$$dh(e_i) = d\eta(e_i)\partial_\eta + d\omega(e_i)\partial_\omega \in T\mathcal{H},$$

and

$$\mathrm{Ric}_f(e_i) = \sum_j \frac{1}{2\eta^2} \left(d\eta(e_i) d\eta(e_j) e_j + d\omega(e_i) d\omega(e_j) e_j \right) + df(e_i) df(e_j) e_j.$$

Therefore, it is exactly

$$\frac{1}{2\eta^4} \left(|\nabla \eta|^4 + 2 \langle \nabla \omega, \nabla \eta \rangle^2 + \langle \nabla f, \nabla \eta \rangle^2 + |\nabla \omega|^4 \right) \geq \frac{\varepsilon^2}{2}.$$

Then, by Lemma 3.1, we have the following bound for the harmonic map energy

$$\varepsilon \leq \frac{C}{\text{dist}^2(p, \partial\mathcal{N})}.$$

Both bounds follow from here. □

One can prove a similar result also for σ.

Corollary 3.2. *There is a constant $C' > 0$ such that for any stationary and axisymmetric orbit data $(\mathcal{S}, \mathfrak{q}, \eta, \omega, \rho)$ and $p \in \mathcal{S}$, we have*

$$|\nabla\sigma|, \quad e^{-\sigma-2\ln\rho}|\nabla\omega| \leq \frac{C'}{dist(p, \partial\mathcal{N})},$$

for all $p \in \mathcal{S}$.

Proof. The second inequality follows directly from Proposition 3.2. For the first one, we have that

$$|\nabla\sigma| - |2\nabla\ln\rho| \leq |\nabla\ln\eta| \leq \frac{C}{\text{dist}(p, \partial\mathcal{N})},$$

and from the estimate for $|\nabla\ln\rho|$ we obtain the result (we can take $C' = 3C$). □

Remark 3.1. *It can be proved, using recursively the previous bounds and standard elliptic estimates, that*

$$|\nabla^{(k)}Ric|_h(p) \leq \frac{c_k}{dist_h^{2+2k}(p, \partial\mathcal{N})}, \quad |\nabla^{(k)}\nabla\ln\rho|_h^2(p) \leq \frac{c_k}{dist_h^{2+2k}(p, \partial\mathcal{N})}.$$

The reader can find this proof in [46, pp. 19-20]. We will use this extension of the results in chapter 4.

3.2 ρ: the good, the bad *or* the ugly coordinate

This section proves that ρ can be taken as a global coordinate (as in the Weyl-Papapetrou method) for the periodic stationary and axisymmetric black hole orbit data. The numerical study of the problem developed in chapter 6 relies heavily on this result.

Consider a periodic stationary and axisymmetric black hole orbit data $(\mathcal{S}, \mathfrak{q}, \eta, \omega, \rho)$. Since in this section (and in what follows later) we focus on the $\{\rho = cnt\}$ loops, we use the following notation:

- given $\rho^* \in \mathbb{R}^+$, the set $\mathcal{C}(\rho*) \subset \mathcal{S}$ is the loop $\{p \in \mathcal{S}, \quad \rho(p) = \rho*\}$.
- Given a sequence $\{p_i\}_{i\geq 0} \subset \mathcal{S}$, we denote by $\mathcal{C}_i$ the loop $\mathcal{C}(\rho(p_i))$ and by l^i the $\mathfrak{q}-$length of $\mathcal{C}_i$.
- Given two loops ℓ_1 and ℓ_2, we denote the compact region between both loops as $\mathcal{D}_{\ell_1,\ell_2}$.
- The distance $\text{dist}(\mathcal{C}_i, \mathcal{C}_0)$ is denoted by r_i, where p_0 is some reference point at $\{\rho = 0\}$.

Let $\{n, s\}$ be $\mathfrak{q}-$unitary vector fields such that n is normal and s is tangent to $\mathcal{C}(\rho)$, for every $\rho \geq 0$. When scaling the metric by a factor of λ^2, i.e., $\bar{\mathfrak{q}} = \lambda^2 \mathfrak{q}$, the scaled vectors $\{\bar{n}, \bar{s}\}$ satisfy the equations $\bar{n} = n/\lambda$, $\bar{s} = s/\lambda$.

We are using the following Lemma (here adapted to periodic stationary and axisymmetric solutions), which can be found in [48] (a similar result can also be found in [47], section 4). It is a consequence of the Bishop-Gromov collapse theorem.

Lemma 3.2. *Given $(\mathcal{S}, \mathfrak{q}, \eta, \omega, \rho)$ a periodic stationary axisymmetric black hole data with $\rho > 0$. Then, ρ is not uniformly bounded.*

Proof. Let us assume that ρ is uniformly bounded by $\bar{\rho} < \infty$.

First, we show that there is a sequence of (rescaled) annuli $\mathcal{A}_i = \mathcal{A}(2r_i, r_i/2, \mathfrak{q}_{r_i})$ and loops $\ell_i \subset \mathcal{A}_i$, isotopic to $\partial\mathcal{S} \simeq S^1$, such that their $q_{r_i}-$length is uniformly bounded.

Consider the function

$$\frac{A(B(\partial\mathcal{S}, r))}{r^2},$$

where $A(\cdot)$ denotes the area function and $B(\partial\mathcal{S}, r)$ is the set $\{x \in \mathcal{S} : \quad \text{dist}(\partial\mathcal{S}, x) < r\}$. By the Bishop-Cheeger-Gromov theorem ([61], Lemma 36), the limiting value when $r \to +\infty$ is either $\mu = 0$ or $\mu > 0$. We proceed to analyze each case.

- Case $\mu = 0$: any annulus $\mathcal{A}_r = \mathcal{A}(2r, r/2, \mathfrak{q}_r)$ satisfies that its area goes to zero as $r \to +\infty$,

$$\lim_{r\to+\infty} A_{\mathfrak{q}_r}(\mathcal{A}_r) = 0.$$

  From proposition 3.1, we have the bound for the gaussian curvature of $\mathfrak{q}_r$, $\kappa_r = \kappa r^2 \leq C$. Then, since the area goes to zero and the Gaussian curvature is uniformly bounded from above, any sequence of annuli $\mathcal{A}_i = \mathcal{A}(2r_i, r_i/2, \mathfrak{q}_{r_i})$, with $\{r_i\}_i$ a diverging sequence, collapse to a segment with bounded curvature. Then, we can choose a sequence $\ell_i \subset \mathcal{A}_i$ such that their $q_{r_i}-$length tends to zero.

- If $\mu > 0$, then the sequence of annuli $\mathcal{A}_r = \mathcal{A}(2r, r/2, \mathfrak{q}_r)$ converge to the flat annulus as $r \to +\infty$ (in fact a "cone" region due to the angle defect at infinity),

$$\mathcal{A}_{\mathbb{R}^2} = B_{\mathbb{R}^2}(0, 2) \setminus B_{\mathbb{R}^2}(0, 1/2), q_{\mathcal{A}} = dR^2 + \frac{\mu^2 R^2}{\pi^2} d\Theta^2,$$

  with (R, Θ) polar coordinates in $\mathbb{R}^2$. Then, the $\mathfrak{q}$-length growth linearly in r. We can take a sequence ℓ_i of loops such that their $\mathfrak{q}_{r_i}$ is less than or equal to a fixed value $\gamma > 0$.

  Observe that in this case, the Gaussian curvature K over the annuli tend to zero as $r \to +\infty$, since the limit manifold is flat,

$$r_i^2 \left(\frac{|\nabla\eta|^2}{\eta^2} + \frac{|\nabla\omega|^2}{\eta^2} \right) \to 0,$$

which, upon rescaling the metric by r_i, $\mathfrak{q} \mapsto \mathfrak{q}/r_i^2$, results in

$$\left(\frac{|\nabla \eta|^2_{\mathfrak{q}_{r_i}}}{\eta^2} + \frac{|\nabla \omega|^2_{\mathfrak{q}_{r_i}}}{\eta^2} \right) \to 0, \tag{3.9}$$

i.e., the curvature decays *sub-quadratically*.

In both cases, we see that for i large enough, there exist loops $\ell_i \subset \mathcal{A}_i$ (isotopic to $\partial\mathcal{S}$) such that their $q_{r_i}-$length is uniformly bounded. Then, take the sequence $\{\ell_i\}_i$ constructed before and compute the integral

$$0 < \int_{\partial\mathcal{S}} \nabla_n \rho dl = \int_{\mathcal{C}_i} \nabla_n \rho dl < \left| \int_{\mathcal{C}_i} \nabla_n \rho dl \right| \leq \bar{\rho} l^i \frac{C}{r_i},$$

where we use that ρ is harmonic and the previous estimates.

In the case $\mu = 0$, we have that the term $\text{length}_{q_{r_i}}(\ell_i) = \frac{l^i}{r_i}$ goes to zero as $r_i \to +\infty$. Then, $\bar{\rho}$ cannot be finite.

In the case $\mu > 0$, $\text{length}_{q_{r_i}}(\ell_i) = \frac{l^i}{r_i} \leq \gamma$ for some $\gamma > 0$.

Consider the function

$$b(\rho) = \int_{\mathcal{C}_\rho} \rho \nabla_n \ln \eta dl.$$

This function is monotonic, by equation (2.17) and is bounded away from zero by the conditions in Definition 3.3. Then, at each l_i, we have

$$0 < \beta \leq |b(\rho)| \leq \bar{\rho} l^i |\nabla_n \ln \eta| = \bar{\rho} \frac{l^i}{r_i} |\nabla_{\bar{n}} \ln \eta| \leq \bar{\rho}\gamma |\nabla_{\bar{n}} \ln \eta|. \tag{3.10}$$

By (3.9), we have that

$$\left(|\nabla \ln \eta|_{q_{r_i}} + \frac{|\nabla \omega|_{q_{r_i}}}{\eta} \frac{|\omega|}{\eta} \right) \gamma \to 0, \quad (i \to +\infty),$$

and thus, we obtain that the right-hand side in equation (3.10) also goes to zero if $\bar{\rho} < \infty$, which is absurd. □

Proposition 3.3. *Let $(\mathcal{S}, \mathfrak{q}, \eta, \omega, \rho)$ be a periodic stationary and axisymmetric black hole data with $\rho > 0$. Consider a divergent sequence of points $\{p_i\}_{i\geq 0} \subset \mathcal{S}$. Then*

$$\rho(p_i) \to +\infty \quad (i \to +\infty).$$

Proof. Consider the rescaled annuli $\mathcal{A}_i = \mathcal{A}(2r_i, r_i/2, \mathfrak{q}_{r_i})$, where $r_i = \text{dist}(p_i, H)$. Then, from Proposition 3.2, on this annuli it holds that

$$|\nabla \ln \rho|_{\mathfrak{q}_{r_i}} \leq C.$$

Consider now a sequence of loops ℓ_i given by the previous Lemma, and denote the uniform

bound for their $q_{r_i}-$length by L. Take p^i_{min} and p^i_{max} the points on ℓ_i where ρ reaches its minimum and maximum, and let $\gamma_i : I \to \ell_i$ the curve joining these points. Then

$$\ln\left(\frac{\rho(p^i_{max})}{\rho(p^i_{min})}\right) = \left|\int_0^1 \langle \nabla \ln\rho, \gamma'\rangle_{q_{r_i}} dt\right| \leq \left|\int_0^1 |\nabla \ln\rho|_{q_{r_i}} |\gamma'|_{q_{r_i}} dt\right| \leq CL, \tag{3.11}$$

for some constant $C \geq 0$ (observe that in the case $\mu > 0$ in the proof of Lemma 3.2 it is indeed zero).

Let us assume that there is a subsequence $\{p^{i_j}_{min}\}$ such that $\rho(p^{i_j}_{min})$ is uniformly bounded. Then, by (3.11), $\rho(p^{i_j}_{max})$ is uniformly bounded also. By the maximum principle (ρ is harmonic)

$$\max_{\mathcal{D}_{\ell_{i_j},\ell_{i_{j+1}}}} \{\rho\} \leq \max\{\max_{\ell_{i_j}}\{\rho\}, \max_{\ell_{i_{j+1}}}\{\rho\}\},$$

and thus ρ is uniformly bounded, which contradicts Lemma 3.2. Then, $\rho(p^{i_j}_{min}) \to +\infty$ as $j \to +\infty$, and thus $\rho \to +\infty$.

Since $\bigcup_j \mathcal{D}_{\ell_{i_j},\ell_{i_{j+1}}} \subset \mathcal{S}$ covers all except a bounded region, we obtained the result. □

Finally, we will prove that ρ is a *possible* coordinate choice by showing that it has no critical points. This proof is analogous to Proposition 8 in [48, p. 12].

Proposition 3.4. *Let $(\mathcal{S}, \mathfrak{q}, \eta, \omega, \rho)$ be a periodic stationary and axisymmetric black hole data. Then, ρ has no critical points.*

Proof. We know that $\rho \to +\infty$ at infinity and that $\rho\,|_{\partial\mathcal{S}} = 0$. Then, the pre-image of any regular value of ρ is necessarily a finite set of circles. As ρ is harmonic, the maximum principle implies that none of such circles can enclose a disc. Hence, every circle is isotopic to $\partial\mathcal{S}$. If there is more than one circle, then any two of them must enclose an annulus, which is again ruled out by the maximum principle. Thus, the pre-image of any regular value of ρ is a circle isotopic to $\partial\mathcal{S}$. Fix two regular values $0 < \rho_1 < \rho_2$. Let $\mathcal{A}_{12}$ be the annulus enclosed by $\mathcal{C}_{\rho_1}$ and $\mathcal{C}_{\rho_2}$.

Observe that, as ρ is harmonic and analytic, the critical points are isolated and of positive (integer) index (standard argument in the complex plane $x + iy$ around a critical point using Cauchy-Riemann equations) and that, by Poincaré-Hopf, the sum of the index of the critical points in $\mathcal{A}_{12}$ must be zero. As this is valid for any $\rho_1 < \rho_2$, it follows that ρ does not have critical points. □

Given the previous proposition, ρ can be chosen as a global harmonic coordinate with

$$\mathfrak{q} = e^{\gamma}(d\rho^2 + dz^2),$$

where z is the harmonic conjugate of ρ, with period L. In the rest of our work, we use the Weyl-Papapetrou method without explicitly stating it.

Next, we want to provide a divergent sequence where we can take a lower bound for the decay of $\ln\rho$. Over this particular divergent sequence, we can prove a lower bound for the curvature, showing that ρ is indeed a *good* coordinate choice.

Proposition 3.5. *Let $(\mathcal{S}, \mathfrak{q}, \eta, \omega, \rho)$ be a periodic stationary and axisymmetric black hole data. There exists a divergent sequence $\{p_i\}_i$ and $b > a > 0$ such that*

$$\frac{a}{r_i} \leq \left|\frac{\nabla\rho}{\rho}\right|(p_i) < \frac{b}{r_i}.$$

Proof. In this proof, we work on the manifold $\mathcal{N} \simeq S^1_\phi \times (\mathbb{R}^+_{0,\rho} \times S^1_z)$ with metric

$$h = \rho^2 d\phi^2 + e^{2q}(d\rho^2 + dz^2).$$

Consider the function $G : \mathbb{R}^+_0 \to \mathbb{R}$ given by

$$G(\rho) := \int_{\mathcal{C}(\rho)} |\nabla \ln \rho|^2 dA,$$

with $dA = \rho e^q dz \wedge d\phi$ and $\mathcal{C}(\rho)$ the set level set of the function ρ. Since we are in $\mathcal{N}$, the sets $\mathcal{C}(\rho)$ have the topology of a torus. As it was shown in [47], the function G satisfies the inequality

$$\left(\frac{G'}{G}\right)' \geq 0.$$

Then

$$G(\rho) \geq C\rho^{\alpha_1}, \tag{3.12}$$

for some constant C that depends on the value of $G(\rho_0)$ and some $\alpha_1 \in \mathbb{R}$. First, we prove that $\alpha_1 < 0$. If $\alpha_1 \geq 0$

$$0 < G(\rho_0) \leq G(\rho) = \int_{\mathcal{C}(\rho)} |\nabla \ln \rho|^2 dA = 2\pi \int_{S^1_z} |\nabla \ln \rho| dz = 2\pi \left(\int_{\mathcal{C}(\rho)} dz\right) (|\nabla \ln \rho|)\,(p),$$

for some point $p \in \mathcal{C}(\rho)$, since $|\nabla_n \rho| dl = dz$. But then, since $\left(\int_{S^1_z} dz\right) = L$, we have

$$0 < G(\rho_0) \leq L \left(\frac{|\nabla\rho|}{\rho}\right)(p),$$

which implies that $\frac{|\nabla\rho|}{\rho}$ does not go to zero at infinity, contradicting Anderson's theorem.

Next, we prove that there is a sequence $\{p_i\}_i$ as in the thesis of the proposition. Let us assume that there is $\epsilon > 0$ such that for all $s > s_0$

$$\frac{|\nabla\rho|}{\rho} \leq \frac{\epsilon}{s}, \quad \forall \rho > \rho_0. \tag{3.13}$$

By integrating from ρ_0, we have

$$\rho \leq C' s^\epsilon.$$

If this is the case, then

$$C'^{-\alpha_1} \epsilon s^{-\alpha_1 \epsilon - 1} \geq \rho^{-\alpha_1} \frac{|\nabla\rho|}{\rho}. \tag{3.14}$$

Consider the integral

$$F(\rho) := \int_{S^1_z} \rho^{-\alpha_1} \frac{|\nabla \rho|}{\rho} dz,$$

which by (3.12) satisfies

$$F(\rho) \geq C' > 0.$$

By mean value theorem, for each ρ there is p_ρ such that

$$\rho^{-\alpha_1} \frac{|\nabla \rho|}{\rho}\Big|_{p_\rho} \geq C'/L.$$

However, condition (3.14) implies that for every $\epsilon = -\frac{1}{2\alpha_1}$ the right-hand side tends to zero as $s \to +\infty$, while the previous identity shows that it is not the case. Therefore, assumption (3.13) is not true. Then, there exists $a > 0$ and a sequence of points $\{p_i\}$ such that

$$\Big|\frac{\nabla \rho}{\rho}\Big|(p_i) \geq \frac{a}{s(p_i)}.$$

By rescaling, we obtain the desired result. □

3.3 T^2-symmetric solutions

In this section, we provide a derivation of Lewis' asymptotic models for the T^2-symmetric solutions and discuss some of their properties. In particular, we are interested in the Smarr identity for these models.

3.3.1 Solving $z-$independent equations

Assuming an extra symmetry along the $z-$axis implies that the metric coefficients are independent of z. If Ω is independent of z, by means of equations (2.20), ω must be independent of ρ.

Let us define $x := \ln \eta - \ln \rho = \sigma + \ln \rho$. Working with equations (2.26) and (2.27), the $z-$independent case is

$$\frac{d^2}{d\rho^2}x + \frac{1}{\rho}\frac{d}{d\rho}x = -\frac{e^{-2x}}{\rho^2}\Big|\frac{d}{dz}\omega\Big|^2,$$
$$\frac{d^2}{dz^2}\omega = 0.$$

The second equation is immediately solved. The function ω depends linearly on z, so $\omega = wz$ for large values of ρ (we can drop off the constant since only derivatives of ω are involved in the equations). Therefore, the equation to solve under z-independence is

$$\rho^2 \frac{d^2}{d\rho^2}x + \rho \frac{d}{d\rho}x = -e^{-2x}w^2. \tag{3.15}$$

If $w = 0$, then the solution is straightforward:

$$x = \beta + \alpha \ln \rho. \tag{3.16}$$

Then, we re-obtain Kasner static solutions, (2.23). In what follows, we assume $w \neq 0$. We integrate (3.15), and obtain the following equation

$$\left(\rho x'\right)^2 = w^2 e^{-2x} + C.$$

The sign of the constant C is significant in the classification of the solutions. We set $C = \epsilon a^2$, with $a \geq 0$ and $\epsilon = -1, 1$. Letting $U = e^{-x} (:= \rho/\eta)$ and using $\zeta = \ln \rho/\rho_0$, for some $\rho_0 > 0$, we get (we use $\dot{}$ as notation for ∂_ζ)

$$\dot{U}^2 = w^2 + \epsilon a^2 U^2,$$

to obtain, after $\zeta-$derivation[1],

$$\ddot{U} = \epsilon a^2 U.$$

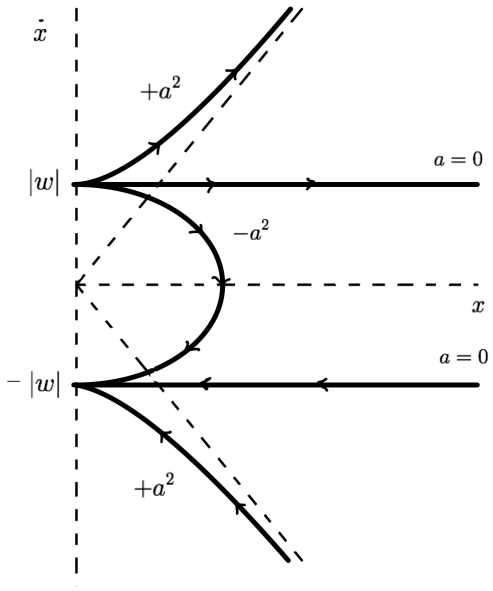

Figure 3.1: Types of $U-$orbits in phase space $(U, \dot{U})$. Those of physical interest are the ones on top $\epsilon = 1$ and $a = 0$.

Let us see the three cases separately.

1. For $\epsilon = -1$,

$$U = \frac{|w|}{a} \sin(\pm a \ln \rho + b),$$

where b is an integration constant. These solutions do not possess clear physical meaning since the sign of η changes infinitely many times as $\rho \to +\infty$.

[1] Recall that $\dot{U} = 0$ and $U = \epsilon w/a$ are not solutions of the original problem.

2. For $a = 0$, we have the following solution

$$U = |w| \left(\pm \ln \rho + d \right)$$

where d is an integration constant. We have two types of solutions. The one corresponding to the minus sign is an *interior* solution since it only exists for $\rho < e^d$, while the solution corresponding to the plus sign is an *exterior* solution, existing for $\rho > e^{-d}$ [2]. Both solutions are related by a $\rho \mapsto \frac{1}{\rho}$ transformation. The metric coefficients for the exterior solution can be calculated straightforwardly,

$$\Omega = \frac{1}{w \left(\ln \rho + d \right)}$$
$$V = \frac{\rho}{\ln \rho + d} \frac{1 - w^4}{w}$$

It is unclear whether this type of solution can be reached or if there is some limit in which they appear. Also, the ergosphere of such a solution can reach infinity if $1 < w^4$. The Kasner exponent is precisely 1; therefore, this solution has the same asymptotic as the Boost solution (up to higher order in ρ).

3. For $\epsilon = 1$ the solution is

$$U = \frac{w}{a} \sinh(\pm a \ln(\rho/\rho_*)), \tag{3.17}$$

where ρ_* is an integration constant. In the limit $\rho \to +\infty$, the plus sign is needed for the solution to exist, whereas the minus sign is the correct one for the existence of the solution in the limit $\rho \to 0$. In this case, we have an "interior" solution and an "exterior" solution, as in the case $\epsilon = 0$. Again, both solutions are related by the symmetry $\rho \mapsto \frac{1}{\rho}$. Observe that for the exterior solution, the function V is given by

$$V = \frac{2a}{w} e^{-b} \rho^{1-a}. \tag{3.18}$$

By inspecting (2.23), the Kasner parameter is $\alpha = 1 - a$.

Observe that not all solutions extend to infinity. Neither those extending to infinity will be physically acceptable since we have a negative Kasner parameter for solutions with $a > 1$.

The three cases presented before are known as *Lewis' models* for stationary spacetimes with cylindrical symmetry. They can also be found as *rotating Kasner* solutions (cf. [53]), a terminology that will be clear in the following subsection.

[2] The names *interior* and *exterior* are not due to some boundary of gluing of the spacetime. They reference whether the solution is complete at infinity or not

Another representation of Lewis' models

As we saw, the case $w = 0$ in the above equations leads to the linear case,

$$x'' + \frac{x'}{\rho} = 0,$$

which is immediately solved by $x = \beta + \alpha \ln \rho$, i.e., a Kasner solution. Next, we are showing a representation of the Lewis' models such that they can be written as a perturbation of the Kasner solutions (2.23). Then, we proceed to show a heuristic by which the limit $w \to 0$ is well defined, in the sense that in that limit, the solutions tend to the Kasner metric. Therefore, we can regard the perturbation as *close* to the static solution. This shows that there is a possibility to find some integral quantity in which the difference can be computed and a notion of *closeness* can be computed.

Let us denote by $\sigma^{K,w}$ the function σ associated with the Lewis model for $w \neq 0$. Then, from (3.17), we have

$$\sigma^{K,w} = \ln\left(\frac{w}{a\rho}\sinh(\pm a\ln(\rho/\rho_*))\right) = \ln\left(\frac{w}{2a\rho_*^a}\right) + (a-1)\ln\rho + \ln\left(1-(\rho_*/\rho)^{2a}\right),$$

and therefore

$$\sigma^{K,w} = \sigma^{K,0} + \ln\left(1-(\rho_*/\rho)^{2a}\right) + b,$$

where b is some constant. For the function η, we have

$$\eta^{K,w} = \eta^{K,0}\left(1-(\rho_*/\rho)^{2a}\right)B, \tag{3.19}$$

for some constant B. By taking a small perturbation of a $w = 0$ solution, such that it does not change β and α, we have that w and ρ_*^a are of the same order,

$$\rho_* = w^{1/a}(1 + o(w)).$$

Equation (3.19) gives us the following heuristics:

- If $a > 0$, then a small perturbation of a static Kasner solution is complete at infinity, with a small scale parameter.
- If $a < 0$, then a small perturbation of a static Kasner solution hits a singularity within a finite distance of the axis.

A formal understanding of this heuristic will be investigated in the next chapter.

3.3.2 Lewis' families of solutions

The Lewis solutions [51] (see also [52]) are cylindrically symmetric (i.e., independent on ϕ and z) stationary vacuum solutions, with off-diagonal terms in the matrix. Some solutions extend

to infinity ($\rho = +\infty$) while others do not. In view of the three cases above, $\epsilon = -1, 0, 1$, the possible forms for η are the following three

$$(\mathrm{I}\pm) : \eta = \rho \frac{|w|}{a} \sin(\pm a \ln(\rho/\rho_*)),\ a > 0,\ \rho_* \in \mathbb{R}^+, \tag{3.20}$$

$$(\mathrm{II}\pm) : \eta = \rho |w| (\pm \ln(\rho/\rho_*)),\ \rho_* \in \mathbb{R}^+, \tag{3.21}$$

$$(\mathrm{III}\pm) : \eta = \rho \frac{|w|}{a} \sinh(\pm a \ln(\rho/\rho_*)),\ a > 0,\ \rho_* \in \mathbb{R}^+, \tag{3.22}$$

where a and ρ_* are free parameters and w is related to the twist potential by

$$\omega = wz, \quad w \neq 0.$$

The solutions extending to infinity are (II+) and (III+) (note that they are positive only after ρ_*, which is where the singularity is located). Also, observe that

$$\lim_{a \to 0} \eta_{III+} = \eta_{II+},$$

i.e., the limit when $a \to 0$ of a sequence of solutions in the family (III+) gives a solution in the family (II+).

Since $e^x \approx \rho^{1+a}$ or $e^x \approx \rho^{1-a}$, depending on whether we are in the case (III+) or (III-), we have two clear behaviors for x. The non-existence Theorem 4.1 contains in its proof some pointers to a phenomenological property of the periodic solutions: given a periodic stationary and axisymmetric black hole orbit data with parameters $(m/L, A, J)$, the solution cannot reach infinity if the asymptotic behavior of $e^x = \eta/\rho$ is forced to be sub-linear (since we would be in case III-). We will study this in more detail in the next chapter, and in chapter 6, we will show the transition from the case (III+) to the case (III-).

For the case (III+), the metric components V, W, η and $e^{2\gamma}/\eta$ get the form

$$V = \frac{2a}{|w|} e^{-b} \rho^{1-a}, \quad W = \mathrm{s}(w) e^{-b} \rho^{1-a}, \tag{3.23}$$

$$\eta = \frac{|w|}{2a} (e^b \rho^{1+a} - e^{-b} \rho^{1-a}), \quad \frac{e^{2\gamma}}{\eta} = c \rho^{(a^2-1)/2}, \tag{3.24}$$

where $\mathrm{s}(w) = w/|w|$ is the sign of w and $c > 0$ is another free parameter. The angular velocity function Ω is

$$\Omega = \frac{2a}{w} \frac{e^{-b} \rho^{-a}}{(e^b \rho^a - e^{-b} \rho^{-a})}.$$

Note that Ω is set to be zero at infinity. It turns out that the solutions (III+) with $a \geq 1$ cannot model the asymptotic behavior ($\rho \to \infty$) of a periodic array of black holes. Indeed, suppose one such array of black holes is asymptotically a solution (III+) with $a \geq 1$. In that case, a simple computation shows that the lapse function (i.e., the component of ∂_t normal to $\{t = 0\}$) would tend to zero at infinity. As it is zero on the horizons, it would have an absolute maximum, thus contradicting the maximum principle on the lapse equation (the Laplacian of the lapse is

always less than or equal to zero). As a tends to zero, η in (III+) degenerates into (II+). The asymptotic models are, therefore, the model (III+) with $0 < a < 1$ and the model (II+).

The metrics of the models (III+) are Kasner to leading order (the cross term $-2\mathrm{s}(w)e^{-b}\rho^{1-a}dtd\phi$ has a subleading fall-off's). Recalling that the Kasner metrics have the form

$$g_{K,0} = -e^{-b}\rho^{\alpha}dt^2 + e^{b}\rho^{2-\alpha}d\phi^2 + c\rho^{\alpha^2/2-\alpha}\left(d\rho^2 + dz^2\right),$$

we see that in case (III+) the Kasner exponent is $\alpha = 1 - a$ (cf. (3.24)).

We can define the asymptotic Lewis' behavior by the same lines of Definition 2.11 and Definition 2.12.

Definition 3.4. *A stationary data set $(N; h, \eta, \omega)$ is asymptotic to a Lewis solution $(\Sigma^K; g^K, \eta^K, \omega^K)$, $\Sigma^K = (0,\infty)\times T^2$, if for any $m \geq 1$ and $n \geq 0$ there is $C > 0$, a bounded set $K \subset N$ and a diffeomorphism into the image $\phi : N \setminus K \to \Sigma^K$ such that*

$$|\partial_I(\phi_* h)_{ij} - \partial_I g^K_{ij}| \leq \frac{C}{x^m},$$
$$|\partial_I(\phi_* \eta)_{ij} - \partial_I \eta^K| \leq \frac{C}{x^m},$$
$$|\partial_I(\phi_* \omega)_{ij} - \partial_I \omega^K| \leq \frac{C}{x^m},$$

for any multi-index I with $|I| \leq n$, where x, y, z are the coordinates in Σ^K.

3.3.3 Smarr formula for Lewis models

Assume we have a periodic stationary and axisymmetric black hole solution, with parameters $(m/L, A, J)$. Consider the right-hand side in (2.29) for a loop ℓ far away from the axis. Then, by direct computation from (3.22) for $a > 0$ and the plus sign,

$$M = \frac{1-a}{4}L,$$

where a is the Kasner parameter. This equation relates the Komar mass of the solution with the period and the Kasner exponent of the corresponding Lewis model. This equation is the stationary analog of the static equation (1.15).

The Smarr formula, (2.33), now reads

$$\frac{1-a}{4}L = m + 2\Omega_{\mathcal{H}} J.$$

This equation implies a relation between the Kasner exponent and the angular velocity of the black hole:

$$\Omega_{\mathcal{H}} = \frac{\frac{(1-a)L}{4} - m}{2J}. \tag{3.25}$$

This equation contains useful information regarding the structure of the moduli space of solutions. First, it gives us another consistency check in the numerical simulations. After com-

puting Ω from the quadrature equations (2.20) and the Kasner exponent a, we can check if its value at the axis satisfies (3.25).

Second, it is connected to the non-existence Theorem 1.1: since $a > 0$, (3.25) tells us that

$$2J\Omega_{\mathcal{H}} \leq L/4 - m. \tag{3.26}$$

If $J \neq 0$, the hypothesis in Definition 3.3 implies the inequality $J\Omega_{\mathcal{H}} \geq 0$. Then, (3.26) implies that $L/4 - m > 0$ is a *necessary condition* for a solution to have the cases III+ or II+ as the model for asymptotic behavior.

Of course, this is not proof of Theorem 1.1 since we do not know a priori which is the asymptotic behavior of the solution and not even if it is T^2-symmetric.

Chapter 4

Non-existence theorems

In this chapter, we are concerned with the obstructions to the existence of solutions. As we saw in the previous chapter, heuristics on the behavior of the possible asymptotic models provide insights into which global properties a solution might have. Based on such insights, we show that if $m/L \in (1/4, 1/2)$, then solutions to the periodic Kerr analog cannot exist.

First, in section 4.1, we provide some decay rates for quantities evaluated at the sequence of points constructed in Proposition 3.5. Then, in section 4.2, we show the non-existence result, Theorem 1.1. We use a monotonic quantity, (4.8), which links the axis behavior of the function σ with the asymptotic region. In section 4.3, we relate the non-existence theorem with the MKN solutions. We prove Theorem 1.2, showing a bound for the quantity D^2/A in terms of m/L, where D is the distance between consecutive black holes. Below this bound, the MKN solutions cannot be put into rotation. This is a key result since it concerns two physical quantities (the distance D and the area A) instead of the gauge-independent quantity m/L, which has no clear physical meaning.

4.1 Preliminary results

First, we study the scaled diameter decay of the transverse circumferences at fixed ρ. This is a significant quantity to have information about since it appears in the integral quantities (e.g., the Komar integrals). It turns out, for a subsequence of points in the sequence $\{p_i\}_{i\geq 0}$ found in Proposition 3.5, the (scaled) diameter of the $\rho = cnt$ loops in $\mathcal{S}$ decays proportionally to the inverse of the distance from the horizon. Then, we study the properties of a monotonic quantity (Proposition 4.3) and the decays of the rotational energy (Lemma 4.1).

4.1.1 Scaled diameter decay

Recall the notation introduced at the beginning of section 3.2.

Proposition 4.1. *Let $(\mathcal{S}, \mathfrak{q}, \eta, \omega, \rho)$ be a periodic stationary and axisymmetric black hole data. Let*

$\{p_i\}_{i\geq 0}$ be the sequence obtained in Proposition 3.5. There is a subsequence $\{p'_{i_j} \in \mathcal{C}_{i_j}\}_{j\geq 0}$ such that

$$\frac{l^{i_j}}{r_{i_j}} \to 0, \quad j \to \infty, \quad \text{,and} \quad \frac{l^{i_j}}{r_{i_j}}\rho_{i_j} \to \ell_0, \quad j \to \infty,$$

for some constant $\ell_0 > 0$.

Proof. For the sequence of points $\{p_i\}_{i\geq 0}$ we have

$$\frac{a}{r_i} \leq \left|\frac{\nabla\rho}{\rho}\right|(p_i) < \frac{b}{r_i}. \tag{4.1}$$

Let $\mathcal{D}_{\rho_*,\rho_{**}} := \{(\rho, z) : \rho_* \leq \rho \leq \rho_{**}\}$, for any two $0 < \rho_* < \rho_{**}$. The function ρ is harmonic on $\mathcal{S}$, therefore

$$0 = \int_{\mathcal{D}} \Delta\rho dA = \int_{\mathcal{C}_*} \nabla_n\rho d\ell - \int_{\mathcal{C}_{**}} \nabla_n\rho d\ell.$$

Then, by taking $\rho_* > 0$ and $\rho_{**} = \rho(p_i)$,

$$0 < C_0 = \int_{\mathcal{C}_*} \nabla_n\rho d\ell = \int_{\mathcal{C}_i} \nabla_n\rho dl,$$

where the first inequality is a consequence of the definition of the data. Then, by the Mean Value Theorem,

$$C_0 = \int_{\mathcal{C}_i} \nabla_n\rho dl = l^i\rho_i\frac{\nabla_n\rho(p'_i)}{\rho_i},$$

for some $p'_i \in \mathcal{C}_i$. The previous equation is invariant under rescaling of the metric by the factor r_i^2 (i.e., $\mathfrak{q} \mapsto \mathfrak{q}/\bar{r}_i^2$). Then, we have

$$C_0 = \left(\frac{l^i}{r_i}\right)\rho_i\frac{\nabla_{\bar{n}}\rho(p'_i)}{\rho_i}, \tag{4.2}$$

where $\bar{n} = nr_i$. As $i \to +\infty$, we know that the scaled quantity $\frac{\nabla_{\bar{n}}\rho(p_i)}{\rho}$ is bounded, $a \leq \left|\frac{\nabla_{\bar{n}}\rho}{\rho}\right|(p_i) \leq b$, since we are computing the derivative with respect to $\bar{n}$. To obtain the same bounds when evaluating at p'_i, we have to use Reiris' bounds (recall Remark 3.1). Indeed,

$$\left|\nabla_n \ln\rho(p_i) - \nabla_n \ln\rho(p'_i)\right| \leq \int_{\mathcal{C}_i} |\nabla_s\nabla_n \ln\rho| d\ell \leq l^i\frac{c_1}{r_i^2}.$$

If $\frac{l^i}{r_i} \to +\infty$, it contradicts the Bishop-Gromov theorem, as shown in the proof of Lemma 3.2. Indeed, we can construct a sequence of (scaled) annuli where the $\mathfrak{q}_{r_i}-$length of the loop $\mathcal{C}_i$ is unbounded, and therefore the area of the annuli diverge.

Then, there is a convergent subsequence of points on which $\frac{l^{i_j}}{r_{i_j}} \to cnt < +\infty$. Therefore,

$\frac{l^{i_j}}{r^2_{i_j}} \to 0$, which implies that

$$\nabla_n \ln \rho(p'_{i_j}) \to \nabla_n \ln \rho(p_{i_j}), \quad j \to \infty.$$

Consequently, (4.1) is valid also at p'_{i_j}, for large j and some $a' < a$,

$$\frac{a'}{r_i} \leq \left| \frac{\nabla \rho}{\rho} \right| (p'_{i_j}) < \frac{b}{r_i}.$$

Considering (4.2), the scaled term $\frac{\nabla_{\bar{n}} \rho(p'_{i_j})}{\rho_{i_j}}$ is bounded from above and from below away from zero. Then, the product $\left(\frac{l^{i_j}}{r_{i_j}} \right) \rho_{i_j}$ is also bounded from above and from below away form zero. Therefore, there exists a subsequence, which we rename as $\{q_{i_j}\}_{j \geq 0}$, such that

$$\left(\frac{l^{i_j}}{r_{i_j}} \right) \rho_{i_j} \to \ell_0 > 0.$$

Finally, since ρ_i tends to infinity as $i \to \infty$, we have

$$\frac{l^{i_j}}{\bar{r}_{i_j}} \to 0, \quad (j \to \infty).$$

□

From now on, we will denote as $\{p'_i\}_{i \geq 0}$ the sequence found in Proposition 4.1. The Bishop-Gromov theorem (recall the proof of Lemma 3.2) plays a central role in the previous proof, although its full strength is still hidden in the geometry. Observe that the previous result is consistent with the case $\mu = 0$ since the length of the scaled loops goes to zero. However, the case $\mu > 0$ seems to be excluded (since it contains loops such that $\frac{l^i}{r_i} \to \beta > 0$). To show that $\mu > 0$ does not hold for periodic solutions, we also need to bound the decay for the curvature and exclude the sub-quadratic decay, (3.9). This will be done in section 5.2.

Two straightforward consequences of the previous result are shown below. First, we show a bound for the functions q and γ on the loops $\mathcal{C}_i$. This result will be useful in the next chapter.

Proposition 4.2. *There is a constant $c > 0$ such that for all i and for any $p', p \in \mathcal{C}_i$ we have,*

$$|e^{\gamma(p') - \gamma(p)} - 1| \leq c \frac{l^i}{\bar{r}_i},$$

and

$$|e^{q(p') - q(p)} - 1| \leq c' \frac{l^i}{\bar{r}_i}.$$

Proof. For the second inequality, observe that

$$|e^{-\gamma(p)} - e^{-\gamma(p')}| = \left| \int_p^{p'} \partial_z \gamma e^{-\gamma} dz \right| \leq \int_p^{p'} \left| \left(\frac{\rho}{2\eta^2} (\partial_\rho \eta \partial_z \eta + \partial_\rho \omega \partial_z \omega) \right) \right| |e^{-\gamma}| dz,$$

from where we can rewrite the last term as

$$|e^{-\gamma(p)} - e^{-\gamma(p')}| \leq \int_p^{p'} \left| \left(\frac{\rho e^{-2\gamma}}{2\eta^2} (\partial_\rho \eta \partial_z \eta + \partial_\rho \omega \partial_z \omega) \right) \right| |e^{\gamma}| dz.$$

Using Anderson's estimates at points in the sequence $\{p_i'\}$, we have

$$|e^{-\gamma(p)} - e^{-\gamma(p')}| \leq \frac{c\rho_i}{r_i^2} \int_p^{p'} |e^{\gamma}| dz \leq \frac{c\rho_i}{r_i^2} l^i.$$

Finally, by taking p' as the point in C_p such that $l^i = e^{\gamma(p')}$ (by Mean Value Theorem), we have

$$|e^{\gamma(q)-\gamma(p')} - 1| \leq \frac{c\rho_i}{r_i^2} (l^i)^2.$$

The result follows from here. The second inequality can be shown analogously. □

Now, we show a lemma in which the asymptotic behavior of $\nabla_s \omega$ is computed, where s is the direction tangent to the level sets of ρ. This result is the first step in our study of the rotational energy.

Lemma 4.1. *Let $(\mathcal{S}, \mathfrak{q}, \eta, \omega, \rho)$ be a periodic stationary and axisymmetric black hole data. Given the sequence of points $\{p_i'\}_{i\geq 0}$ in Proposition 4.1, we have that*

$$\frac{\nabla_{\bar{s}} \omega(p_i'')}{\rho_i} \to \frac{8J}{\ell_0},$$

as $i \to +\infty$, for some $p_i'' \in \mathcal{C}_i$.

Proof. For each p_i', the Komar integral for the angular momentum implies the following identity

$$0 < 8J = \int_{\mathcal{C}_i} \nabla_s \omega dl,$$

where J is the total angular momentum enclosed by the surface $\mathcal{C}_i$. By the mean value theorem, there exists $p_i'' \in \mathcal{C}_i$ such that

$$l_i \nabla_s \omega(p_i'') = 8J.$$

Scaling the metric $\mathfrak{q}$ by $r_i = \text{dist}(\mathcal{C}_i, \mathcal{C}_0)$, we obtain

$$\rho_i \frac{l^i}{r_i} \frac{\nabla_s \omega(p_i'')}{\rho_i} = 8J,$$

where $\bar{s} = sr_i$. By Proposition 4.1, the sequence $\rho_i \frac{l^i}{r_i}$ converges to ℓ_0 as $i \to +\infty$. Then

$$\frac{\nabla_{\bar{s}}\omega(p_i'')}{\rho_i} \to \frac{8J}{\ell_0}$$

□

Lemma 4.1 is directly related to the convergence and collapse results stated in [56]. Consider the family of scaled annuli $\{\mathcal{A}_i(1/2, 2, p_i''), \mathfrak{q}_{r_i}\}_{i\geq 0}$. If the annuli collapse to a segment in the moduli space of data, the function ω will converge to a linear function $wz + c_0$ in the universal cover $\tilde{\mathcal{S}}$. Lemma 4.1 states that, over the sequence of points $\{p_i''\}_{i\geq 0}$, $w = \frac{8J}{\ell_0}$ holds.

However, because of the possible asymptotic models given in section 3.3, there is a clear obstruction in Lewis families $III+$ or $II+$. If η has a sublinear growth with respect to ρ, then the collapse is faster than in these families, and therefore no Lewis family models the asymptotic behavior of the solution (complete at infinity). As we will prove in the next section, this represents the central obstruction to the existence of solutions.

4.1.2 A monotonic quantity

Let $(\mathcal{S}, \mathfrak{q}, \eta, \omega, \rho)$ be a periodic stationary and axisymmetric black hole data. In what follows, we are using the function $x := \ln(\eta/\rho)$ (as in the derivation of Lewis' models, cf. section 3.3). Observe that $x = \sigma + \ln\rho$.

In section 3.3, we already saw the advantage of taking x as a variable since it has a *positive* leading Kasner exponent in the Lewis models (in case (III+)). The equation for x is now,

$$\Delta_\rho x = -\frac{e^{-2x}}{\rho^2}|\nabla\omega|^2, \tag{4.3}$$

which is not surprising in view of Lemma 2.1 in section 2.7.

Lemma 4.2. *Let $(\mathcal{S}, \mathfrak{q}, \eta, \omega, \rho)$ be a periodic stationary and axisymmetric black hole data. Then, for $p \in \mathcal{S}$ and some constant $C > 0$,*

$$|\nabla x|(p) \leq \frac{C}{r(p)},$$

where $r(p) = dist(p, \partial\mathcal{S})$.

Proof. From Reiris' estimate, we have the quadratic bound for the Gaussian curvature

$$K \leq \frac{C}{r^2},$$

and therefore by (2.5)

$$\frac{|\nabla\eta|^2 + |\nabla\omega|^2}{\eta^2} \leq \frac{C}{r^2}.$$

Since each term is positive, we have two sets of inequalities

$$|\nabla \ln \eta| \leq \frac{C}{r}, \quad \frac{|\nabla \omega|}{\eta} \leq \frac{C}{r},$$

with $\nabla_s X = e^{-\gamma}\partial_z X$ and $\nabla_n X = e^{-\gamma}\partial_\rho X$ for any function X. Then

$$|\nabla_s(x + \ln \rho)| = |\nabla_s \ln \eta|,$$

and

$$\left|\nabla_n x\right| - \left|\nabla_n \ln \rho\right| \leq \left|\nabla_n x + \nabla_n \ln \rho\right| = |\nabla_n \ln \eta| \leq \frac{C}{r}.$$

By the estimate on $|\nabla_n \ln \rho|$ in Proposition 3.2, the result follows. □

Lemma 4.3. *Consider the sequence of points $\{p_i'\}_{i\geq 0}$, and let $y, y' \in \mathcal{C}_i$. Then there are constants $D_0, D_0', J_0 > 0$ such that*

$$|x(y) - x(y')| \leq D_0 \frac{l^i}{r_i} \tag{4.4}$$

$$\left|\frac{\eta(y)}{\eta(y')} - 1\right| \leq D_0' \frac{l^i}{r_i} \tag{4.5}$$

$$|\nabla x(y) - \nabla x(y')| \leq D_0 \frac{l^i}{r_i^2} \tag{4.6}$$

$$\left|\frac{\nabla_s \omega(y)}{\nabla_s \omega(y')} - 1\right| \leq J_0 \frac{l^i}{r_i} \tag{4.7}$$

Proof. For the first inequality, we use Lemma 4.2

$$|x(y) - x(y')| = \left| \int_q^p (e^{-\gamma}\partial_z x) e^{\gamma} dz \right| \leq c \frac{l_i}{r_i}.$$

Then, the difference between distinct values of x tends to zero as $i \to +\infty$. Inequality (4.5) is immediate after the computation

$$\left|\frac{\eta(y)}{\eta(y')} - 1\right| = \left|e^{x(y)-x(y')} - 1\right| \leq e^{|x(y)-x(y')|} - 1 \leq e^{D_0 \frac{l^i}{r_i}} - 1.$$

Inequalities (4.6) and (4.7) are analogous to the previous ones, having in mind Remark 3.1. □

Let $a(\rho)$ be the following integral on the level sets of ρ,

$$a(\rho) := \int_{\mathcal{C}(\rho)} \rho \nabla_n x dl. \tag{4.8}$$

This function resembles the Komar Mass functional (cf. subsection 2.6.3). In this case, we are missing the term containing the contribution from ω (which, intuitively, contains the informa-

tion regarding the rotational energy).

Proposition 4.3. *The function $a(\rho)$ decreases monotonically and is bounded. Therefore, it converges to a finite limiting value,*

$$a(\rho) \to a > -\infty, \quad \rho \to \infty$$

Proof. Let $\rho_* < \rho_{**}$ and $\mathcal{D}_{\rho_*,\rho_{**}} := \{(\rho, z) : \rho_* \leq \rho \leq \rho_{**}\}$. By the Stokes' Theorem,

$$a(\rho_*) - a(\rho_{**}) = \int_{\mathcal{C}_{**}} \rho \nabla_n x dl - \int_{\mathcal{C}_*} \rho \nabla_n x dl = \int_{\mathcal{D}_{\rho_*,\rho_{**}}} \Delta_\rho x dv < 0,$$

where in the last inequality we use (4.3) and the fact that in at least one point on $\mathcal{D}_{\rho_*,\rho_{**}}$ we have $\nabla\omega \neq 0$ (otherwise we are in a static solution). Then, $a(\rho)$ is monotonically decreasing.

To prove boundedness, observe that on the loops $\mathcal{C}_i$ (given by the sequence $\{p_i'\}_{i\geq 0}$ obtained in Proposition 4.1),

$$\left| \int_{\mathcal{C}_i} \rho \nabla_n x dl \right| \leq \rho_i \int_{\mathcal{C}_i} |\nabla_n x| dl \leq \rho_i \frac{C}{r_i} l^i \to C\ell_0,$$

where in the last inequality we use that $\rho_i \frac{l^i}{r_i} \to \ell_0 > 0$. Since it is valid for the points in the sequence $\{p_i'\}_{i\geq 0}$ and the function is monotonically decreasing, we have that it is valid for all the points where $\rho \in (0, +\infty)$. □

4.2 A non-existence theorem when $m/L > 1/4$

In this section, we will prove a non-existence result for the periodic Kerr analogs. Let $(\mathcal{S}, \mathfrak{q}, \eta, \omega, \rho)$ be a periodic stationary and axisymmetric black hole solution with parameters $(m/L, A, J)$. Recall from section 2.3 that ρ is a harmonic function (taken as coordinate in the Weyl-Papapetrou coordinates).

At each level set of ρ, we define $\bar{x}(\rho) := \max\{x(p) : p \in \mathcal{C}(\rho)\}$ and $\underline{x}(\rho) := \min\{x(p) : p \in \mathcal{C}(\rho)\}$.

Proposition 4.4. *Let $(\mathcal{S}, \mathfrak{q}, \eta, \omega, \rho)$ be a periodic stationary and axisymmetric black hole solution. Either $\underline{x}$ is strictly monotonically increasing, or it is strictly monotonically decreasing on $[\rho_*, +\infty)$ for certain $\rho_* > 0$.*

Proof. Suppose that we have three points $p_1, p_2, p_3 \in \mathcal{S}$ on which $\rho(p_1) < \rho(p_2) < \rho(p_3)$ and such that $\underline{x}(\rho(p_1)) \geq \underline{x}(\rho(p_2))$ and $\underline{x}(\rho(p_3)) \geq \underline{x}(\rho(p_2))$. To simplify the notation, we denote $\rho(p_i)$ as ρ_i[1]. Then, using the minimum principle in the domain $\mathcal{D}_{1,3} := \{(\rho, z) : \rho_1 \leq \rho \leq \rho_3\}$ we obtain

$$\underline{x}(\rho_2) \geq \min_{\mathcal{D}_{1,3}} x \geq \min_{\partial\mathcal{D}_{1,3}} x = \min\{\underline{x}(\rho_1), \underline{x}(\rho_3)\} \geq \underline{x}(\rho_2),$$

which implies that the function $\underline{x}$ is constant on the interval $[\rho_1, \rho_2]$ or $[\rho_2, \rho_3]$. Then, by the strong minimum principle, x is constant. In that case, ω is also constant, and the solution is the

[1]Not to be confused with the values of ρ at the points in the sequence from subsection 4.1.1.

flat solution on that interval. This is a contradiction. Then the function $\underline{x}$ cannot *increase* once it decreases.

Either $\underline{x}$ is strictly monotonically increasing or not. If $\underline{x}$ is not strictly monotonically increasing, then there exist two points $\rho_*(p_*) < \rho_{**}(p_{**})$ such that

$$\underline{x}(\rho_*) = \underline{x}(\rho_{**}).$$

In the interval $[\rho_*, \rho_{**}]$ there is $\hat{\rho}$ such that $\underline{x}$ attains its maximum. If $\underline{x}(\hat{\rho}) = \underline{x}(\rho_*)$, then $\underline{x}$ is constant on $[\rho_*, \rho_{**}]$ (it cannot increase after it decreases). By the strong minimum principle (again), this is a contradiction.

Therefore, $\rho_* < \hat{\rho} < \rho_{**}$ and $\underline{x}(\hat{\rho}) > \underline{x}(\rho_*)$. In the interval $[\rho_*, \hat{\rho}]$ the function $\underline{x}$ is increasing and in $[\hat{\rho}, \rho_{**}]$ decreases.

If we take any other $\rho > \rho_{**}$, we can repeat the argument and therefore $\underline{x}$ is decreasing on the interval $[\hat{\rho}, \rho]$ (see Figure 4.1). Then, it is a monotonically decreasing function on the interval $[\rho_*, +\infty)$.

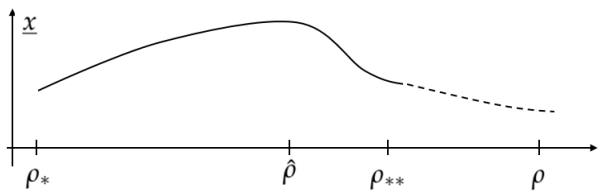

Figure 4.1: Schematic representation of $\underline{x}$ decreasing after $\hat{\rho}$.

□

Now, we will use the sequence of points, $\{p_i'\}_{i\geq 0}$, in order to establish a bound for $\underline{x}$, relating it to the sequence in Lemma 4.1.

Proposition 4.5. *There is $d \in \mathbb{R}$ such that $\underline{x}(\rho_i) \geq d$, $\forall i$. Therefore, either $\lim_{\rho\to+\infty} \underline{x}(\rho) = +\infty$ or $\lim_{\rho\to+\infty} \underline{x}(\rho) = h < +\infty$.*

Proof. Consider the sequence of values $\{\underline{x}(\rho(p_i'))\}_i$. By Proposition 4.4, it satisfies

$$\underline{x}(\rho_{i_k}) \to x_\infty \quad (k \to +\infty),$$

where $-\infty \leq x_\infty \leq +\infty$. Assume $x_\infty = -\infty$. Then, there is a sequence of points $\{p_i'' \in \mathcal{C}_i\}_{i\geq 0}$ such that

$$0 = \lim_{i\to+\infty} e^{\underline{x}_i(\rho_i)} = \lim_{i\to+\infty} e^{x_i(p_i'')} = \lim_{i\to+\infty} \frac{\eta(p_i'')}{\rho_i}.$$

But in that case, we have

$$\frac{\nabla_{\bar{s}}\omega(p_i')}{\eta(p_i')}\frac{\eta(p_i'')}{\rho_i} = \frac{\nabla_{\bar{s}}\omega(p_i')}{\rho_i}\frac{\eta(p_i'')}{\eta(p_i')} \to \frac{8J}{\ell_0},$$

where we use Proposition 4.1 together with (4.5) and (4.7).

By Reiris' estimates, on the left-hand side

$$\frac{\nabla_{\bar{s}}\omega(p_i')}{\eta(p_i')} \leq C,$$

recall that $\bar{s}$ is the scaled vector. Then, we have that $\frac{8J}{\ell_0} = 0$, which is a contradiction since by Lemma 4.1, $\frac{\nabla_{\bar{s}}\omega(p_i')}{\rho_i}$ must tend to a non-vanishing constant. Then, $x_\infty > -\infty$. □

Observe that if $\lim_{i\to+\infty} \eta(p_i')/\rho_i = +\infty$, then

$$\frac{|\nabla_{s_{r_i}}\omega|_{q_i}}{\eta_i} \to 0,$$

and the limit is positive if $\lim_{i\to+\infty} \eta(p_i')/\rho_i = h < +\infty$. In that case, as we will see below, the rotational energy attains its slower decay possible (quadratic decay).

Now, we are in a position to prove Theorem 1.1.

Theorem 4.1. *Let $(\mathcal{S}, \mathfrak{q}, \eta, \omega, \rho)$ be a periodic stationary and axisymmetric black hole solution with parameters $(m/L, A, J)$. Then $m/L \leq 1/4$.*

Proof. Assume $L < 4m$. We will show that $\underline{x} \to -\infty$ and reach a contradiction by Proposition 4.5. Observe that

$$\rho\nabla_n x dl = (\rho\nabla_\rho\sigma + 1)dz.$$

By the boundary conditions for σ at the horizon (cf. section 2.5), we have that

$$\lim_{\rho\to 0}\int_{\mathcal{C}(\rho)} \rho\nabla_n x dl = -4m + L < 0.$$

By Proposition 4.3, the function $a(\rho)$ is monotonically decreasing and tends to a limiting value a when $\rho \to +\infty$,

$$0 > -4m + L \geq \int_{\mathcal{C}(\rho)} \rho\nabla_n x dl = a(\rho) \searrow a.$$

Consider $\zeta := \ln\rho$, and let us define the function

$$F(\zeta) := \int_{C_\zeta} x dz.$$

After derivation under the integral, we get that

$$a(\zeta) = \frac{d}{d\zeta}F(\zeta).$$

Then, $F(\zeta)$ is a decreasing function with derivative satisfying

$$\frac{d}{d\zeta}F(\zeta) \leq -4m + L < 0.$$

Therefore

$$\underline{x}L \leq F(\zeta) \leq (-4m + L)\zeta \to -\infty \quad \rho \to +\infty.$$

Then, by Proposition 4.5, we have a contradiction. □

Using the proof of the theorem, we can show the following two results for a generic periodic stationary and axisymmetric solution.

Corollary 4.1. *Let $(\mathcal{S}, \mathfrak{q}, \eta, \omega, \rho)$ be a periodic stationary and axisymmetric black hole solution with $J > 0$ and $m/L < 1/4$. Then $a(\rho) > 0$ for all $\rho > 0$.*

Proof. If exists $\rho^* > 0$ such that $a(\rho^*) \leq 0$ (remember that is a monotonically decreasing), then we take such ρ^* as the initial ρ in the argument of the proof of Theorem 4.1, and deduce $\underline{x} \to -\infty$, which is a contradiction. □

Proposition 4.6. *Consider the sequence of points $\{p_i'\}_{i\geq 0}$ from Proposition 4.1. Then there are constants D_1, D_2 such that the following identities hold*

$$\left|\nabla_{\bar{n}} x(p_i') - \bar{a}\right| \to 0, \tag{4.9}$$

$$\left.\frac{\eta}{\rho^{1+\tilde{a}}}\right|_{p_i'} \to D_1, \tag{4.10}$$

$$\left.\frac{|\nabla_{s_{r_i}}\omega|\rho^{1+\tilde{a}}}{\eta}\right|_{p_i'} \to D_2,$$

with $\tilde{a} = \frac{1}{\ell_0}\lim_{\rho\to\infty} a(\rho)$.

Proof. We have that

$$a = \lim_{i\to+\infty} \int_{\mathcal{C}_i} \rho \nabla_n x d\ell,$$

with a the limiting value of $a(\rho)$. By the mean value theorem, there exists $y_i \in \mathcal{C}_i$ such that

$$a = \lim_{i\to+\infty} l^i \rho_i \nabla_n x(y_i) = \lim_{i\to+\infty} \ell_0 \nabla_{\bar{n}} x(y_i).$$

Then

$$\left|\nabla_{\bar{n}} x(y_i) - \bar{a}\right| \to 0,$$

where $\bar{a} = \frac{a}{\ell_0}$. The results follows from equation (4.6).

For the second limit, let $p_{i,m}$ and $p_{i,M}$ be the points where x attains its minimum and maximum, respectively, at $\mathcal{C}(\rho)$. Then

$$l^i(\partial_\zeta x)(p_{i,m}) \leq a(\zeta_i) \leq l^i(\partial_\zeta x)(p_{i,M}).$$

Reestablishing ρ as variable and using the bound (4.4), we have

$$l^i\rho_i(\partial_\rho x)(p_{i,m}) \leq a(\rho_i) \leq l^i\rho_i(\partial_\rho x)(p_{i,m}) + l^i\rho_i D_0 \frac{l^i}{r_i^2},$$

and therefore,

$$(\partial_\rho x)(p_{i,m}) \leq \frac{a}{\ell_0} \leq (\partial_\rho x)(q_{i,m}) + D_0 \frac{l^i}{r_i}.$$

In the limit $i \to +\infty$, both sides of the inequality are equal, and we have,

$$\frac{x(p_i)}{\bar{a} \ln \rho(p_i)} \to 1 \in \mathbb{R},$$

thus identity (4.9) holds.

Finally, the third limit is a consequence of

$$\frac{|\nabla_{s_{r_i}} \omega|_{q_i}}{\eta_i} \frac{\eta_i}{\rho_i} \to \frac{8J}{\ell_0},$$

and (4.10). □

4.3 Distance-Area bound for MKN Solutions

In this section, we establish Theorem 1.2. Regarding our orbit data, an MKN solution is given by a periodic stationary and axisymmetric black hole solution with parameters $(m/L, A, 0)$. Recall that we say that it can be *put into rotation* if there exists a periodic Kerr analog with the same m/L and A (cf. Definition 1.3).

Theorem 4.2. *Given a MKN solution with parameters $(m/L, A)$, the distance D between the horizons is bounded by,*

$$D \geq \frac{\pi}{6} \Gamma_{\min} \left(1 - \frac{2m}{L}\right) \sqrt{\frac{L}{2m}} \sqrt{A},$$

where $\Gamma_{\min}$ is the minimum of the gamma function in $\mathbb{R}^+$. Therefore, in view of Theorem 4.1, no MKN solution with $D < \frac{\pi \Gamma_{\min}}{6\sqrt{2}} \sqrt{A}$ can be put into rotation. As a reference, $\frac{\pi \Gamma_{\min}}{6\sqrt{2}} \approx 0.3279....$

Proof. Recall that a stationary metric in Weyl-Papapetrou form is written as

$$g_{MKN} = e^\sigma \left(e^{2q}(d\rho^2 + dz^2) + \rho^2 d\phi^2\right) - e^{-\sigma} dt^2.$$

Therefore, the distance between two consecutive horizons is given by

$$D = \int_m^{L-m} e^{\sigma/2} dz,$$

since $q = 0$ (recall that the metric is regular at the axis, cf. subsection 2.5.3). The area of the horizon is given by

$$A = 4\pi m \kappa^{-1}.$$

We want to relate the values of σ with the value of κ. As we show in (2.31), the surface gravity has a simple expression in terms of $\gamma_{\mathcal{H}}$, and it can be computed from a direct formula, (2.30).

Then, we have

$$\begin{aligned}\kappa &= \frac{1}{2}\left(e^{-2\gamma}\rho^2|\nabla\sigma|^2\right)^{1/2}\Big|_{\mathcal{H}} \\ &= \frac{1}{2}\left(e^{-2\gamma+2q+\sigma}\rho^2|\bar{\nabla}\sigma|^2\right)^{1/2}\Big|_{\mathcal{H}}, \\ &= \frac{1}{2}\left(e^{-\sigma}|\bar{\nabla}\sigma|^2\right)^{1/2}\Big|_{\mathcal{H}} = -|\bar{\nabla}e^{-\sigma/2}|\Big|_{\mathcal{H}},\end{aligned}$$

where $\bar{\nabla}$ is the covariant derivative of the metric $e^{\sigma}\left(e^{2q}(d\rho^2+dz^2)\rho^2 d\phi^2\right)$. This formula is exactly the characterization of the surface gravity by the Lapse associated with the metric g_{MKN} (in this case, $N = e^{-\sigma/2}$),

$$\kappa = |\bar{\nabla}N|_{\mathcal{H}},$$

which, for Killing horizons, is equivalent to Definition 2.5. If we compute at the north pole at $(0,m)$, then the normal direction to the horizon is ∂_z. Then

$$\kappa = -\frac{e^{-\sigma}}{2}\partial_z\sigma\Big|_{(0,m)} = \frac{\partial_z e^{-\sigma}}{2}\Big|_{(0,m)},$$

where we use that $q = 0$ at the pole. Next, to compute the previous expression, we use the formula in [2] for $e^{-\sigma}$ evaluated at the segment $z \in (m, L-m)$

$$e^{-\sigma} = e^{4\gamma_{EM}m/L}\frac{\Gamma\left(\frac{z+m}{L}\right)\Gamma\left(1-\frac{z-m}{L}\right)}{\Gamma\left(\frac{z-m}{L}\right)\Gamma\left(1-\frac{z+m}{L}\right)}, \tag{4.11}$$

where γ_{EM} is the Euler-Mascheroni constant and Γ the usual gamma function. Observe that the function has a zero of order one at $(z = m)$ since $\Gamma\left(1-\frac{z-m}{L}\right)$ has a simple pole at $z = 0$. Therefore

$$\kappa = \frac{e^{4\gamma_{EM}m/L}}{2L}\frac{\Gamma\left(\frac{2m}{L}\right)}{\Gamma\left(1-\frac{2m}{L}\right)}.$$

Then, the area is given by the following expression

$$A = 8\pi m L e^{-4\gamma_{EM}m/L}\frac{\Gamma\left(1-\frac{2m}{L}\right)}{\Gamma\left(\frac{2m}{L}\right)}.$$

Next, we compute the distance. In view of (4.11), we have

$$D = \int_m^{L-m} e^{-2\gamma_{EM}m/L}\left(\frac{\Gamma\left(\frac{z-m}{L}\right)\Gamma\left(1-\frac{z+m}{L}\right)}{\Gamma\left(\frac{z+m}{L}\right)\Gamma\left(1-\frac{z-m}{L}\right)}\right)^{1/2} dz.$$

Both poles at the numerator can be isolated by using the identity $\Gamma(1+z) = z\Gamma(z)$,

$$D = \int_m^{L-m} e^{-2\gamma_{EM}m/L}\left(\frac{\Gamma\left(1+\frac{z-m}{L}\right)\Gamma\left(2-\frac{z+m}{L}\right)}{\Gamma\left(\frac{z+m}{L}\right)\Gamma\left(1-\frac{z-m}{L}\right)}\right)^{1/2}\frac{1}{\sqrt{1-\frac{z+m}{L}}\sqrt{\frac{z-m}{L}}}dz. \tag{4.12}$$

We will use a couple of properties for Γ, namely

$$\Gamma(x) \geq \Gamma_{\min} \approx 0.88560..., \quad x \in (0,2),$$

where the minimum is attained at $x_{\min} \approx 1.46163...$, and, Γ is decreasing in $x \in (0,1)$. Then, since $2m < L$, we have

$$\Gamma\left(1+\frac{z-m}{L}\right)\Gamma\left(2-\frac{z+m}{L}\right) \geq \Gamma_{\min}^2,$$

and

$$\Gamma\left(\frac{z+m}{L}\right)\Gamma\left(1-\frac{z-m}{L}\right) \leq \Gamma\left(\frac{2m}{L}\right)\Gamma\left(1-\frac{2m}{L}\right) = \frac{\pi}{\sin\left(\pi\frac{2m}{L}\right)}.$$

With this in mind, the integral (4.12) is bounded from below by

$$D \geq \frac{e^{-2\gamma_{EM}m/L}}{\sqrt{\pi}}\Gamma_{\min}\left(\sin\left(\pi\frac{2m}{L}\right)\right)^{1/2}\int_m^{L-m}\frac{1}{\sqrt{1-\frac{z+m}{L}}\sqrt{\frac{z-m}{L}}}dz.$$

We can compute exactly the last term,

$$D \geq \frac{e^{-2\gamma_{EM}m/L}}{\sqrt{\pi}}\Gamma_{\min}\left[\sin\left(\pi\frac{2m}{L}\right)\right]^{1/2}\frac{\pi L}{3}.$$

The area can be rewritten as

$$A = 8\pi m L e^{-4\gamma_{EM}m/L}\Gamma^2\left(1-\frac{2m}{L}\right)\sin\left(\pi\frac{2m}{L}\right).$$

Then, we can establish a bound for D in terms of the area,

$$D^2 \geq A\frac{\pi^2 L}{72m}\frac{\Gamma_{\min}^2}{\Gamma^2\left(1-\frac{2m}{L}\right)}.$$

Finally, since

$$x = \frac{\Gamma(1-x)}{\Gamma(x)} \leq \frac{1}{\Gamma(x)}, \quad x \in (0,1],$$

we arrive at

$$D^2 \geq A\frac{\pi^2}{36}\Gamma_{\min}^2\frac{L}{2m}\left(1-\frac{2m}{L}\right)^2,$$

which is the lower bound stated in the theorem. Next, assume $D < \frac{\pi\Gamma_{\min}}{6\sqrt{2}}\sqrt{A}$. Then

$$\frac{\pi^2}{36}\Gamma_{\min}^2\frac{L}{2m}\left(1-\frac{2m}{L}\right)^2 \leq \frac{D^2}{A} < \frac{\pi^2\Gamma_{\min}^2}{72},$$

which implies

$$\frac{L}{2m}\left(1-\frac{2m}{L}\right)^2 < \frac{1}{2} \quad \Leftrightarrow \quad \frac{2m}{L} > \frac{1}{2}.$$

Then, $4m > L$ and therefore no periodic analog of Kerr can be constructed by Theorem 4.1. □

Chapter 5

Asymptotic behavior

In this chapter, we assume the existence of solutions and focus on the possible asymptotic behaviors. After an overview of the approach, in section 5.2 we prove a decay condition for the curvature, which implies the collapse of the (rescaled) asymptotic region to a segment. In section 5.3, we use such collapse to prove Theorem 1.3, namely, that in a neighborhood of each point in the sequence $\{p_i'\}_{i\geq 0}$ from Proposition 4.1 we have a Lewis model. As a consequence of this result, when $i \to \infty$, we have a limiting model for the asymptotic behavior. Finally, we comment on the asymptotic behavior in the definition 3.4.

5.1 Approach to the asymptotic study: an overview

Let us consider a periodic stationary and axisymmetric black hole solution, $(\mathcal{M}, g)$, with parameters $(m/L, A, J)$. As we explained in the previous chapter, the Lewis models are the only known stationary solutions that happen to be cylindrically symmetric. Also, they are the stationary generalization of Kasner solutions. Therefore, it is natural to ask whether $\mathcal{M}$ is *close* to a Lewis model in the asymptotic region. Intuitively, we want to show that the solution g becomes $z-$independent the further away we go in the ρ direction.

Consider the orbit data $(\mathcal{S}, \mathfrak{q}, \eta, \omega, \rho)$ associated to $(\mathcal{M}, g)$. Let $\mathcal{A}_{\rho_0} = \{\rho_0 < \rho < 2\rho_0\}$ be an annulus cut from the manifold $\mathcal{S}$. The restriction of the metric $\mathfrak{q}$ on $\mathcal{A}_{\rho_0}$ becomes $z-$independent as $\rho_0 \to +\infty$ if some sequence of annuli $\{\mathcal{A}_{\rho_i}\}_i$ converges to a *collapsed* 1-manifold where ρ can also be used as a coordinate, via the projection of the coordinate from the annuli to the limiting 1-manifold.

In modern geometry, the approach given by the Cheeger-Gromov Theory (see [61] and references therein) is well-suited for the interplay between geometry, topology and analysis. Here, the notions of collapse and convergence of sequences of Riemannian manifolds are defined in geometrical terms. The curvature of the metrics plays a central role, as well as the diameter and volume of the manifolds.

In this context, the problem we are studying in this thesis (cf. Problem 1.1) is an exciting and interesting application of results of Riemannian geometry in the context of General Relativity. Recall that the scalar curvature of the three-manifold $\mathcal{N}$, which can be computed from (2.5), is

quadratic in η and ω and therefore non-negative.

The main argument behind the proof of Theorem 5.2, which is contained in Proposition 5.2, is the following. Assume that we have established the collapse of $\{\mathcal{A}_{\rho_i}\}_i$ to a z-independent solution as $\rho_i \to +\infty$. Then, we have a *sufficiently enough* z-independent solution for large ρ's. For each $\mathcal{A}_{\rho_i}$, the equations (2.26) and (2.27) can be approximated with two ODE equations plus some perturbation which we will have to control as well. Recall that the $z-$independent versions of (2.26) and (2.27) have already been solve in section 3.3, leading to the Lewis' models.

From all the possible models, the families III^+ and II^+ are the only ones that reach infinity. One of the technical points is that we must ensure that when we go further away from the axis, the perturbation of the ODE decreases. The solutions obtained converge to some Lewis model. Showing that the perturbation is uniformly bounded by the diameter of the loops $\ell \subset \mathcal{A}_{\rho_0}$ is a critical element in this reasoning.

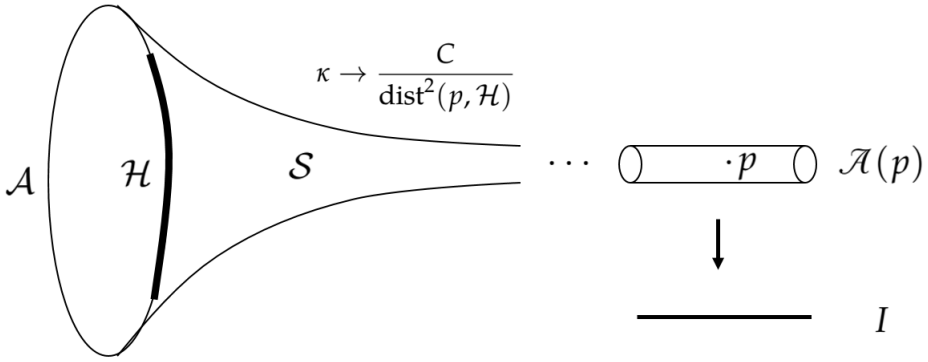

Figure 5.1: Diagram schematically representing the collapse to a segment of the annulus at increasingly diverging points. As we will see, the quadratic decay of the Gaussian curvature is a key property.

Let us comment on the intuitive approach in an informal language, expressed schematically in Figure 5.1.

- How does the z direction become *irrelevant* the further we go away from the axis?

  In this regard, as we mentioned before, the geometric meaning of a coordinate to become irrelevant is a certain *collapse* of the geometry. The celebrated theorems due to Cheeger, Gromomov and Bishop establish general conditions on moduli spaces under which the collapse occurs. For stationary orbit data, Anderson [56] shows two possible collapses: to a segment or to a two-manifold. In our case, the properties of the curvature and the volume of the manifold imply a collapse of the transverse two-torii to points and, therefore, the three-manifold N to a segment.

- What does it mean for a solution to be *sufficiently enough* z-independent for large ρ's?

  This is clearly in analogy with the definition of asymptotically flat spacetimes (Definition 2.11) or asymptotically Kasner spacetimes (Definition 2.12). In this case, we are looking

for an asymptotically Lewis model. However, there is no a priori knowledge of *which* Kasner exponent the asymptotic model will have. One possible procedure by which we obtain the correct Lewis model is constructive: taking increasingly large portions of the manifold as $\rho \to +\infty$. This is compatible with the notion of geometric collapse we discussed before.

This question has naturally two parts:

1. If a solution is *close* to a z-independent model for large enough ρ's, does it stay *close* to a $z-$independent model for an even larger ρ's?
2. If a solution is close to a *particular* z-independent model for a large enough ρ's, does it stay close to *that* z-independent model for even larger ρ's?

- In answering the previous two questions, we are dealing with the more technical part of the asymptotic behavior problem.

  The first deals with the proximity to a Lewis model for a large ρ, which can be deduced from the collapse of the annuli centered at the $\{p_i\}$ to a segment. On each annulus, we can define a Lewis model such that the distance to the actual solution is bounded by the diameter of the loops at constant ρ. The second question deals with the convergence of those Lewis models near the metric on the annuli to a limiting Lewis model.

- The construction of the final Lewis model that satisfies Definition 3.4 has to be done telescopically, in the same manner as it was done for the static case in [47]. We will not provide the details here, leaving it for future work.

5.2 Curvature decay and collapse

In the rest of this chapter, we will assume that $(\mathcal{S}, \mathfrak{q}, \sigma, \omega)$ is the orbit data for a periodic stationary and axisymmetric black hole solution with parameters $(m/L, A, J)$ (recall that ρ is coordinate). Our interest is to understand the asymptotic behavior of σ and ω. In view of Corollary 4.1, we will assume $a(\rho) > 0$ for all $\rho > 0$ (although the limiting value when $\rho \to +\infty$ can be zero).

Consider the function

$$b(\rho) := \int_{\mathcal{C}(\rho)} \rho \nabla_n \ln \eta dl,$$

which is similar to the definition of $a(\rho)$ in Proposition 4.3.

Lemma 5.1. *The function $b(\rho)$ is monotonically decreasing, bounded and satisfies*

$$b(\rho) \geq a(\rho) + L.$$

Proof. Analogous to Proposition 4.3. □

Proposition 5.1. *There exist a constant C_0 and a divergent sequence of points $\{y_i\}_{i>0} \subset \mathcal{S}$ such that*

$$K(y_i) \geq \frac{C_0}{dist^2(y_i, \partial\mathcal{S})}.$$

Proof. Since $a(\rho) > 0$, then $b(\rho) > L$. Consider the sequence of points $\{p_i'\}_{i\geq 0}$ obtained in Proposition 4.1. For the values of ρ at each p_i', we can use the mean value theorem for the integrals,

$$L < \int_{\mathcal{C}_i} \rho \nabla_n \ln \eta dl = \rho_i l^i \nabla_n \ln \eta(y_i),$$

for some $y_i \in \mathcal{C}_i$. Upon a scaling of the metric $\mathfrak{q}$ by the factor $1/r_i^2$, the left-hand side remains L, since it is a coordinate parameter. The inequality is then

$$L < \left(\rho_i \frac{l^i}{r_i}\right) \nabla_{\bar{n}} \ln \eta(y_i),$$

where $\bar{n} = nr_i$. The first factor converges to ℓ_0 in the limit $i \to +\infty$, due to Proposition 4.1. Therefore, the second term is bounded from above and below away from zero,

$$0 < C_1 < \nabla_{\bar{n}} \ln \eta(y_i) < C_2,$$

where C_2 can be considered as the constant C in Proposition 3.2. Restoring the scale of $\mathfrak{q}$, $r_i = \text{dist}(y_i, \partial\mathcal{S})$, we obtain that there is a sequence of points $\{y_i\}_{i>0}$ such that

$$|\nabla \ln \eta|(y_i) \geq \frac{C_1}{\text{dist}(y_i, \partial\mathcal{S})}$$

This is sufficient to prove the statement of the proposition, given the formula

$$K = \frac{1}{4}\left(\frac{|\nabla\eta|^2 + |\nabla\omega|^2}{\eta^2}\right),$$

and Proposition 3.2. □

Observe that the sequence of points $\{y_i\}_{i\geq 0}$ can be taken as the sequence $\{p_i'\}_{i\geq 0}$, due to Remark 3.1 and in analogy with Lemma 4.3.

The next lemma can be found in [56], and it follows from the Cheeger-Gromov theory of the collapse of Riemannian manifolds [61].

Lemma 5.2. *Let $(\mathcal{S}_i, \mathfrak{q}_i, \eta_i, \omega_i)$ represent data for a sequence of solutions to the stationary vacuum equations. Suppose that on the domains $(\mathcal{S}_i, \mathfrak{q}_i)$ we have that*

$$|R(\mathfrak{q}_i)| \leq \Lambda, \quad diam\mathcal{S}_i \leq D, \quad vol\mathcal{S}_i \to 0, \quad dist(x_i, \partial\mathcal{S}_i) \geq \delta,$$

for some $x_i \in \mathcal{S}_i$ and constants $\Lambda, D, \delta > 0$. Then, for any $\epsilon(\delta) > 0$ there are domains $U_i \subset \mathcal{S}_i$, with $\epsilon/2 \leq dist(\partial U_i, \partial\mathcal{S}_i) \leq \epsilon$ with $x_i \in U_i$, such that U_i is either

- *a Seifert fibered space, or*

- *a torus bundle over an interval.*

In both cases, the $\mathfrak{q}_i-$diameter of any fiber F (a S^1 of a T^2) goes to 0 as $i \to +\infty$, and $\pi_1(F)$ injects in $\pi_1(U_i)$.

We arrive at the main result of this section.

Theorem 5.1. *Let $(\mathcal{S}, \mathfrak{q}, \sigma, \omega)$ be the orbit data for a periodic stationary and axisymmetric black hole solution with $J > 0$ and $4m < L$, and let $\{p_i'\}_{i\geq 0}$ be the sequence of points obtained in Proposition 4.1. Then, the sequence $(\mathcal{A}_{r_i}(p_i'; 1/2, 2); \mathfrak{q}_{r_i})$ of scaled annuli collapse to the segment $([1/2, 2]; |.|)$ (in the Bishop-Gromov sense).*

Proof. Recall the proof of Lemma 3.2. Consider the function

$$\lim_{r\to+\infty} \frac{A(B(\partial\mathcal{S}, r))}{r^2} = \mu,$$

where $A(\cdot)$ denotes the area function and $B(\partial\mathcal{S}, r)$ is the set $\{x \in \mathcal{S} : \text{dist}(\partial\mathcal{S}, x) < r\}$. By the Bishop-Cheeger-Gromov theorem [61, Lemma 36], $\mu = 0$ or μ is a positive finite number.

If $\mu > 0$, then $(\mathcal{S}, \mathfrak{q})$ is asymptotically a flat cone, but then the curvature would decay sub-quadratically (cf. (3.9)), which is a contradiction in view of Proposition 5.1.

If $\mu = 0$, consider the sequence of metric spaces $\{(\mathcal{A}_{r_i}(p_i'; 1/2, 2); \mathfrak{q}_{r_i})\}_{i\geq 0}$, i.e., the annuli centered at p_i' with the rescaled metric $\mathfrak{q}_{r_i}$. Observe that the scalar curvature of each annulus is bounded. The diameter of the annuli is bounded from below by $3/2$, and the volume of each annulus is bounded from above by

$$vol(\mathcal{A}_{r_i}) \leq \frac{3}{2} C' \frac{l^i}{r_i} \to 0,$$

where C' is some positive constant. The limit vanishes due to Proposition 4.1. Observe that $\text{dist}(y, \partial\mathcal{S}) > 0 \; \forall y \in \mathcal{A}_{r_i}$ by definition of the annuli.

Then, by Lemma 5.2 the sequence $\{(\mathcal{A}_{r_i}(p_i'; 1/2, 2); \mathfrak{q}_{r_i})\}_{i\geq 0}$ of scaled annuli collapse to the segment $((1/2, 2), |.|)$. □

5.3 Lewis-like asymptotic behavior

In terms of the monotonic quantity $a(\rho)$ and its limit a when $\rho \to \infty$, the statement of Theorem 1.3 in chapter 1 can be rewritten as follows.

Theorem 5.2. *Given a periodic stationary and axisymmetric black hole solution with orbit data $(\mathcal{S}, \mathfrak{q}, \sigma, \omega)$ and parameters $(m/L, A, J)$ (satisfying $m/L \leq 1/4$), there is a divergent sequence of points $\{y_i\}_{i\geq 0} \subset \mathcal{S}$ and a sequence of rescaled annuli $\{(\mathcal{A}_{r_i}(y_i; 1/2, 2), \mathfrak{q}_{r_i})\}$ on $\mathcal{S}$ such that $\mathfrak{q}_{r_i} \to C\bar{\rho}^{\alpha}(d\bar{\rho}^2 + d\bar{z}^2)$. The parameters C, α and J determine a unique Lewis' model from family (III+) (3.22) in the case $a > 0$ and a model from family (II+) (3.21) in the case $a = 0$.*

In what follows, we will consider the divergent sequence of points $\{y_i\}_{\geq 0}$ constructed in Proposition 5.1.

5.3.1 Scaling of transverse tori

In this subsection, we see how the rescaling of a metric on a two-torus affects its diameter. This is important in the following subsections. Recall that we are denoting by a the limit of the monotonic function $a(\rho)$ when $\rho \to +\infty$.

Definition 5.1. *The Kasner exponent at a given ρ is denoted as*

$$\tilde{a}(\rho) := \frac{a(\rho)}{L},$$

and its limit when $\rho \to +\infty$ simply as $\tilde{a}$.

Observe that $0 \leq \tilde{a} < 1$. For the Lewis model in the case (III+), (3.22), with Kasner exponent $\tilde{a}$, the two-dimensional metric $\mathfrak{q}$ have the following form

$$\mathfrak{q} = c\rho^{(\tilde{a}^2-1)/2}e^b(d\rho^2 + dz^2)$$

while the transverse metrics on the $z - \phi$ tori $\mathcal{C}(\rho)$ are given by

$$c\rho^{(\tilde{a}^2-1)/2}e^b dz^2 + \frac{\rho w}{\tilde{a}}\sinh(\tilde{a}\ln\rho + b)d\phi^2.$$

In the next subsections, we will rescale the metric $\mathfrak{q}$. We will need to ensure collapsing in the transverse direction. Rescaling the metric by a factor $\frac{1}{l^2}$ and calculating the metric of the torus at $\mathcal{C}(\rho = l)$, we have

$$cl^{(\tilde{a}^2-5)/2}e^b dz^2 + \frac{A}{\tilde{a}}\frac{l^{\tilde{a}-1}e^b - l^{-\tilde{a}-1}e^{-b}}{2}d\phi^2.$$

Consider

$$l^*(\tilde{a}) = \max\left\{e^{-\frac{2}{\tilde{a}-1}}, e^{-\frac{2}{-\tilde{a}-1}}, e^{-\frac{4}{\tilde{a}^2-5}}\right\}.$$

If $l > l^*(\tilde{a})$, then

$$diam_{\mathfrak{q}}(\mathcal{C}(\rho = l)) \leq \frac{1}{2}diam_{\mathfrak{q}}(\mathcal{C}(\rho = l)).$$

Observe that $l^*(\tilde{a}) \leq e^2$, and in the limit $\tilde{a} \to 1$ the value $l^*(\tilde{a})$ diverges, while in the limit $\tilde{a} \to 0$ the value is e^2. Given $a^* \geq 0$, define

$$l_*(a^*) = \max\{l^*(a) : \frac{a^*}{2} \leq \tilde{a} < \frac{1+a^*}{2}\}$$

We drop the a^* explicit dependency when it is clear by context.

5.3.2 Asymptotic geometry of the periodic Kerr analogs

Based on Theorem 5.1, we will prove that at each y_i, we can define a *close enough* Lewis model, whose distance to the solution is controlled by the diameter of the transverse tori $\mathcal{C}(\rho)$. Since the diameter of those tori tends to zero as $\rho \to 0$, the approximations improve as $i \to +\infty$. However, there can be arbitrarily large distances between the annuli, so this step will provide us with a *candidate* for the asymptotic behavior.

The following lemmas will be helpful in the proof of Proposition 5.2. Their proofs can be found in [47].

Lemma 5.3. *Let (T,h) be a flat two-torus. Let W be a smooth tensor field, such that it vanishes at some point. Then, for any $0 \leq j \leq k$, we have*

$$\|W\|_{C_h^j} \leq c(k_{ij}) diam_h^{k-j}(T) \|W\|_{C_h^k}.$$

Lemma 5.4. *Let (T,h) be a Riemannian two-torus and let $p \in T$. Then there is a unique flat metric h_F, conformally related to h and $h_F(p) = h(p)$. Moreover, for any integer $k \geq 1$, and reals $K_1, K_k > 0$ there are constants $D(K_1), C(k,K_k) > 0$ such that if*

$$\|\kappa\|_{C_h^1} \leq K_1, \quad \|\kappa\|_{C_h^k} \leq K_k \quad \text{and} \quad diam_h(T) \leq D,$$

with κ the Gaussian curvature of h, then

$$e^{-C} h_F \leq h \leq e^C h_F, \quad \text{and} \quad \|h\|_{C_{h_F}^k} \leq C$$

Instead of ω, we will work with Ω. Then, equations (2.26) and (2.27) change as follows,

$$\begin{aligned} \Delta_\rho x &= -e^{2x} |\nabla \Omega|^2, \\ \Delta_\rho \Omega &= -2 \langle \nabla \Omega, \nabla x \rangle , \end{aligned}$$

in order to control the bounds with respect to the diameter of the loops $\mathcal{C}(\rho)$ on the surface.

Proposition 5.2. *Consider a periodic stationary and axisymmetric black hole solution with orbit data $(\mathcal{S}, \mathfrak{q}, \sigma, \omega)$ and parameters $(m/L, A, J)$ (satisfying $4m \leq L$). Let $0 \leq a^* < 1$. There exist positive constants $\epsilon_j, r^*, \epsilon_d, \epsilon_m > 0$ such that if at a point p with $r(p) > r^*$ we have*

1. $d_{GH}(\mathcal{A}_r(p, 1/2, 2), d_r), ([1/2, 2], |.|) < \epsilon_d$,
2. $|\tilde{a}(\rho(p)) - a^*| < \epsilon_m$,
3. $|\frac{|\nabla \omega|_r}{\rho_r}(p) - w^*| < \epsilon_j$,

then,

a. *we can foliate a neighbourhood $\mathcal{U}_p$ of $(\mathcal{A}_r(p; 1/(2l_*), 2l_*; \mathfrak{q}_r)$ by the level sets of ρ, each of which is a two-torus.*

b. *There is a Lewis model in the family (III+) or (II+), $(\Sigma^L; h^L, x^L, \Omega^L)$, and a diffeomorphism $\phi : \mathcal{U}_p \to \Sigma^L$ such that the distance from the three dimensional metric h and h^L is bounded by the diameter of the transverse tori,*

$$\|\phi_* h_r - h^L\|_{C_{h^L}^j} \leq C^* diam_{h^L}^m(\phi(\mathcal{C}_p)) \tag{5.1}$$

where $\mathcal{C}_\rho$ is the level set of ρ containing p.

Proof. a. Let us assume, by contradiction, that 1.,2. and 3. hold for every $\epsilon_d, \epsilon_m, \epsilon_j = 1/i$ and $r^* = i$ but that there exists a point y_i such that (a.) does not hold. Take the sequence of points $\{y_i\}_{i\geq 0}$ and consider the sequence of annuli $\{(\mathcal{A}_{r_i}(y_i; 1/(2l_*), 2l_*); \mathfrak{q}_{r_i})\}_i$. Since (a.) is true, then the annuli metrically collapses to a segment of length $2l_* - (1/(2l_*) < \infty$. By Lemma 5.2 we know that there are neighborhoods U_i of each $(\mathcal{A}_{r_i}(y_i; 1/(2l_*), 2l_*); \mathfrak{q}_{r_i})$ such that $(U_i; \mathfrak{q}_i)$ converges to a torus bundle over the interval. Then, for i large enough, the level sets of ρ foliate U_i, thus a contradiction.

b. We prove this part in three steps. Each step is done such that the bounds are in terms of $\mathrm{diam}^m_{g^K}(\phi(\mathcal{C}_p))$ (see Figure 5.2).

(a) First we define a flat metric on $\mathcal{U}_p$, denoted h_F.

(b) Then we approximate the real solution by a T^2-symmetric metric (not necessarily a solution), $h^{(1)}$.

(c) Finally, we prove that this approximation is near (in the ODE-perturbation sense) a Lewis model $h^{(2)}$.

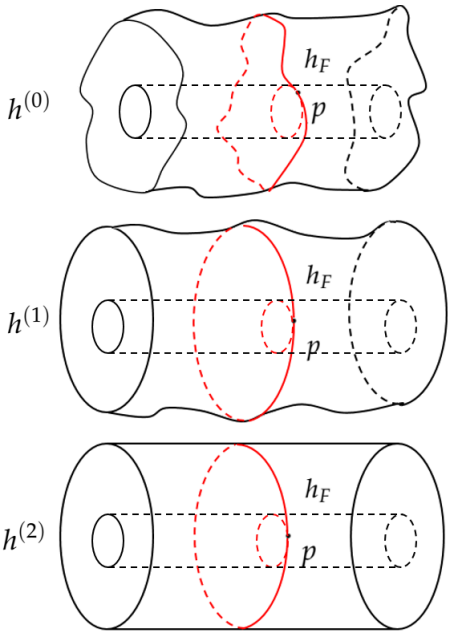

Figure 5.2: Schematic depiction of the steps involved in the proof.

For simplicity, let us denote the starting metric on $\mathcal{N}$ as $h^{(0)}$,

$$h^{(0)} = e^{2q-x-\ln\rho}(d\rho^2 + dz^2) + \rho e^x d\phi^2.$$

This metric is the spatial part of the complete solution from the orbit data $(\mathcal{S}, \mathfrak{q}, \sigma, \omega)$. Let us denote the metric on the transverse tori as $\mathfrak{h}$.

Step (a): In this part we are using Lemma 5.4. We define a flat metric on $\mathcal{U}_p$ as follows

$$h_F = C_0(d\rho^2 + dz^2) + C_1 d\phi^2$$

for some constants C_0, C_1 such that $h_F(p) = h(p)$. At any point $q \in \mathcal{C}_{\rho=q}$, we can take a neighborhood and coordinates $\bar{z}, \bar{\phi}$ such that

$$h_F = C_0 d\rho^2 + d\bar{z}^2 + d\bar{\phi}^2.$$

Let us denote the flat metric on the transverse tori as $\mathfrak{h}_F$. We take ϵ_d sufficiently small enough, so that $\mathrm{diam}_{\mathfrak{h}^{(0)}}(\mathcal{C}_q)$ satisfies the hypothesis in Lemma 5.4 for each $q \in \mathcal{U}_p$. Then, at each $q \in \mathcal{U}_p$,

$$e^{-C(q)}\mathfrak{h}_F \leq \mathfrak{h}^{(0)} \leq e^{C(q)}\mathfrak{h}_F, \quad \text{and} \quad \|\mathfrak{h}^{(0)}\|_{C^k_{\mathfrak{h}_F}} \leq C(q). \tag{5.2}$$

Now, this constant $C(q)$ is uniform. Indeed, the Gaussian curvature $K(\mathfrak{h}_F)$ of the tori at fixed ρ is uniformly bounded due to the estimates for the curvature in $\mathcal{N}$ derived in chapter 3, Remark 3.1 and Proposition 4.2. Then, (5.2) can be taken to be true on $\mathcal{U}_p$, and therefore

$$e^{-\tilde{C}}h_F \leq h^{(0)} \leq e^{\tilde{C}}h_F, \quad \text{and} \quad \|h^{(0)}\|_{C^k_{h_F}} \leq \tilde{C}. \tag{5.3}$$

We can further show that for any $m \geq 0$ and $j \geq 0$

$$\|\partial^m_\rho \partial^j h^{(0)}\|_{h_F} \leq \tilde{C}_{mj}. \tag{5.4}$$

This last uniform bound contemplates the $\rho-$derivatives (this is the case because of the collapse to a segment).

Step (b): Consider a ray emanating from H, which we will call γ. Such ray can be for example $\gamma = \{z = 0\}$, i.e., the integral curve of $\nabla\rho$ starting at $(0,0)$. By the z-even symmetry acting on our orbit data, it is quite straightforward to prove that the set $\{z = 0\} \subset \mathcal{S}$ is a $\mathfrak{q}$-geodesic. Its lift to $\mathcal{N}$, denoted as $\gamma_{\mathcal{N}}$, is also a $h^{(0)}-$geodesic by also fixing the angle ϕ.

Given a function $f : \mathcal{U}_p \to \mathbb{R}$, we define its $\mathfrak{h}-$*extension* as the function $\bar{f} : \mathcal{U}_p \to \mathbb{R}$ such that

$$\bar{f}(p) = \bar{f}(q), \quad \text{if } p \in \mathcal{C}_q.$$

In other words, $\bar{f}$ is constant at each level set of ρ, equal to the value at $q \in \gamma_{\mathcal{N}}$.

With the previous definition at hand, for each $q \in \gamma_{\mathcal{N}}$ we define the $\mathcal{C}_q-$extensions of x, Ω and q. Let them be $\bar{x}, \bar{\Omega}$ and $\bar{q}$ respectively.

The three functions define a 3-metric on $\mathcal{U}_p$, $h^{(1)}$, which is T^2-symmetric,

$$h^{(1)} = e^{\bar{q}-\bar{x}-\ln\rho}(d\rho^2 + dz^2) + \rho e^{\bar{x}} d\phi^2.$$

Observe that, by hypothesis (section 2.5), $\partial_z\Omega$ and $\partial_z x$ vanish along γ (not necessarily $\partial^2_z x$ and $\partial^2_z\Omega$). Of course, $g^{(1)}$ is not a solution to Einstein equations. We will see that it is a solution to perturbed T^2-symmetric equations on γ.

Let us now compute the bounds for the distance from $h^{(1)}$ to $h^{(0)}$. In view of Lemma 5.3, and by the $z-$even symmetry imposed on the solution, we have that for every $m \geq 0$ and $j \geq 0$,

there is a uniform C such that (for further details, see [47, p. 44]),

$$|\partial_\rho^m \partial^{(j)}(e^x - e^{\bar{x}})|_{\mathfrak{h}_F} \leq C_{mj} \mathrm{diam}^m_{\mathfrak{h}_F}(\mathcal{C}_p),$$
$$|\partial_\rho^m \partial^{(j)}(e^q - e^{\bar{q}})|_{\mathfrak{h}_F} \leq C_{mj} \mathrm{diam}^m_{\mathfrak{h}_F}(\mathcal{C}_p),$$
$$|\partial_\rho^m \partial^{(j)}(\Omega - \bar{\Omega})|_{\mathfrak{h}_F} \leq C_{mj} \mathrm{diam}^m_{\mathfrak{h}_F}(\mathcal{C}_p).$$

Then, the distance between $h^{(1)}$ and $h^{(0)}$ is controlled by $\mathrm{diam}_{\mathfrak{h}_F}(\mathcal{C}_p)$.

Step (c): In this step, we prove that there is a Lewis model $g_L^{(2)}$ such that the C^j-distance to $g^{(1)}$ is controlled by the $\mathfrak{h}_F-$diameter of $\mathcal{C}_p$. First, assume that $a^* > 0$.

Let us consider the equations for a T^2-symmetric solutions, x_L and Ω_L, given by

$$\left\{ \begin{array}{rcl} x_L'' + \frac{x_L'}{\rho} & = & -e^{2x_L}(\Omega_L')^2, \\ \Omega_L'' + \frac{\Omega_L'}{\rho} & = & -2\Omega_L' x_L', \end{array} \right.$$

with initial values at $q \in \gamma$ given by

$$\left\{ \begin{array}{rcl} (\rho x_L')^2 & = & \left(\frac{|\nabla\omega|_r}{\rho_r}(q)\right)^2 e^{-2x_L} + \tilde{a}(\rho(q)), \\ \frac{e^{2x_L}}{\rho}\Omega_L' & = & -\frac{|\nabla\omega|_r}{\rho_r}(q), \end{array} \right. \qquad \left\{ \begin{array}{rcl} x_L(q) & = & \bar{x}(q), \\ \Omega_L(q) & = & \bar{\Omega}(q). \end{array} \right. \tag{5.5}$$

The solution to these equations, (x_L, Ω_L), is a Lewis model with angular momentum proportional to $\frac{|\nabla\omega|_r}{\rho_r}(p) > 0$ and constant $\tilde{a}(\rho(p)) \geq a^* > 0$ (due to monotonicity of a).

The solution has a singularity at ρ_*, cf. (3.22). We derive the position of the singularity by the initial data (5.5) and formula (3.23). Observe that in terms of $x_L(q)$ and $\Omega_L(q)$, the position of the singularity is given by

$$\rho_* = \left(\rho(e^{x_L}\Omega_L)^{1/\bar{a}}\right)|_q .$$

At each $\{p_i\}_{i\geq 0}$, we have derived in Proposition 4.6 the decays for each of the functions involved in the formula for ρ_*. We prove below that in the limit $i \to +\infty$, and this limit is bounded. Take $q_i \in \gamma \cap \mathcal{C}(\rho(p_i))$, then, in virtue of the boundary condition $\Omega(\rho = \infty) = 0$ and the fourth and fifth bounds in Proposition 4.6, we have

$$|\Omega(q_i)| = \left| \int_{+\infty}^{\rho(q_i)} \nabla_n \Omega dl \right| = \left| \int_{+\infty}^{\rho(q_i)} \frac{\rho}{\eta}\frac{\nabla_n \omega}{\eta} dl \right| \leq C_3 \int_{+\infty}^{\rho(q_i)} \frac{1}{\rho^{1+2a}} d\rho = \frac{C_3}{\rho(q_i)^{2a}},$$

for some constant C_3. Then

$$\lim_{i\to+\infty} \left(\rho(\eta\Omega)^{1/\bar{a}}\right)|_{q_i} = C_4 > 0.$$

Therefore, by taking r^* sufficiently big enough, we have that $\rho^* < \rho/(2l_*)$. Then, the position of the singularity can be taken to be outside of $\mathcal{U}_p$. We call $h^{(2)}$ the Lewis models that results from (x_L, Ω_L),

$$h^{(2)} = e^{q_L - x_L - \ln\rho}(d\rho^2 + dz^2) + \rho e^{x_L} d\phi^2.$$

Next, consider the perturbation of the previous equations, which is still an ODE along γ,

$$\begin{cases} x'' + \frac{x'}{\rho} + f_x &= -e^{2x}(\Omega')^2, \\ \Omega'' + \frac{\Omega'}{\rho} + f_\Omega &= -2\Omega' x', \end{cases}$$

by taking $f_x = \partial_z^2 x \mid_\gamma$ and $f_\Omega = \partial_z^2 \Omega \mid_\gamma$, with the same initial conditions (5.5). Then, observe that $(\bar{x}, \bar{\Omega}) \mid_\gamma$ *are* a solution of the perturbed system (since on γ they are a solution to the full equations). Both $\partial_z^2 \Omega$ and $\partial_z^2 x$ vanish in at least one point along the circle at p, since they are periodic in z and $\partial_z x = \partial_z \Omega = 0$ on γ. Then, their $C^m_{\mathfrak{h}_F}-$norms are controlled by the diameter of the transverse circles, $\mathcal{C}_p$.

Therefore, using the usual perturbation results for ODEs, for every $m, j \geq 0$

$$\begin{aligned} |\partial_\rho^m \partial^{(j)}(e^{\bar{x}} - e^{x_L})|_{\mathfrak{h}_F} &\leq C'_{mj} \mathrm{diam}^m_{\mathfrak{h}_F}(\mathcal{C}_p), \\ |\partial_\rho^m \partial^{(j)}(e^{\bar{q}} - e^{q_L})|_{\mathfrak{h}_F} &\leq C'_{mj} \mathrm{diam}^m_{\mathfrak{h}_F}(\mathcal{C}_p), \\ |\partial_\rho^m \partial^{(j)}(\bar{\Omega} - \Omega_L)|_{\mathfrak{h}_F} &\leq C'_{mj} \mathrm{diam}^m_{\mathfrak{h}_F}(\mathcal{C}_p). \end{aligned}$$

Finally, putting everything together, we obtain

$$\begin{aligned} |\partial_\rho^m \partial^{(j)}(e^{x} - e^{x_L})|_{\mathfrak{h}_F} &\leq C^*_{mj} \mathrm{diam}^m_{\mathfrak{h}_F}(\mathcal{C}_p), \\ |\partial_\rho^m \partial^{(j)}(e^{q} - e^{q_L})|_{\mathfrak{h}_F} &\leq C^*_{mj} \mathrm{diam}^m_{\mathfrak{h}_F}(\mathcal{C}_p), \\ |\partial_\rho^m \partial^{(j)}(\Omega - \Omega_L)|_{\mathfrak{h}_F} &\leq C^*_{mj} \mathrm{diam}^m_{\mathfrak{h}_F,}(\mathcal{C}_p) \end{aligned}$$

This is equivalent to (5.1) due to (5.3) and (5.4).

The case $a^* = 0$ is analogous and can be thought of as a limit when $a^* \to 0$ of the previous case (recall that the limit when the Kasner exponent goes to zero of the solutions in the family (III+) gives a solution in the family (II+), and the limit preserves the bounds).

□

5.3.3 Proof of the asymptotic behavior theorem

Having Proposition 5.2 at our disposal, the proof of Theorem 5.2 is straightforward.

Proof of Theorem 5.2. Let $(\mathcal{S}, \mathfrak{q}, x, \Omega)$ be the orbit data for a periodic stationary and axisymmetric black hole solution, with parameters $(m/L, A, J)$. Assume $a \geq 0$.

Consider the sequence of annuli $\{(\mathcal{A}_{r_i}(p'_i; 1/2, 2), \mathfrak{q}_{r_i})\}$. As we showed previously, they collapse to the segment $((1/2, 2), |\cdot|)$. Therefore, for sufficiently small constants $\epsilon_j, \epsilon_d, \epsilon_m > 0$ and sufficiently big $r_i > 0$, the conditions *1.*, *2.* and *3.* are satisfied.

Indeed, the first condition is satisfied due to the collapse. The second condition is held by the existence of the limit for a, Proposition 4.3. The third condition is a consequence of Lemma 4.1.

Since, as $i \to +\infty$, we have

$$\frac{l^i}{\bar{r}_i} \to 0, \quad \operatorname{diam}_{h^L}(\mathcal{C}(\rho)) \to 0,$$

then by (5.1) there is a unique Lewis model $(\Sigma^L, h^L, x^L, \Omega^L)$ such that the metric on the annuli converges to h^L. If $a > 0$, then the limit model is in the Lewis family (III+), and if $a = 0$, then it is in the Lewis family (II+).

The metric $\mathfrak{q}_{r_i}$ on the annuli converges to $\bar{C}\bar{\rho}^(\bar{a}^2 - 1)/2)(d\bar{\rho}^2 + dz^2)$, for some constant $\bar{C} > 0$. Then, the constant $\bar{C}$ (related to ρ_*, the position of the singularity), the angular momentum J and the value a determine a unique Lewis model. □

5.3.4 Discussion and further work

Two questions remain unanswered:

- How is a related to the original parameters $(m/L, A, J)$?
- Can it be shown that the Lewis model found satisfies Definition 3.4?

The first question is more compelling because we have no a priori knowledge of the functional relation between a and the parameters. At least a bound for the rotational energy term must be obtained to relate a with m/L and J. This will be studied in more detail in the next chapter.

The second question is of a technical nature. Following [47], we can proceed to use Proposition 5.2 as the first step (together with the collapse result) in a telescopic argument. For certain p_i, it can be shown that at a point p_i' such that $r(p_i') = l_* r_i$, the distance from the Lewis model near the solution on $\mathcal{A}_{p_i'}$ is *closer* than that on $\mathcal{A}_{p_i}$. The distance is controlled in terms of the diameter of the transverse tori (see [47, Proposition 4.2.6]). Then, by gluing the tori and taking the candidate Lewis model, we can show that Definition 3.4 holds indeed. The detailed exposition of the previous argument will be in a future work.

Chapter 6

Numerical results

In this chapter, we present and discuss the results of our numerical exploration (from [55]).

First, in section 6.1, we review the main results of our numerical exploration. Then, in section 6.2, we define the boundary conditions for the harmonic map heat flow. In particular, we introduce a new type of dynamical condition at the asymptotic region related to the Smarr identity. In section 6.3, we describe how the numerical simulations were implemented to solve the equations from the harmonic map heat flow. The results are presented in section 6.4 for two different sets of parameters. In section 6.5, we discuss further extensions of the numerical analysis. In particular, we show numerical results for the counter-rotating case where the total angular momentum is zero.

In Appendix B, we present some preliminary results concerning the numerical construction of solutions to the periodic set-up using the Inverse Scattering Method. It serves as an independent validation of our numerical solutions, although the details of this approach are still work in progress.

6.1 Overview of results

We will look for stationary states of the *harmonic map heat flow* equations (see, e.g., [54]),

$$\begin{cases} \partial_\tau \eta &= -\Delta\eta + \dfrac{|\nabla\eta|^2 - |\nabla\omega|^2}{\eta}, \\ \partial_\tau \omega &= -\Delta\omega + 2\langle\nabla\omega, \dfrac{\nabla\eta}{\eta}\rangle, \end{cases} \tag{6.1}$$

where τ is the flow time, starting from certain initial data (ω_0, η_0). Observe that we have a solution to the harmonic map at a stationary state of the heat flow.

Thus, to numerically solve the harmonic map equations, we evolve the heat flow on a finite rectangle $[0, \rho_{\text{MAX}}] \times [-L/2, L/2]$. This adds the extra difficulty of finding natural boundary conditions also at $\rho = \rho_{\text{MAX}}$, for ω and η (see Figure 6.1).

As we prove in Theorem 5.2, one expects the solutions to become asymptotically independent of z as $\rho \to \infty$ and to approach a Lewis model (in particular, one of the solutions in the family (III+) or (II+) for $L > 4m$). The problem, quite recurrent by now, is that one does not

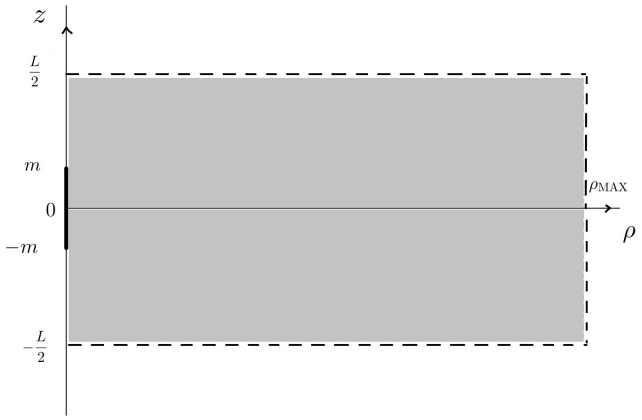

Figure 6.1: The numerical domain with the horizon indicated by the thick interval on the z-axis.

know a priori which Lewis solution shows up for the given m/L, A and J, i.e., we do not know which Kasner exponent will appear.

Now, all Lewis solutions (see section 3.3) have $\omega = wz$, so we fix $\omega(\rho_{\text{MAX}}, z) = wz$. For η, however, no such single choice is possible. We set Neumann-type boundary condition for η using that, on actual solutions, the Komar mass expression $M(\rho)$ is constant (cf. (6.6)). Then, $M(\rho_{\text{MAX}}) = M(\rho)$ easily relates $\partial_\rho \eta(\rho_{\text{MAX}})$ to η and ω at any $\rho < \rho_{\text{MAX}}$. To define the condition for η, we make use of this relation, equating $\partial_\rho \eta(\rho_{\text{MAX}})$ to the average of the Komar mass expression in the bulk set $0 < \rho < \rho_{\text{MAX}}$, see (6.6). This peculiar boundary condition for η[1] at ρ_{MAX} gave us the best numerical results with respect to a standard Neumann-type boundary condition, when considering the speed and stability of our code.

We obtain strong numerical evidence of the existence of periodic analogs of Kerr, for a wide range of parameters $(m/L, A, J)$. We show that the Komar mass M per black hole satisfies the relevant inequality,

$$M \geq \sqrt{\frac{A}{16\pi} + \frac{4\pi J^2}{A}},$$

and equality is approached when the separation between the black holes grows unboundedly and the geometry near the horizons approaches that of Kerr.

In relation with Theorem 4.1, the impossibility of a complete (at infinity) solution when $m/L > 1/4$ follows by fitting the resulting η with Lewis models. We obtained numerically the transition from super-linear to sub-linear growth for η, depending on ρ. This was a fundamental property to validate the code.

As a result of our numerical implementations in the study of Problem 1.1, and due to the simple implementation of the boundary conditions, we also study multi-horizon periodic configurations. We wrote a code that numerically solves the harmonic map equations for the case of two identical, equidistant, counter-rotating black holes and provides further evidence of the existence of solutions in the multi-horizon case.

[1] Recall that $\sigma = \ln \eta - 2 \ln \rho$ and therefore $\frac{\partial_\rho \eta}{\eta} = \frac{2}{\rho} + \partial_\rho \sigma$.

6.2 Boundary conditions for the harmonic map heat flow

Consider a periodic stationary and axisymmetric black hole solution with parameters $(m/L, A, J)$. While A and J are *physical*, the meaning of the parameter m/L is completely obscure. Given the results in chapter 3 and chapter 4, there are two clear sets of physical parameters,

1. The area A, the angular momentum J and the total energy of the system M.
2. The area A, the angular momentum J and the separation D between two consecutive black holes.

Of course, writing M or D as functions depending on $(m/L, A, J)$ is still an open problem in the stationary case, cf. section 4.3 for the static case. In the numerical approach, we take as input parameters $(m/L, A, J)$ since they can be naturally incorporated into the boundary conditions of the harmonic map equations (6.1) for η and ω. First, the area allows us to compare the numerical results with the Kerr solutions or MKN solutions. By (2.32) and Remark 2.2, if we give A as a parameter, then m is equal to the surface gravity, κ, of the horizons times $A/4\pi$. To compare with Kerr solutions, the surface gravity can be fixed using the horizon gauge (cf. Remark 2.1).

6.2.1 Boundary conditions for the fields

It will be more convenient to work with σ instead of η (this choice has some numerical advantages, see [42, 54]). We need then to provide boundary conditions for the heat flow associated with the equations (2.26) and (2.27), i.e.,

$$\begin{cases} \partial_\tau \sigma &= -\Delta\sigma - \frac{e^{-2\sigma}}{\rho^4}|\nabla\omega|^2, \\ \partial_\tau \omega &= -\Delta\omega + 2\langle\nabla\omega, \nabla(\sigma + 2\ln\rho)\rangle. \end{cases} \tag{6.2}$$

As we look for metrics periodic in z, we keep appropriate periodicity conditions on the top and bottom lines $\{\rho \geq 0,\ z = \pm L/2\}$ of the numerical domain. The equations for ω and η must be supplied with boundary data on both boundaries $\{\rho = 0\}$ and $\{\rho = \rho_{\text{MAX}}\}$.

The first boundary contains the horizon, from now on denoted as $\mathcal{H}$, and two components of the axis $\mathcal{A}$, which is the complement of $\mathcal{H}$. Here, the boundary conditions arise from the natural conditions that η and ω must verify on horizons and axes (cf. Definition 2.15) and from fixing the values of A and J. The angular momentum J is set by specifying Dirichlet data for ω on the axis. In contrast, the area A is set by specifying the limit for σ/σ_0 at the poles $z = \pm m$ (here σ_0 is from the reference Kerr solution for which $\kappa = \kappa_K$).

Boundary conditions on $\mathcal{A}$ and $\mathcal{H}$. First, recall that ω has to satisfy

$$\omega\big|_{\mathcal{A}_+} = 4J, \quad \omega\big|_{\mathcal{A}_-} = -4J,$$
$$\partial_\rho\omega\big|_{\mathcal{H}} = 0.$$

These conditions are minimal in that they guarantee that the total angular momentum of the solution is J and the regularity of ω at the horizon.

Observe that the Dirichlet-type condition on the axis imposes a non-periodic ω. This is consistent with the fact that it is *locally* the potential of the twist θ^ξ, see Definition 2.1. It enters the metric through Ω, which *is* periodic under these boundary conditions. Similarly, the second condition, of Neumann type, can be obtained by demanding the spacetime smoothness of $\Omega = W/\eta$, linked to ω by (2.20).

The boundary conditions for σ are

$$\begin{aligned}
&\partial_\rho \sigma\big|_{\mathcal{A}} = 0,\\
&\partial_\rho(\sigma + 2\ln\rho)\big|_{\mathcal{H}\setminus\partial\mathcal{H}} = 0,\\
&\lim_{(\rho,z)\to(0,\pm m)} \frac{\sigma}{\sigma_0} = 1,
\end{aligned}$$

where σ_0 is the reference Kerr solution given A, J.

The first condition is necessary for the final metric to be regular at the axis. The second condition is the prescribed singularity at the horizon. For the third condition, recall that for Kerr

$$m = \sqrt{\frac{A}{16\pi}}\frac{1-(8\pi J/A)^2}{\sqrt{1+(8\pi J/A)^2}}.$$

As mentioned in the previous section, this is the choice of m we make when constructing the computational domain in Weyl coordinates. On the other hand, the condition (6.2.1) enforces γ on $\mathcal{H}$ (which is constant) to be also that of Kerr,

$$\gamma_{\mathcal{H}} = \gamma_{0,\mathcal{H}}.$$

The computation of this formula can be found in section A.2. As $e^{-\gamma}|_{\mathcal{H}} = \kappa$, we deduce that

$$\text{Area}(\mathcal{H}) = 2\pi\int_{-m}^{m} e^{\gamma} dz = 2\pi\int_{-m}^{m}\frac{1}{\kappa}dz = \frac{4\pi m}{\kappa} = A.$$

So, the area of the horizon is indeed A. This prescribes an indirect normalization of the Killing vector field ∂_t outside the ergoregion.

Boundary conditions at ρ_{MAX}. Since we expect a Lewis asymptotic model and the Komar angular momentum to be J (Theorem 5.2), the asymptotic behavior of ω is set as the one in Lewis models (cf. section 3.3),

$$\omega(\rho_{\text{MAX}}, z) = (8J/L)z.$$

The boundary condition for σ is more delicate to define and we motivate it as follows. Given a stationary solution to the harmonic heat flow (6.2), i.e. a solution to (2.26)-(2.27), one can compute a renormalized Komar Mass M (renormalizing it per black hole) by a straightforward

computation from (2.28), giving the following expression,

$$M(\rho) = \left[\frac{1}{4}\int_{-L/2}^{L/2}(-\rho\partial_\rho\sigma + \Omega\partial_z\omega)dz\right]_\rho, \tag{6.3}$$

which we know indeed to be $\rho-$independent under the assumption that (σ,ω) are solutions, i.e., $M(\rho)\equiv M$. For the Lewis solutions in the family (III+) (and similarly for the case (II+)) we have $\Omega, \partial_z\Omega \to 0$ as $\rho\to\infty$, $\rho\partial_\rho\sigma \to a-1$ as $\rho\to\infty$, and $\omega = wz$ is bounded, so we obtain,

$$M = \frac{L}{4}(1-a).$$

Recall that a is the limiting value of the integral $a(\rho)$, cf. Proposition 4.3. Thus, the Kasner exponent $\alpha = 1-a$ is equal to $4M/L$. Hence, for any solution asymptotically like (III+) or II+, we have the decay

$$\partial_\rho\sigma\big|_\rho = -\frac{4M}{L\rho} + o(1/\rho), \quad \rho\gg 1.$$

Therefore, for a solution, we have a Neumann-like type of boundary condition

$$\partial_\rho\sigma\big|_{\rho_{\text{MAX}}} = -\frac{4M}{L\rho_{\text{MAX}}}, \quad \text{as} \quad \rho_{\text{MAX}}\to\infty. \tag{6.4}$$

This suggests taking a boundary condition that depends on the renormalized Komar mass.

Building such conditions faces a couple of problems. First, we do not know the a priori dependence of M with $(m/L, A, J)$. Second, since we are evolving a harmonic map heat flow, at any time $\tau\geq 0$, the integral in (6.3) associated to (σ,ω) at τ is not necessarily constant as a function of ρ. Moreover, the function Ω is not well defined since the integrability conditions (2.20) do not hold. Therefore, we have to define $M(\rho,\tau)$ to use (6.4) as a boundary condition. By integrating by parts the last term in (6.3), and using (2.20), we have the candidate

$$M(\rho,\tau) = 2\Omega(\rho,\tau)J\Big|_{z=-L/2} - \frac{1}{4}\int_{-L/2}^{L/2}(\rho\partial_\rho\sigma + \frac{\rho}{\eta^2}\partial_\rho\omega\omega)dz,$$

where $\Omega(\rho,\tau)$ is prescribed to be

$$\Omega(\rho,\tau) = \int_{\rho_{\text{MAX}}}^{\rho}\frac{\rho'}{\eta^2}\partial_z\omega d\rho', \quad \Omega(\rho_{\text{MAX}},z) = 0, \tag{6.5}$$

with the functions evaluated at $z=-L/2$. That is, Ω is the integration from ρ_{MAX} to ρ of (2.20) with boundary condition $\Omega\,|_{\rho_{\text{MAX}}}(z) = 0$.

Observe that *if* $(\sigma(\tau),\omega(\tau))$ converge to a solution (σ,ω), *then* $M(\rho,\tau)$ converges to a constant function (by taking ∂_ρ in (6.3) and computing). Considering this, a natural dynamical condition arises by taking the *ρ-average* of $M(\rho,\tau)$ over the numerical domain. At each time step τ, we define the mean renormalized Komar mass as follows,

$$\overline{M}(\tau) := \overline{M(\rho,\tau)},$$

which in particular links the values of M near the axis with those far away. We use a simple, uniform average in the interior of the interval $(0, \rho_{\text{MAX}})$[2]. Then, our boundary condition for σ at ρ_{MAX} is given by,

$$\partial_\rho \sigma(\tau)\big|_{\rho_{\text{MAX}}} = -\frac{4\overline{M}(\tau)}{L\rho_{\text{MAX}}}. \tag{6.6}$$

It is essential to notice that there is no reference to any specific Kasner exponent for the asymptotic model in this condition. The only assumption is $z-$independence as $\rho \to +\infty$. Such universality in the asymptotic condition for σ was, in part, our motivation for its construction, and we will discuss it further in section 6.5 when applying the code to multiple horizons per period.

Quadrature integration for Ω, q and γ. It remains to fix the boundary conditions for integrating the quadratures (2.20) and (2.22). For Ω, we impose

$$\Omega\big|_{\rho_{\text{MAX}}} = 0,$$

which is the natural condition for the asymptotic models and also consistent with (6.5). The boundary condition for q is just the vanishing of the function at one point in $\mathcal{A}$. As it is explained in subsection 2.5.3, the symmetries on σ and ω and the integrability equations (2.22) imply this same condition holds at any other point of the axis. Then, we will have no struts. This is also a convenient numerical check test once the solutions are computed.

Finally, the function γ is found via equation $\gamma = q + \ln\rho + \sigma$. A valid check for the numerical study is to compute the difference,

$$|A - 4\pi m e^{\gamma_{\mathcal{H}}}|,$$

once a solution is found. It should be zero in the ideal case where the final output is an exact solution.

6.2.2 Initial data for the harmonic map heat flow

We will call *seed* the initial condition at $\tau = 0$ for the heat flow. In particular, the seed should contain the prescribed singular behaviors of the solutions at the horizons to absorb the singularities. Let us decompose σ and ω as follows (see [54]): we split them as a sum of known solutions to the non-periodic problem plus a perturbation $\bar{\sigma}, \bar{\omega}$. In the case of a single horizon per period, the sum of known solutions can be computed in the same fashion as the function σ_{MKN} was defined in [1,2] (cf. (1.14)): as a series of superimposed solutions. Let $\sigma_0(\rho, z)$ and $\omega_0(\rho, z)$ be the solutions to the asymptotically flat Kerr black hole with momentum J and area A, with horizon located at $\{|z| < m\}$, and define

$$\begin{aligned} \sigma(\rho, z; \tau) =& \sigma_0(\rho, z) + \sigma_r(\rho, z) + \bar{\sigma}(\rho, z; \tau), \\ \omega(\rho, z; \tau) =& \omega_0(\rho, z) + \omega_r(\rho, z) + \bar{\omega}(\rho, z; \tau), \end{aligned} \tag{6.7}$$

[2] In our numerical codes, this means taking a uniform average of the values corresponding to the interior points of the discretized ρ coordinate, excluding just the values at the boundary $\rho = 0$ and the two grid points next to it, and the values at the outer boundary $\rho = \rho_{\text{MAX}}$.

where,

$$\sigma_r(\rho,z) = C + \sum_{n=1}^{\infty}\left(\sigma_0(\rho,z-nL,J) + \sigma_0(\rho,z+nL,J) - \frac{4M_0}{nL}\right), \tag{6.8}$$
$$\omega_r(\rho,z) = \sum_{n=1}^{\infty}\left(\omega_0(\rho,z-nL,J) + \omega_0(\rho,z+nL,J)\right),$$

and where C is a constant such that $\sigma_r \mid_{\partial\mathcal{H}} = 0$, i.e. its value at the poles is zero. The constant $M_0 = \sqrt{\frac{A}{16\pi} + \frac{4\pi J^2}{A}}$ is the ADM mass of the Kerr solution (σ_0, ω_0). The terms $4M_0/nL$ are needed for the series to converge at each point (ρ, z) (since asymptotically, each term goes as $-2M_0/\sqrt{(x-nL)^2+\rho^2}$, and therefore we need to cancel out this divergent term, as in [2]). In our actual numerical calculations, we use a cut-off value $N_d \gg 1$ for n, which can be thought of as the number of "domains" we stack on both the top and below the central domain.

We expect $(\bar{\sigma}(\rho,z;\tau), \bar{\omega}(\rho,z;\tau))$ to be regular throughout the evolution. By inserting the decomposition (6.7) into (6.2), and using the fact that the pair (σ_0, ω_0) is a solution, we obtain the evolution equations for $\bar{\sigma}$ and $\bar{\omega}$

$$\partial_\tau\bar{\sigma} = \Delta\bar{\sigma} + \Delta\sigma_r + \frac{e^{-2\sigma_0}|\nabla\omega_0|^2}{\rho^4}\left(e^{-2(\bar{\sigma}+\sigma_r)} - 1\right)$$
$$+ \frac{e^{-2(\sigma_0+\sigma_r+\bar{\sigma})}}{\rho^4}\left(|\nabla\omega_r|^2 + |\nabla\bar{\omega}|^2 + 2\left(\partial_i\omega_r\partial^i\omega_0 + \partial_i\omega_r\partial^i\bar{\omega} + \partial_i\bar{\omega}\partial^i\omega_0\right)\right), \tag{6.9}$$

$$\partial_\tau\bar{\omega} = \Delta\bar{\omega} + \Delta\omega_r - \frac{4}{\rho}\left(\partial_\rho\omega_r + \partial_\rho\bar{\omega}\right) - 2\Big(\partial_i\omega_0\partial^i\sigma_r$$
$$+\partial_i\omega_0\partial^i\bar{\sigma} + \partial_i\omega_r\partial^i\sigma_0 + \partial_i\omega_r\partial^i\sigma_r + \partial_i\omega_r\partial^i\bar{\sigma} + \partial_i\bar{\omega}\partial^i\sigma_0 + \partial_i\bar{\omega}\partial^i\sigma_r + \partial_i\bar{\omega}\partial^i\bar{\sigma}\Big). \tag{6.10}$$

where summation convention was used for the index i that runs from 1 to 2 (i.e., representing ρ and z). Equations (6.9) and (6.10) are the equations that we solve numerically. The boundary conditions for $(\bar{\sigma}, \bar{\omega})$ can be read off from the conditions for (ω, σ) (explained in the previous section). For $\bar{\omega}$ we have

$$\bar{\omega}(\rho_{\mathrm{MAX}}) = 0, \quad \partial_\rho\bar{\omega} \mid_{\mathcal{H}} = 0, \quad \bar{\omega} \mid_{\mathcal{A}} = 0, \tag{6.11}$$

since $\omega_0 + \omega_r$ already satisfies asymptotically the linear behavior for ω (see next subsection). For $\bar{\sigma}$, the conditions at the axis are

$$\partial_\rho\bar{\sigma} \mid_{(\mathcal{A}\cup\mathcal{H})\setminus\partial\mathcal{H}} = 0, \quad \bar{\sigma} \mid_{\partial\mathcal{H}} = 0. \tag{6.12}$$

The asymptotic condition is given by

$$\partial_\rho\bar{\sigma}\big|_{\rho_{\mathrm{MAX}}} = -\frac{4\overline{M}^{\rho}(\tau)}{L\rho_{\mathrm{MAX}}} - \overline{\partial_\rho(\sigma_0+\sigma_r)}^{z}\big|_{\rho_{\mathrm{MAX}}} \equiv \beta, \tag{6.13}$$

where we are denoting by $\overline{X}^x$ the average along x coordinate of the variable X. This expression needs further explanation. The term $\partial_\rho(\sigma_0+\sigma_r)$ is not $z-$independent, since the series for σ_r is truncated, and therefore we take its average on z. We will call β the dynamical quantity given by the right-hand side of equations (6.13).

At $\tau=0$, we initialize $(\bar{\sigma}(\tau=0),\bar{\omega}(\tau=0))$ as two vanishing functions, $(0,0)$. Observe that they satisfy trivially the boundary conditions at the axis and horizon. Of course, as the flow evolves $(\bar{\sigma}(\tau),\bar{\omega}(\tau))\neq(0,0)$[3].

6.2.3 Some comments on the seed

The infinite superposition of solutions in equation (6.8) resembles the static case (1.14). The difference in the stationary case is that a perturbation has to be present to account for the non-linearity of the problem. In this subsection, we present some properties of the seed similar to those of the static case.

Definition 6.1. *We will denote the seeds as $\sigma_s := \sigma_0+\sigma_r$ and $\omega_s := \omega_0+\omega_r$.*

Asymptotic behavior

The function σ_s can be shown to be asymptotically Kasner with Kasner parameter $\alpha_0 = 4M_0/L$.

Proposition 6.1. *The asymptotic behavior of (σ_s,ω_s) is given by*

$$\sigma_s = -\frac{4M_0}{L}\ln\rho + q_0(z,\rho), \qquad \omega_s = \frac{8J}{L}z + r_0(z,\rho), \qquad (\rho\to+\infty),$$

where $q_0(z,\rho)$ is a subleading function with respect to $\ln\rho$ and $r_0(z,\rho)$ is a function of order $o(1)$ in z and exponential decay in ρ. Then, the asymptotic behavior of the pair (σ_s,ω_s) is that of a Lewis' model, with exponent $\frac{4M_0}{L}$.

Proof. The proof of this result is in the same lines as [2, Theorem 4], using the expressions for σ_0 and ω_0 (cf. Appendix A). The verification that it is indeed a Lewis' model has to be carried for large ρ in the series, neglecting the value of z, and showing that the equation (3.15) indeed holds for σ_s. □

Observe that $\alpha_0=\frac{4M_0}{L}$ is not necessarily the *final* Kasner parameter of the stationary solution since the rotational energy contributes in a non-negligible quantity.

Behavior at the axis

Here we provide a close formula, akin to (4.11), for the value of σ_s at the axis.

Proposition 6.2. *The expression for $e^{-\sigma_s}$ at the points $\{(z,\rho):|z|>m,\rho=0\}$ is*

$$e^{-\sigma_s}(z,0) = \frac{e^{\frac{4\gamma M_0}{L}}}{\pi^2}\frac{\Gamma^2\left(\frac{z+M_0}{L}\right)}{\Gamma^2\left(\frac{z-M_0}{L}\right)}\csc^{-2}\left(\pi\frac{z+M_0}{L}\right)\frac{\sin\left(\pi\frac{z-m}{L}\right)\sin\left(\pi\frac{z+m}{L}\right)}{\sin^2\left(\pi\frac{z+M_0}{L}\right)+\sinh^2\left(\frac{a}{L}\right)},$$

[3] Except if we take $J=0$: in that case the seed is already a solution.

and 0 *otherwise.*

Proof. The function $e^{-\sigma_s}$ can be trivially extended to the horizon, taking the value 0, due to the prescribed singular behavior for σ_s (cf. Definition 2.15). Given the parameters M_0 and $a = J/M_0$, we have

$$e^{-\sigma_0}(z,0) = \frac{z^2 - M_0^2 + a^2}{(z+M_0)^2 + a^2}, \quad z \geq m.$$

For $a = 0$, the static case, we obtain

$$e^{-\sigma_{Sch}}(z,0) = \frac{z - M_0}{z + M_0}.$$

Let us review the derivation of (4.11) first. Upon imposing periodicity and rewriting the series, we have

$$e^{-\sigma_{KNM}}(z,0) = \frac{(z-M_0)/L}{(z+M_0)/L} \prod_{n=1}^{\infty} \frac{(z-M_0)/L + n}{(z+M_0)/L + n} \frac{(z-M_0)/L - n}{(z+M_0)/L - n} e^{\frac{4M_0}{nL}}.$$

By using Weierstrass's identity

$$\Gamma(\zeta) = \frac{e^{-\gamma\zeta}}{\zeta} \prod_{n=1}^{\infty} \frac{n}{n+\zeta} e^{\zeta/n},$$

and therefore we have the identity

$$\frac{\Gamma(\frac{z+M_0}{L})\Gamma(1-\frac{z-M_0}{L})}{\Gamma(\frac{z-M_0}{L})\Gamma(1-\frac{z+M_0}{L})} = e^{-\gamma 4M_0/L} \frac{\frac{z-M_0}{L}(1-\frac{z+M_0}{L})}{\frac{z+M_0}{L}(1-\frac{z-M_0}{L})} \prod_{n=1}^{\infty} \frac{(n+\frac{z-M_0}{L})(n+1-\frac{z+M_0}{L})}{(n+\frac{z+M_0}{L})(n+1-\frac{z-M_0}{L})} e^{-4M_0/nL}.$$

We thus obtain the expression in [2]. For $a \neq 0$, the infinite product results

$$e^{-\sigma_s}(z,0) = \frac{z^2 - M_0^2 + a^2}{(z+M_0)^2 + a^2} \prod_{n=1}^{\infty} \frac{(z+nL)^2 - M_0^2 + a^2}{(z+nL+M_0)^2 + a^2} \frac{(z-nL)^2 - M_0^2 + a^2}{(z-nL+M_0)^2 + a^2} e^{\frac{4M_0}{nL}}.$$

We rewrite this product as

$$e^{-\sigma_s}(z,0) = \prod_{n=-\infty}^{+\infty} \frac{1 - \frac{(m/L)^2}{(n+z/L)^2}}{1 + \frac{(a/L)^2}{(n+(z+M_0)/L)^2}} \frac{1}{\left(1 + \frac{M_0/L}{n+z/L}\right)^2} e^{\frac{4M_0}{nL}}.$$

Next, we multiply and divide by $\prod_{n=-\infty}^{+\infty} \frac{1-\left(\frac{M_0/L}{n+z/L}\right)^2}{1-\left(\frac{M_0/L}{n+z/L}\right)^2}$. Then

$$e^{-\sigma_s}(z,0) = \prod_{n=-\infty}^{+\infty} \frac{1 - \frac{(m/L)^2}{(n+z/L)^2}}{1 + \frac{(a/L)^2}{(n+(z+M_0)/L)^2}} \frac{1}{1 - \left(\frac{M_0/L}{n+z/L}\right)^2} \frac{1 - \frac{M_0/L}{n+z/L}}{\left(1 + \frac{M_0/L}{n+z/L}\right)} e^{\frac{4M_0}{nL}}.$$

Observe that the last two factors are the same as in the MKN solutions, while the first two correspond to contributions due to the non-zero angular momentum.

Using the following identities [71]

$$\prod_{k\in\mathbb{Z}}\left(1-\frac{a^n}{(k+b)^n}\right)=\csc^n(b\pi)\prod_{k=0}^{n-1}\sin(\pi(b-ae^{2k\pi i/n})),$$

$$\prod_{k\in\mathbb{Z}}\left(1+\frac{a^n}{(k+b)^n}\right)=\csc^n(b\pi)\prod_{k=0}^{n-1}\sin(\pi(b-ae^{(2k+1)\pi i/n})),$$

and after a long but straightforward calculation we have

$$e^{-\sigma_s}(z,0)=e^{\frac{4\gamma M_0}{L}}\frac{\Gamma\left(\frac{z+M_0}{L}\right)\Gamma\left(1-\frac{z-M_0}{L}\right)}{\Gamma\left(\frac{z-M_0}{L}\right)\Gamma\left(1-\frac{z+M_0}{L}\right)}\csc^{-2}\left(\pi\frac{z+M_0}{L}\right)\times$$
$$\times\frac{\sin\left(\pi\frac{z-m}{L}\right)\sin\left(\pi\frac{z+m}{L}\right)}{\sin\left(\pi\frac{z+M_0-ai}{L}\right)\sin\left(\pi\frac{z+M_0+ai}{L}\right)\sin\left(\pi\frac{z-M_0}{L}\right)\sin\left(\pi\frac{z+M_0}{L}\right)}$$

By Euler's reflection formula,

$$\Gamma(1-\zeta)\Gamma(\zeta)=\frac{\pi}{\sin(\pi\zeta)},\quad \zeta\neq\mathbb{Z},$$

we can rewrite the expression above to obtain

$$e^{-\sigma_s}(z,0)=\frac{e^{\frac{4\gamma M_0}{L}}}{\pi^2}\frac{\Gamma^2\left(\frac{z+M_0}{L}\right)}{\Gamma^2\left(\frac{z-M_0}{L}\right)}\csc^{-2}\left(\pi\frac{z+M_0}{L}\right)\frac{\sin\left(\pi\frac{z-m}{L}\right)\sin\left(\pi\frac{z+m}{L}\right)}{\sin\left(\pi\frac{z+M_0-ai}{L}\right)\sin\left(\pi\frac{z+M_0+ai}{L}\right)}.$$

The denominator of the last factor can be rewritten as

$$e^{-\sigma_s}(z,0)=\frac{e^{\frac{4\gamma M_0}{L}}}{\pi^2}\frac{\Gamma^2\left(\frac{z+M_0}{L}\right)}{\Gamma^2\left(\frac{z-M_0}{L}\right)}\csc^{-2}\left(\pi\frac{z+M_0}{L}\right)\frac{\sin\left(\pi\frac{z-m}{L}\right)\sin\left(\pi\frac{z+m}{L}\right)}{\sin^2\left(\pi\frac{z+M_0}{L}\right)+\sinh^2\left(\frac{a}{L}\right)},$$

showing that, indeed, it does not vanish on the domain $|z|>m$. □

6.3 Numerical Implementation

This section explains the numerical implementation based on [55]. We use a grid adapted to a finite computational region where the Weyl-Papapetrou coordinates range as follows,

$$(\rho,z)\in[0,\rho_{\text{MAX}}]\times[-L/2,L/2].$$

We use an $N_\rho+1$-point Chebyshev grid in the ρ direction and a uniform grid of N_z points, which are semi-displaced with respect to the boundaries $z=\pm L/2$, in the z direction. Along

this section, we use sub-indexes to identify grid points and grid values:

$$\begin{aligned} \rho_i &= \frac{1}{2}\rho_{\text{MAX}}\left(1-\cos\left(\frac{\pi}{N_\rho}i\right)\right) \quad i=0,...,N_\rho, \\ z_j &= -\frac{L}{2}+\frac{L}{N_z}\left(j+\frac{1}{2}\right), \quad j=0,...,N_z-1. \end{aligned} \tag{6.14}$$

Observe that the symmetry axis, $\{\rho=0\}$, is included in the grid while the axis $\{z=0\}$ is not. Also, the z-grid is defined so that the poles $H\cap\mathcal{A}$ are at the middle of two consecutive grid points. See Figure 6.2 as a reference.

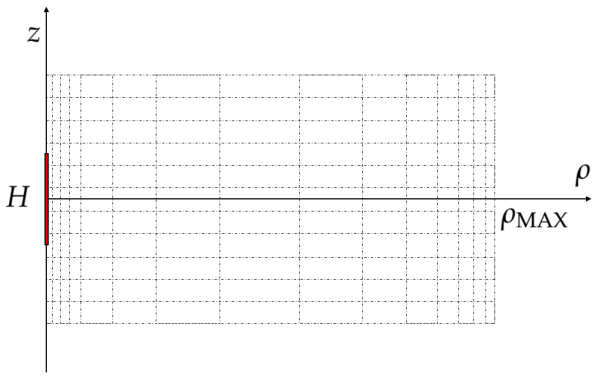

Figure 6.2: Schematic representation of the $\rho-z$ grid defined. Observe that the poles $H\cap\mathcal{A}$ are in the middle of two consecutive grid points.

Derivatives with respect to ρ are approximated by the derivatives of the polynomial interpolation on the Chebyshev grid. In contrast, derivatives with respect to z are approximated as the derivatives of the standard Fourier interpolation on the uniform grid. We use pseudo-spectral and spectral collocation methods in ρ and z, respectively.

We wrote two independent versions of Python codes to conduct the numerical computations to cross-check the results. The implementation of the spectral method is through the standard `rfft` routines provided by `NumPy`, while for the pseudo-spectral derivatives and integrals, we tried various matrix implementations [72–74] that produce no significant differences between them. The values of the analytic expressions from the Kerr solution and their derivatives were obtained symbolically by using the Python package `SymPy` and `Maple`.

Every solution to our problem is obtained by evolving the parabolic flow (6.9)-(6.10), with stopping time selected under certain criteria discussed below. The singular behavior of σ at H, and the starting point for the evolution of the parabolic flow, are handled via the splitting of σ and ω as in equation (6.7) with the introduction of the seed (σ_s,ω_s). That is, the initial value for $\bar{\sigma}$ and $\bar{\omega}$ is always taken as zero, and the boundary conditions are given by equations (6.11)–(6.13).

A particular numerical problem is defined once the following input parameters are specified:

- the values of the physical parameters $(m/L, A, J)$,
- the value of N_d, which amounts to the number of periods we stack to build the seed,

- the values of the grid input: ρ_{MAX}, N_ρ and N_z.

As explained before, we choose the values of L judiciously so that the poles fall in the middle of two consecutive grid points at $\rho = 0$. Section 6.4 shows the precise values used in our runs.

The time evolution for the parabolic flow is implemented with Euler's method. One could argue that Euler's method is a low-precision method for a parabolic flow with these features. However, it is explicit and simple to implement, and, more importantly, we are only seeking the final stationary solutions of the parabolic equations. All time variations at each final stationary state go to zero together with the associated truncation error. Thus, we are not interested in the precision along the time evolution. Near the stationary state, the truncation error is dominated by that of the space discretization. Of course, the time step is subordinated to the grid sizes to always obtain a numerically stable scheme. The closer to the symmetry axis, the stricter the Courant-Friedrichs-Lewy (CFL) condition becomes since the Chebyshev mesh size gets smaller and the derivatives of various functions involved are larger. Since the smallest spatial step was $\delta\rho \approx 10^{-2}$, a time step $\delta\tau = 10^{-4}$ was suitable in most of our runs.

Numerical handle of the boundary conditions. Let us denote the grid functions as

$$\bar{\sigma}_{i,j}(\tau) = \bar{\sigma}(\rho_i, z_j, \tau), \quad \text{and} \quad \bar{\omega}_{i,j}(\tau) = \bar{\omega}(\rho_i, z_j, \tau),$$
$$i = 0, \ldots, N_\rho, \quad j = 0, \ldots, N_z - 1,$$

and the pseudo-spectral derivative matrix associated with the Chebyshev ρ grid as

$$D_{i,k}, \quad i, k = 0, \ldots, N_\rho.$$

Given the grid functions at time τ, a single Euler step determines both grid functions at time $\tau + \delta\tau$ in all grid points with $1 \leq i \leq N_\rho - 1$. Periodicity in z is an intrinsic part of the implementation. The values at $i = 0$ (axis and horizon) and $i = N_\rho$ (outer boundary) at time $\tau + \delta\tau$ are determined by the following boundary conditions.

1. $\bar{\omega}_{N_\rho,j}(\tau + \delta\tau) = 0$ for all j (homogeneous Dirichlet condition for $\bar{\omega}$ at ρ_{MAX}).

2. $\bar{\omega}_{0,j}(\tau + \delta\tau) = 0$ for all j such that $z_j \in \mathcal{A}$ (homogeneous Dirichlet condition for $\bar{\omega}$ at the axis).

3. Solve $\sum_{k=1}^{N_\rho} D_{0,k}\bar{\omega}_{k,j}(\tau + \delta\tau) = 0$ for $\bar{\omega}_{0,j}(\tau + \delta\tau)$, for those j such that $z_j \in \mathcal{H}$ (homogeneous Neumann condition for $\bar{\omega}$ on the horizon).

4. $\bar{\sigma}_{0,j}(\tau + \delta\tau)$ and $\bar{\sigma}_{N_\rho,j}$ are determined by solving a 2×2 system that implements the homogeneous Neumann condition for $\bar{\sigma}$ at the axis and the dynamical inhomogeneous Neumann condition for $\bar{\sigma}$ at the outer boundary $\rho = \rho_{\text{MAX}}$. For each value of j the system is

$$\begin{pmatrix} D_{0,0} & D_{0,N_\rho} \\ D_{N_\rho,0} & D_{N_\rho,N_\rho} \end{pmatrix} \begin{pmatrix} \bar{\sigma}_{0,j}(\tau + \delta\tau) \\ \bar{\sigma}_{N_\rho,j}(\tau + \delta\tau) \end{pmatrix} = \begin{pmatrix} c \\ d \end{pmatrix}$$

where the inhomogeneity is

$$c = -\sum_{i=1}^{N_\rho - 1} D_{0,i}\bar{\sigma}_{i,j}(\tau + \delta\tau),$$
$$d = -\sum_{i=1}^{N_\rho - 1} D_{N_\rho,i}\bar{\sigma}_{i,j}(\tau + \delta\tau) + \beta,$$

where β is the dynamical value given by the right-hand side of equation (6.13).

5. Finally, to keep the homogeneous Dirichlet condition for $\bar{\sigma}$ at the poles, we compute the (minimal) violation $\bar{\sigma}_{\text{pole}}$ as the average of the $\bar{\sigma}(\tau + \delta\tau)$ values at the two nearest neighbor grid points on $\rho = 0$ to any of the poles, and subtract this value from $\bar{\sigma}(\tau + \delta\tau)$ on the whole grid.

The evolution of the parabolic flow approaches the stationary state only in an asymptotic manner. To measure the distance to the stationary point, we compute the L^2 norm of the right-hand side equations (6.9),(6.10). This is an absolute measure of the "error". Then, we compute the relative errors

$$\varepsilon_{\bar{\sigma}} = \frac{\|\text{rhs}(\bar{\sigma})\|}{\|\bar{\sigma}\|}, \quad \varepsilon_{\bar{\omega}} = \frac{\|\text{rhs}(\bar{\omega})\|}{\|\bar{\omega}\|},$$

$$\varepsilon_{\sigma} = \frac{\|\text{rhs}(\bar{\sigma})\|}{\|\sigma\|}, \quad \text{and} \quad \varepsilon_{\omega} = \frac{\|\text{rhs}(\bar{\omega})\|}{\|\omega\|}.$$

Finally, the quadrature equations (2.20)–(2.21) are implemented by standard spectral `rfft` routines along z direction and Clenshaw-Curtis integration along ρ direction. The choice of N_z to be such that the poles $H \cap \mathcal{A}$ are between two consecutive grid points is to avoid catastrophic cancellations in the computation of such quadrature equations since, at the poles, both the z-derivatives and the ρ-derivatives of σ diverge as z^{-k} and ρ^{-k}.

6.4 Results

In this section, we present two series of simulations computed with our code for two different values of angular momentum: $J = 1/4$ and $J = 1/2$. For the case $J = 1/4$, we present and analyze several aspects of the solutions obtained in detail. For the case $J = 1/2$, not to be redundant, we simply show a table with some relevant quantities computed. We choose to compute solutions whose horizon area is $A = 16\pi$. Thus, recalling that κ is the Kerr temperature given A and J, the horizon semi-length becomes

$$m = \frac{4 - J^2}{2\sqrt{4 + J^2}}.$$

In the particular cases presented here, $m = 0.9095$ for $J = 1/2$ and $m = 0.9768$ for $J = 1/4$. The various solutions in each series correspond to different values of the parameter L, that we choose as

$$L = \frac{N_z}{N_h} m,$$

where N_h is the number of z-grid points inside each horizon. In all cases, the computational domain has $\rho_{\text{MAX}} = 40$, and the computing grid is defined with $N_\rho = 79$ and $N_z = 100$ (see (6.14)).

6.4.1 First series: $J = 1/4$

Convergence of the parabolic flow and regularity of the solution. The convergence of the parabolic flow to a stationary state is slow. For all the solutions in this series, we stopped the flow after computing 8×10^6 steps with $\delta\tau = 10^{-4}$, where we found that the relative errors $\varepsilon_{\bar{\sigma}}$ and $\varepsilon_{\bar{\omega}}$ are comparably small. Typical plots of $\varepsilon_{\bar{\sigma}}$ and $\varepsilon_{\bar{\omega}}$ along the evolution of the flow are shown in Figure 6.3, in logarithmic scale.

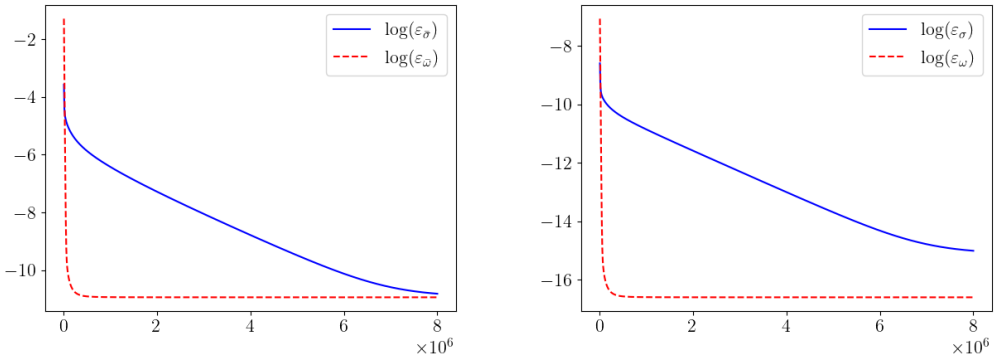

Figure 6.3: Convergence of the parabolic flow to stationary state as a function of time steps for the solution with $N_h = 40$ in Table 6.1.

We now check that $\rho_{\text{MAX}} = 40$ defines a computational domain that is large enough so as not to alter significantly the asymptotic behavior of the solutions (in the spirit explained at the end of section 6.2). To this end, we compute some solutions using $\rho_{\text{MAX}} = 60$ and compare the results. The most sensitive function to compare is $\bar{\sigma}$. In Figure 6.4 we show the plots of $\bar{\sigma}(\rho, z = 0)$ (i.e., we plot $\bar{\sigma}$ on the geodesic with image $\{z = 0\}$) for the case $L = 6.9770$. It is clear that the difference between both solutions is not significant.

Also, the regularity of the solution at this final time is checked by computing $\Delta q = q(0, L/2) - q(0, -L/2)$ (cf. subsection 2.5.3). This is done by integrating on a path around the horizon from just above the upper pole to just below the lower pole. As can be seen, the violation of regularity turns out to be extremely small. The final values of the relative errors for all the runs in this series, together with the values of Δq, are shown in table 6.1.

We choose the run with $L = 4.8839$ (corresponding to $N_h = 40$) as an example to show the solution plots and relevant functions. Figure 6.5 shows the plots of $\bar{\sigma}$, $\bar{\omega}$, σ and ω.

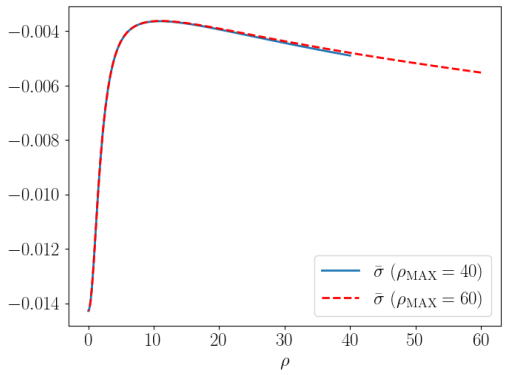

Figure 6.4: Plot of $\bar{\sigma}(z=0)$ when computed using two values of ρ_{MAX} for the case $L = 6.9770$.

N_h	L	$\varepsilon_{\bar{\sigma}}$	$\varepsilon_{\bar{\omega}}$	ε_{σ}	ε_{ω}	Δq
22	8.8798	2.19×10^{-6}	1.40×10^{-6}	7.94×10^{-8}	3.22×10^{-9}	-6.66×10^{-15}
28	6.9770	2.21×10^{-5}	4.83×10^{-6}	1.31×10^{-7}	1.29×10^{-8}	-4.17×10^{-14}
34	5.7457	2.46×10^{-5}	1.06×10^{-5}	2.34×10^{-7}	3.25×10^{-8}	-5.10×10^{-14}
40	4.8839	2.01×10^{-5}	1.78×10^{-5}	3.04×10^{-7}	6.19×10^{-8}	-1.50×10^{-13}
46	4.2468	1.59×10^{-5}	2.62×10^{-5}	3.84×10^{-7}	1.03×10^{-7}	2.49×10^{-14}
50	3.9071	1.47×10^{-5}	3.27×10^{-5}	4.89×10^{-7}	1.40×10^{-7}	4.39×10^{-14}
52	3.7568	1.47×10^{-5}	3.63×10^{-5}	5.77×10^{-7}	1.62×10^{-7}	4.59×10^{-14}
54	3.6177	1.52×10^{-5}	4.01×10^{-5}	7.07×10^{-7}	1.87×10^{-7}	-2.07×10^{-13}
56	3.4885	1.63×10^{-5}	4.42×10^{-5}	9.04×10^{-7}	2.16×10^{-7}	-8.26×10^{-14}
58	3.3682	1.83×10^{-5}	4.87×10^{-5}	1.22×10^{-6}	2.48×10^{-7}	-1.32×10^{-13}
60	3.2559	2.17×10^{-5}	5.36×10^{-5}	1.75×10^{-6}	2.85×10^{-7}	-2.35×10^{-13}

Table 6.1: Relative error after 8×10^6 time steps and violation of regularity, Δq, for the solutions in the series.

Convergence with respect to grid size and time step. We also want to check the convergence of the numerical solution with respect to the smallness of the discretization parameters (mesh sizes and time step). Let h denote the smallness parameter of the numerical method. Formally, the limit $h \to 0$ applied to the discrete method gives the differential equation plus boundary conditions. Let $v^h(x,\tau)$ denote a solution to the numerical method and $u(x,\tau)$ the solution of the differential equation plus boundary conditions. The function $v^h(x,\tau)$ converges to $u(x,\tau)$ in order k when $h \to 0$ if there is some $k > 0$ such that $v^h(x,\tau) = u(x,\tau) + \mathcal{O}(h^k)$ for all (x,τ) in the numerical domain. The constant k is called the order of convergence of the method. In a nonlinear problem like ours, we can compute k by evaluating the quotient,

$$Q = \frac{\|v^h - v^{h/2}\|}{\|v^{h/2} - v^{h/4}\|}, \tag{6.15}$$

where v^h, $v^{h/2}$ and $v^{h/4}$ are three numerical approximations of the same differential problem (same parameters, initial data and boundary data) computed on different grids or with different time steps. The norm $\|\ \|$ is the discrete version of the L^1 norm on the numerical domain. This

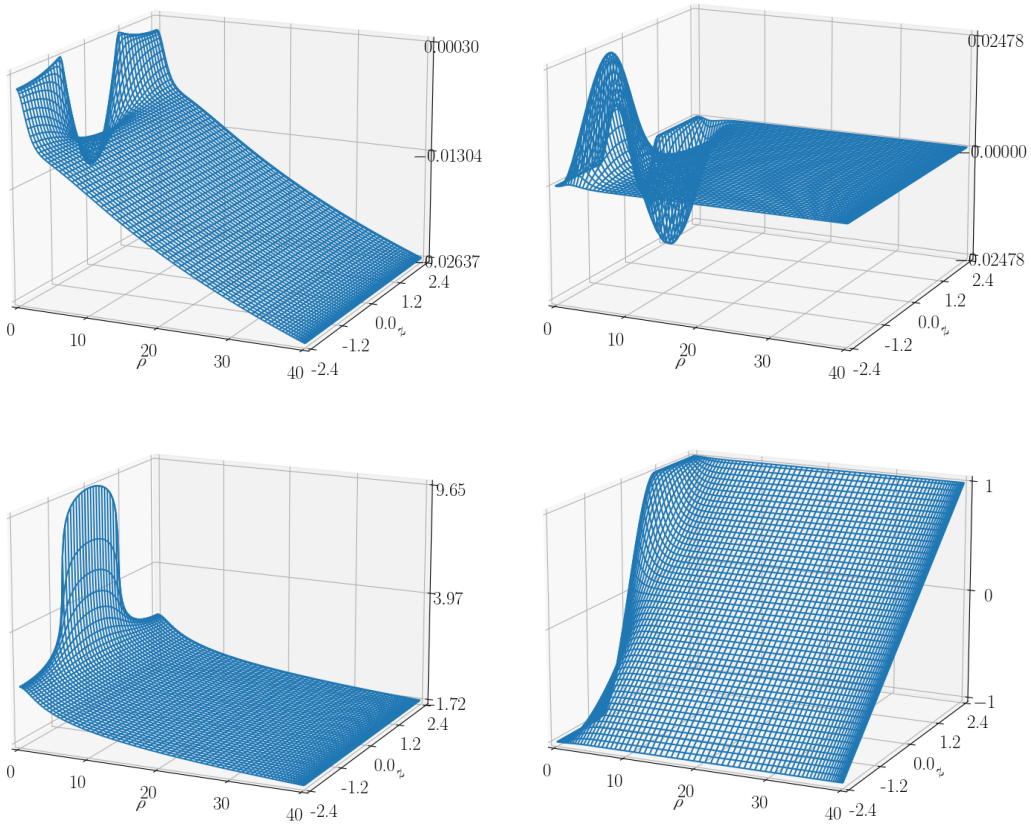

Figure 6.5: Plots of the solution corresponding to $L = 4.8839$ of Table 6.1. From left to right, from top to bottom: $\bar{\sigma}$, $\bar{\omega}$, σ, ω.

quotient should be, for h small enough, close to 2^k.

We first test the convergence of the time discretization (Euler method) by fixing the space discretization (i.e., by fixing N_ρ and N_z). To do this, we take a solution already close to the stationary state with parameters: $J = 1/4$, $L = 6.9770$, $\rho_{\text{MAX}} = 40$, $N_\rho = 80$, $N_z = 100$ and $\tau = 500$, and compute from there three solutions with three time steps $\delta\tau = 10^{-5}$, $\delta\tau = 2 \times 10^{-5}$, and $\delta\tau = 4 \times 10^{-5}$ up to a time $\tau_1 = 510$[4]. We then compute the quotient Q as in (6.15). We obtain linear convergence, as expected for Euler's method. For example, for $\bar{\sigma}$, we get

$$\frac{\|\bar{\sigma}^{4\delta\tau} - \bar{\sigma}^{2\delta\tau}\|}{\|\bar{\sigma}^{2\delta\tau} - \bar{\sigma}^{\delta\tau}\|} = 2.00068$$

indicating linear convergence ($k = 1$).

We now study the convergence of the complete numerical scheme we use to compute the parabolic flow. There are three smallness parameters: the time step $\delta\tau$ of Euler's method, the mesh size of the uniform grid for the z coordinate, which is proportional to $1/N_z$, and the mesh

[4]Since we are already in a near-stationary solution to the parabolic flow, we consider $\tau_1 - \tau$ equivalent to $\approx 10^6$ time steps, to avoid further computational cost.

size of the nonuniform grid for the ρ coordinate (see (6.14)) which, close to the boundaries $\rho = 0$ and $\rho = \rho_{\text{MAX}}$, have values proportional to $1/(N_\rho)^2$.

Numerical stability for Euler's method applied to a parabolic problem like ours requires that the following CFL condition holds

$$\delta\tau \leq C \min\left\{\left(\frac{1}{N_\rho^2}\right)^2, \left(\frac{1}{N_z}\right)^2\right\}, \tag{6.16}$$

where C is some positive constant depending on the equation and the exact solution we are approximating. The limit $\delta\tau \to 0$, $N_z \to \infty$ and $N_\rho \to \infty$ that recovers the differential problem needs to be taken always satisfying (6.16).

To check the order of convergence of our method, we compute the solution on three different grids. Starting with a solution on a coarse grid, already close to the stationary state with parameters $J = 1/4$, $L = 6.9770$, $\rho_{\text{MAX}} = 40$, $N_\rho = 40$, $N_z = 50$ and $\tau = 500$, we refine this solution to obtain initial data on two finer grids, with $N_\rho = 80$, $N_z = 100$ and with $N_\rho = 160$, $N_z = 200$. To do this refinement, we use quadratic interpolation on the seed. Then, we evolve these initial data with different time steps chosen to fulfill the relation (6.16) until time $\tau_1 = 510$ (see Table 6.2)

grid #	N_ρ	N_z	$\delta\tau$	Solution
1	40	50	2×10^{-3}	$\bar{\sigma}^1(x,\tau_1)$, $\bar{\omega}^1(x,\tau_1)$
2	80	100	1.25×10^{-4}	$\bar{\sigma}^2(x,\tau_1)$, $\bar{\omega}^2(x,\tau_1)$
3	160	200	7.2185×10^{-6}	$\bar{\sigma}^3(x,\tau_1)$, $\bar{\omega}^3(x,\tau_1)$

Table 6.2: Three solutions computed to evaluate the quotient (6.15)

We now compute the quotient (6.15). We need to subtract the solutions on the same grid to do this. We use quadratic interpolation to restrict the solution on grid 2 to grid 1 and the solution on grid 3 to grid 2. Then we use grid 1 and grid 2 to compute the numerator and denominator, respectively, in (6.15), obtaining

$$\frac{\|\bar{\omega}^1 - \bar{\omega}^2\|}{\|\bar{\omega}^2 - \bar{\omega}^3\|} = 4.881215, \qquad \frac{\|\bar{\sigma}^1 - \bar{\sigma}^2\|}{\|\bar{\sigma}^2 - \bar{\sigma}^3\|} = 1.742365.$$

These values show convergence at different rates. For $\bar{\omega}$ we obtain higher than quadratic convergence $k = 2.29$; for $\bar{\sigma}$ we obtain a sub-linear convergence ($k = 0.80$). We believe that the difference in the convergence rates is because of the boundary conditions. For $\bar{\omega}$ the boundary conditions (homogeneous Dirichlet and homogeneous Neumann) are fixed along the evolution. For $\bar{\sigma}$, on the other hand, the boundary condition at the outer boundary ($\rho = \rho_{\text{MAX}}$) is dynamic; the boundary data depends on the solution in the bulk. Thus, the evolution changes the boundary condition at every time step, making the convergence rate for $\bar{\sigma}$ low.

Mass, angular velocity and Kasner parameter. The mass M is computed as the Komar mass integral (6.3) at ρ_{MAX}. The horizon angular velocity is obtained as the averaged value of $\Omega(\rho =$

0) in one of the horizons[5]. We also compute the Kasner exponent in two different ways. The first value is obtained from the mass, as $4M/L$, while the second value is obtained from the asymptotic behavior of the function V (cf. (3.23)). More precisely, we compute it as the slope of a linear regression of $\ln(V)$ as a function of $\ln(\rho)$ in the *asymptotic region* of the computational domain, see (3.23). We arbitrarily define the *asymptotic region* of the domain as the portion of the domain, adjacent to ρ_{MAX}, corresponding to 30% of ρ grid points[6]. The two values obtained for the Kasner exponent are in excellent agreement. All these quantities are shown in Table 6.3 for the solutions in this series.

L	M (mass)	Angular velocity	α (from M)	α (from V)
8.8798	1.0095	6.5753×10^{-2}	4.5476×10^{-1}	4.5477×10^{-1}
6.9770	1.0119	7.0513×10^{-2}	5.8014×10^{-1}	5.8017×10^{-1}
5.7457	1.0164	7.9507×10^{-2}	7.0758×10^{-1}	7.0768×10^{-1}
4.8839	1.0250	9.6689×10^{-2}	8.3947×10^{-1}	8.3977×10^{-1}
4.2468	1.0422	1.3130×10^{-1}	9.8167×10^{-1}	9.8264×10^{-1}
3.9071	1.0640	1.7495×10^{-1}	1.0893	1.0916
3.7568	1.0807	2.0831×10^{-1}	1.1506	1.1541
3.6177	1.1036	2.5413×10^{-1}	1.2202	1.2257
3.4885	1.1358	3.1881×10^{-1}	1.3024	1.3113
3.3682	1.1831	4.1348×10^{-1}	1.4050	1.4201
3.2559	1.2557	5.5907×10^{-1}	1.5426	1.5698

Table 6.3: Relevant quantities computed for the solutions in the series with $J = 1/4$.

Recall that, for an asymptotically flat Kerr black hole, the mass M_0, area A and angular momentum J are related by

$$M_0 = \sqrt{\frac{A}{16\pi} + \frac{4\pi J^2}{A}}.$$

For a general axisymmetric black hole solution, with mass M, the inequality

$$M \geq \sqrt{\frac{A}{16\pi} + \frac{4\pi J^2}{A}},$$

is known as a *generalized Penrose inequality*, conjectured to be true for an asymptotically flat solution under general hypotheses. Observe that in our case, the right-hand side of the inequality is

$$\sqrt{1 + \frac{1}{256}} = 1.00778...$$

Then, the solutions we found are within the range of validity of the generalized Penrose inequality. Similar results hold for exact solutions of black hole binaries (e.g., [75–77]), although they possess angle defects along the axis.

[5]The computation of Ω is singular at the horizon; we compute Ω strictly in the interior of H and get the value of $\Omega(\rho = 0)$ by simple linear extrapolation from the first and second internal grid points.

[6]Since the Chebyshev is defined on the interval $[0, \rho_{\text{MAX}}]$, we have a good resolution near the asymptotic region. Defining half a grid, i.e., a Chebyshev grid defined on the interval $[0, 2\rho_{\text{MAX}}]$ but taking only up to ρ_{MAX}, would have improved the code velocity, to the detriment of resolution.

Figure 6.6 shows the plots of relevant metric functions obtained for the solution corresponding to $N_h = 40$.

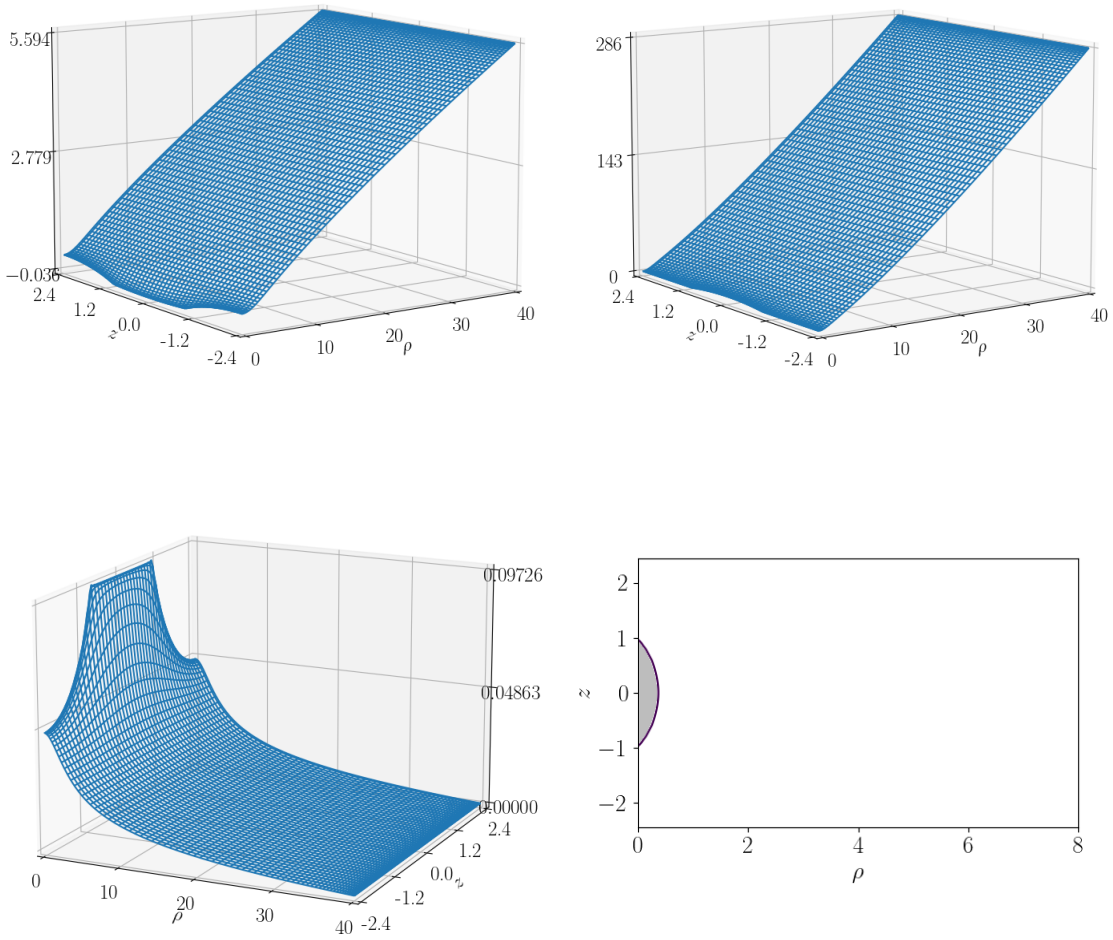

Figure 6.6: Plots of the metric functions V (top left) and η (top right), and plot of Ω and the ergosphere (as a gray region) at the bottom for the solution with $N_h = 40$ of Table 6.1.

The Smarr identity. A very sensitive test for convergence of the heat flow is the validity of the Smarr identity. This is, the constancy of $M(\rho)$ (see equation 6.3) as a function of ρ. In this regard, the $M(\rho)$ plot became crucial to test the correctness of the outer boundary condition for $\bar{\sigma}$. Also, it provides a heuristic for the mass contribution at the axis and horizon. In particular, from the numerical analysis, the $\bar{\sigma}$ values appear to be of the order of 10^{-4}. This is comparable with the error from the truncation of the series (6.8). This could be used, in principle, to establish a similar result as in Theorem 4.2 by using Proposition 6.2.

In Figure 6.7, we show plots that compare $M(\rho)$ computed for the seed (initial data for the flow) and $M(\rho)$ at final time for the six numerically computed solutions with larger L in the series.

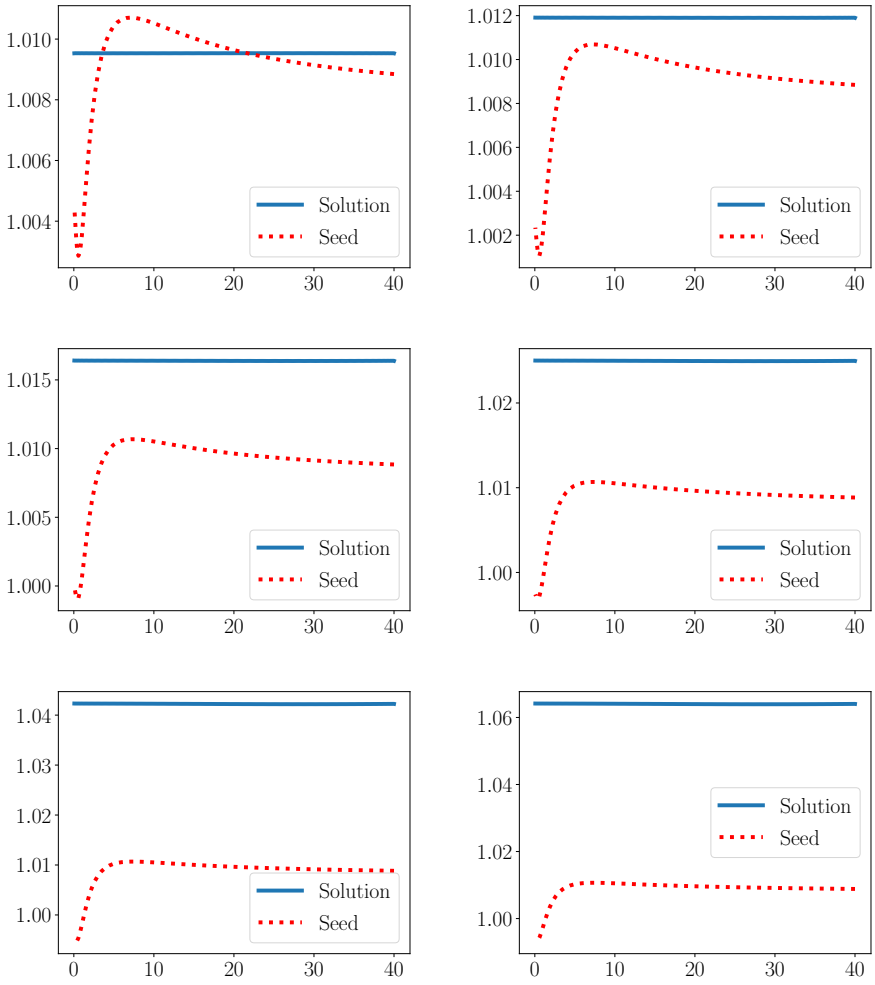

Figure 6.7: Plots of $M(\rho)$ for the seed and for the numerically computed solution compared for six of the solutions in the series. From left to right, from top to bottom, the plots correspond to the cases with $N_h = 22, 28, 34, 40, 46, 50$ in Table 6.1.

Best-fitting asymptotic models We want to check which of the asymptotic candidate solutions best fits the numerically computed solution. To this end, we take the average on the z axis for the function η to get a z-independent function $\bar{\eta}(\rho)$. We then compute the best fitting model η-function for the six posibilities given by models (I+), (I-), (II+), (II-), (III+) and (III-) (see equations (3.20), (3.21), and (3.22)). To do this, we minimize the deviation of the model $\eta(a, b, \rho)$ from $\bar{\eta}$ by varying the parameter a or taking $a = 0$ for the models (II+) and choosing b in such a way that the η-functions are coincident at the outer boundary. We measure the mentioned deviation by computing the integrated square difference in the asymptotic region,

$$\Delta\eta = \int_{\text{asympt. region}} \Big(\bar{\eta}(\rho) - \eta(a, b, \rho)\Big)^2 \, d\rho.$$

The results of fitting the eleven solutions in Table 6.1 are shown in Table 6.4. It is interesting

	(III+)			(II+)		(I+)		
L	a	b	$\Delta\eta$	b	$\Delta\eta$	a	b	$\Delta\eta$
8.8798	0.5451	2.6149	$\mathbf{2.4\times10^{-7}}$	89.9297	5.2×10^{1}	0.0001	0.0090	5.2×10^{1}
6.9770	0.4194	2.2513	$\mathbf{1.4\times10^{-7}}$	49.4932	1.6×10^{1}	0.0001	0.0049	1.6×10^{1}
5.7457	0.2906	1.8077	$\mathbf{9.0\times10^{-9}}$	26.8568	3.2	0.0001	0.0027	3.2
4.8839	0.1500	1.1372	$\mathbf{1.5\times10^{-8}}$	13.7707	2.3×10^{-1}	0.0001	0.0014	2.3×10^{-1}
4.2468	0.0001	0.0006	6.5×10^{-2}	6.0951	6.5×10^{-2}	0.1005	1.0170	$\mathbf{6.0\times10^{-7}}$
3.9071	0.0001	0.0003	2.9×10^{-1}	2.8198	2.9×10^{-1}	0.1536	0.9808	4.3×10^{-2}
3.7568	0.0001	0.0002	4.0×10^{-1}	1.5649	4.0×10^{-1}	0.1903	0.8483	8.5×10^{-2}
3.6177	0.0001	0.0001	5.0×10^{-1}	0.5104	5.0×10^{-1}	0.2381	0.6756	1.3×10^{-1}
3.4885	0.0001	-0.0000	5.9×10^{-1}	-0.3766	5.9×10^{-1}	0.3019	0.4511	1.6×10^{-1}
3.3682	0.0001	-0.0001	6.5×10^{-1}	-1.1241	6.5×10^{-1}	0.3898	0.1107	1.9×10^{-1}
3.2559	0.0001	-0.0002	7.1×10^{-1}	-1.7558	7.1×10^{-1}	0.5172	-0.3566	2.1×10^{-1}
	(I−)			(II−)		(III−)		
L	a	b	$\Delta\eta$	b	$\Delta\eta$	a	b	$\Delta\eta$
8.8798	0.0106	1.4862	5.4×10^{1}	97.3074	5.6×10^{1}	0.0001	0.0097	5.6×10^{1}
6.9770	0.0188	1.6213	1.7×10^{1}	56.8710	1.9×10^{1}	0.0001	0.0057	1.9×10^{1}
5.7457	0.0327	1.6434	4.2	34.2346	5.1	0.0001	0.0034	5.1
4.8839	0.0572	1.7306	5.9×10^{-1}	21.1485	1.1	0.0001	0.0021	1.1
4.2468	0.1022	1.9351	3.6×10^{-3}	13.4728	1.4×10^{-1}	0.0001	0.0013	1.4×10^{-1}
3.9071	0.1250	1.4114	$\mathbf{8.5\times10^{-9}}$	10.1975	2.1×10^{-2}	0.0001	0.0010	2.1×10^{-2}
3.7568	0.1164	1.0874	$\mathbf{1.6\times10^{-9}}$	8.9426	5.8×10^{-3}	0.0001	0.0009	5.8×10^{-3}
3.6177	0.0909	0.7270	$\mathbf{1.1\times10^{-9}}$	7.8882	8.4×10^{-4}	0.0001	0.0008	8.4×10^{-4}
3.4885	0.0001	0.0007	2.3×10^{-7}	7.0012	2.3×10^{-7}	0.0147	0.1029	$\mathbf{1.4\times10^{-9}}$
3.3682	0.0001	0.0006	2.6×10^{-4}	6.2537	2.6×10^{-4}	0.1089	0.6775	$\mathbf{2.2\times10^{-9}}$
3.2559	0.0001	0.0006	4.7×10^{-4}	5.6220	4.7×10^{-4}	0.1629	0.9108	$\mathbf{3.3\times10^{-9}}$

Table 6.4: Fit of the solutions of Table 6.1 with the six possible models given by equations (3.20),(3.21), and (3.22). The best-fitting models are shown in boldface for each case.

to see how well the z-averaged η-function of our numerically computed solution fits, in the whole ρ range, one of the model η-functions. As expected, for large values of L, the best-fitting model is (III+). Then, for decreasing values of L, the best fitting model becomes (I+), then (I-), and finally (III-). Figure 6.8 shows six examples from Table 6.4.

It is interesting to observe here that, on theoretical grounds, there must indeed be a critical L below which no solution solutions extending to infinity exist. Assume that we have an actual solution extending to infinity with any of the two possible asymptotic models given by Theorem 5.2. As we mentioned in subsection 3.3.3, for the asymptotic models (III+) or (II+) with $0 \leq a < 1$, Smarr formula gives the following identity

$$(1-a)L/4 = \frac{1}{4\pi}\kappa A + 2\Omega_{\mathcal{H}} J.$$

Now, the condition $a \geq 0$ allows us to obtain the lower bound for L

$$0 < 2\Omega_{\mathcal{H}} J \leq \frac{L}{4} - \frac{1}{4\pi}\kappa A = \frac{L}{4} - m,$$

and therefore, $L > 4m$. In Theorem 4.1, we showed that below this lower bound, there is no black hole solution that is complete at infinity. This relation is easily verified in the numerical

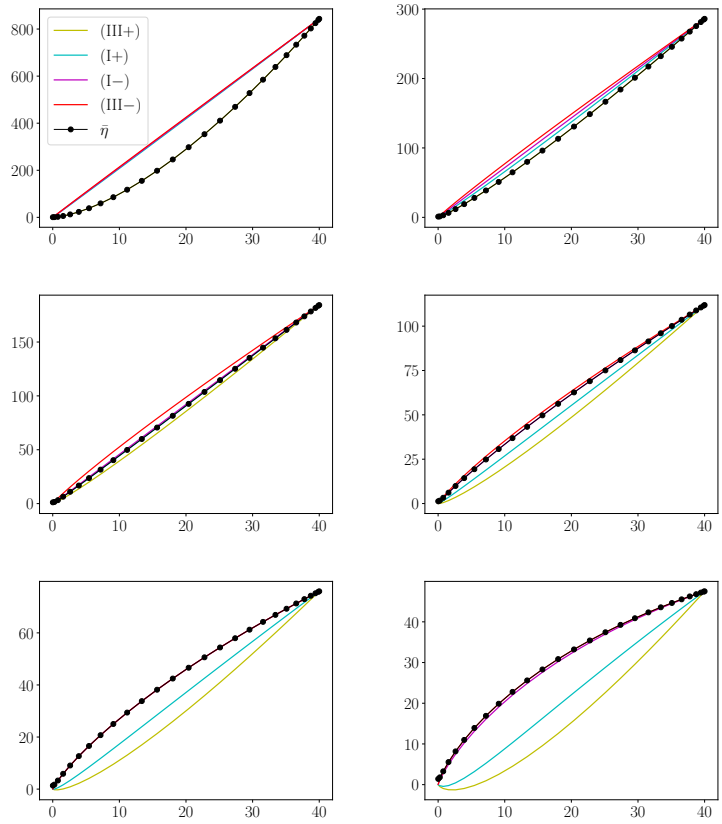

Figure 6.8: Plots of $\bar{\eta}$ together with the fitting models (III+), (I+), (I+) and (III+) for the six solutions in Table 6.4 corresponding, from left to right, from top to bottom, to $L = 8.8798,\ 4.8839,\ 4.2468,\ 3.7568,\ 3.4885,\ 3.2559$. The $\bar{\eta}$ curve overlaps the best-fitting model in all cases, while some of the bad-fitting model curves overlap among themselves; that is why not all curves are visible in all plots.

tables.

Ergo-region merging. Recall that the region $\{V \leq 0\}$ is called ergo-region, and its boundary is called ergosphere.

For large values of L, the ergo-region associated with the horizon does not touch the $z = \pm L/2$ boundaries of the domain. The boundary of the ergo-region is thus topologically S^2. When the value of L decreases, the ergo-region gets closer to the boundaries and, at some point, touches them. At a critical value of L, the outer boundary of the ergo-region changes topology, becoming a torus T^2. However, the change takes place for L below the critical value, so such solutions do not extend to infinity. Topological changes in the Ergo-regions have been studied in binary systems (e.g., [78]), so seeing this phenomenon in the periodic setup is unsurprising. This process is shown in Figure 6.9.

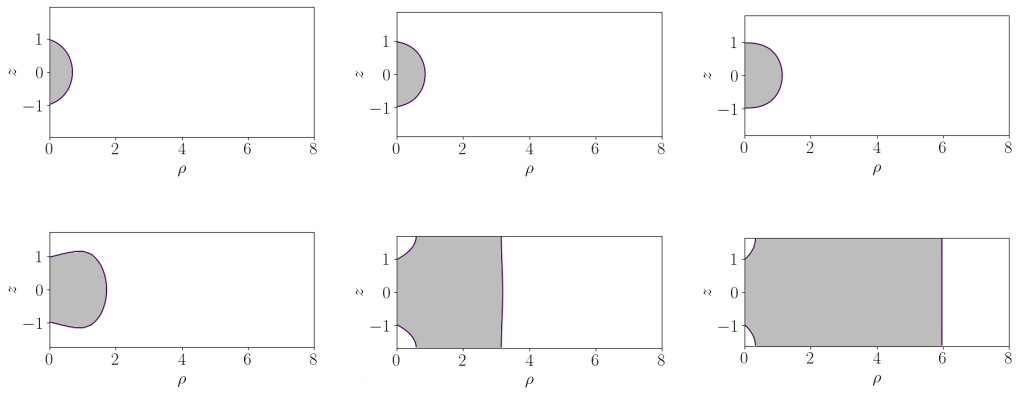

Figure 6.9: The shaded regions are the ergospheres of the last six solutions of Table 6.1. From left to right, from top to bottom, the six plots correspond to $L = 8.8798,\ 4.8839,\ 4.2468,\ 3.7568,\ 3.4885,\ 3.2559$.

6.4.2 Second series: $J = 1/2$

For the sake of comparison, we include results corresponding to a series of four solutions with a higher value of J and the same horizon area as the previous series. The three solutions with larger values of L are better fitted by the asymptotic model (III+) of (3.22). The solution with $L = 4.5475$ is better fitted with the model (II+) of equation (3.20). These results are consistent with the heuristics we obtain from Smarr identity.

Table 6.5 shows the relevant physical quantities of the solutions in this series.

N_h	L	M (mass)	Angular velocity	α (from M)	α (from V)
22	8.2683	1.0391	1.3024×10^{-1}	5.0272×10^{-1}	5.0278×10^{-1}
28	6.4965	1.0518	1.4287×10^{-1}	6.4761×10^{-1}	6.4781×10^{-1}
32	5.3501	1.0775	1.6860×10^{-1}	8.0560×10^{-1}	8.0632×10^{-1}
40	4.5475	1.1340	2.2516×10^{-1}	9.9745×10^{-1}	1.0003

Table 6.5: Relevant quantities computed for solutions with $J = 1/2$.

6.5 Multi-horizon set ups

In this section, we will discuss further improvements on the code to analyze the existence of solutions with more than one connected component of the horizon per period. In particular, we are interested in two counter-rotating axially symmetric black holes in a periodic setup.

We want periodic stationary and axisymmetric black hole data to satisfy the hypotheses of Proposition 2.4 to avoid angle defects on the axis. It remains an open problem to prove whether there is any other data with no struts at the axis.

Recall that for a z-even or z-odd periodic stationary and axisymmetric black hole data on the hypotheses of Proposition 2.4, we have that the area of each horizon is the same, they are equidistant and $|J_i| = J$ the same for all i. Then, once the number $j > 0$ of horizons is fixed, the

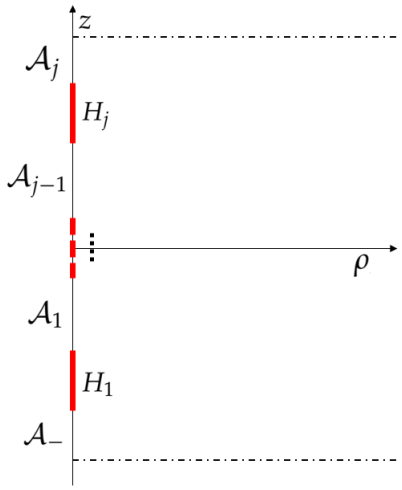

Figure 6.10: Schematic representation of a multi-horizon set-up, for j horizons. The data is either $z-$odd or $z-$even.

parameters $m/L, \{A_i\}_{i=1}^{j}, \{J_i\}_{i=1}^{j}$ have been set, and the parity of the solution has been decided, the boundary conditions are quite straightforward. Let

$$J_T = \sum_{i}^{j} J_i,$$

be the total angular momentum of the solution with j horizons, and let

$$J_{\uparrow j} = \sum_{i=1}^{j} J_i,$$

be the sum up to j. Let $\mathcal{A}_-$ be the axis component with the lowest values of z, $\mathcal{A}_i$ the axis component between the $i-$th and the $(i+1)-$th horizons and $\mathcal{A}_j$ the axis component with the highest values of z. In Figure 6.10, we show a diagram representing the periodic setup for the black hole data.

Boundary conditions on $\mathcal{A}$ and $\mathcal{H}$: we distinguish between $z-$even and odd cases.

- If the data is z-even: the boundary conditions for ω are Dirichlet on the axis and Neumann on the horizon,

$$\omega\,|_{\mathcal{A}_-} = -4J_T, \quad \omega\,|_{\mathcal{A}_j} = -4J_T + 8J_{\uparrow j}, \quad \partial_\rho \omega\,|_{\mathcal{H}} = 0,$$

  while for σ are Neumann on both the axis and the horizon,

$$\partial_\rho \sigma\,|_{\mathcal{A}} = 0, \quad \partial_\rho(\sigma + 2\ln\rho)\,|_{\mathcal{H}\setminus\partial\mathcal{H}} = 0,$$

with a Dirichlet condition at the poles,

$$\lim_{(\rho,z)\to(0,z_i\pm m)} \frac{\sigma}{\sigma_i} = 1, \quad \forall 1 \leq i \leq j,$$

where σ_i is the reference Kerr solution with same A and J.

- If the data is z-odd: the conditions on σ are the same, while for ω we have

$$\omega \mid_{\mathcal{A}_-} = 0, \quad \omega \mid_{\mathcal{A}_j} = 8J_{\uparrow j}, \quad \partial_\rho \omega \mid_{\mathcal{H}} = 0,$$

since $J_T = 0$ in this case.

Boundary condition at ρ_{MAX}: we use the same as in the one-horizon case,

$$\omega(\rho_{\text{MAX}}, z) = \frac{8J_T}{L} z, \quad \partial_\rho \sigma \mid_{\rho_{\text{MAX}}} = -\frac{4\overline{M}(\tau)}{L\rho_{\text{MAX}}}.$$

The quadrature equations (2.20) and (2.21), for Ω and γ, respectively, are solved in the same way as in the single horizon case.

6.5.1 Construction of the seed

The construction of a general seed at $\tau = 0$ to initialize the heat flow is done analogously as in subsection 6.2.2. Let $\sigma_{0,i}(\rho, z)$ and $\omega_{0,i}(\rho, z)$ be the solutions to the asymptotically flat Kerr black hole with area A and angular momentum J_i (cf. subsection 2.4.1), located at $\mathcal{H}_i = \{|z - z_i| \leq m\}$ with $z_i = -L/2 + N/2j + (i-1)N/j$. Consider

$$\sigma_0(\rho, z) = \sum_{i=1}^{j} \sigma_{0,i}(\rho, z), \quad \omega_0(\rho, z) = \sum_{i=1}^{j} \omega_{0,i}(\rho, z) + C_0, \tag{6.17}$$

where C_0 is such that ω_0 satisfies the Dirichlet conditions defined above, given the data is either $z-$even or $z-$odd. Next, we use the same splitting as in (6.7),

$$\begin{aligned} \sigma &= \sigma_0 + \sigma_r + \bar{\sigma}, \\ \omega &= \omega_0 + \omega_r + \bar{\omega}, \end{aligned}$$

for σ_r and ω_r defined as follows

$$\begin{aligned} \sigma_r(\rho, z) &= C + \sum_{n=1}^{\infty} \left(\sigma_0(\rho, z - nL, J) + \sigma_0(\rho, z + nL, J) - \frac{4jM_0}{nL} \right), \\ \omega_r(\rho, z) &= \sum_{n=1}^{\infty} \left(\omega_0(\rho, z - nL, J) + \omega_0(\rho, z + nL, J) \right), \end{aligned}$$

where C is, again, the constant such that $\sigma_r \mid_{(\rho=0, z_i \pm m)} = 0$ for all $i = 1, ..., N$. Observe that $\frac{4jM_0}{nL}$ fulfills the same role as $\frac{4M}{nL}$ in the case of a single horizon.

Equations for $(\bar{\sigma}, \bar{\omega})$ are the same as (6.9) and (6.10), as well as their boundary conditions, (6.11), (6.12), (6.13).

For $j = 2$, we can, in principle, use any pair of functions (σ_0, ω_0) that represent a binary Kerr solution. In particular, the binary solutions presented in [75–77, 79–81] constructed via the Tomimatsu method [82, 83] can be another candidate as (σ_0, ω_0). For $j > 2$, solutions constructed with the Inverse Scattering Method can be also taken as (σ_0, ω_0). Heuristically, one of the advantages of working with an already binary Kerr solution would be an initially *closer* expression for the asymptotic Kasner exponent already in the seed, $4M_{binary}/L$ instead of $8M_0/L$. The general feature of the metrics constructed in this fashion is that they are not regular in at least one component of the axis due to the presence of struts, and their expressions are algebraically more costly to manipulate symbolically with the computer. Therefore, we opt for the sum of Kerr solutions to approximate the binary/multi-horizon solution on each strip, (6.17).

6.5.2 Two counter-rotating black holes

This subsection presents preliminary results on some numerical solutions we constructed for two counter-rotating horizons. The methodology is identical to the one exposed in section 6.3, evolving a heat flow from the harmonic map equations for (σ, ω).

For two counter-rotating black holes, we take $j = 2$, $J_1 = J$, $J_2 = -J$ and fix the area to be $A = 16\pi$ for each black hole. The positions of the black holes are $z_1 = -L/4$ and $z_2 = L/4$. The semi-length of each horizon is m, and the periodic length is L. The inequality $L > 4m$ becomes the condition for the non-overlapping of horizons.

In the counter-rotating case, the seed is asymptotically Kasner-like, as in (1.15). This can be explicitly computed, since $\omega_0 + \omega_r$ vanishes at first order in z, and therefore (σ_s, ω_s) is asymptotically a Lewis model with $x = \beta + \alpha \ln \rho$, cf. (3.16).

We present three series of runs. To observe contrast with the single horizon case, we consider first $J = \pm 1/4$ and $J = \pm 1/2$. We also present a run for $J = 0.3$ where the horizons get as "close" as numerically possible for a given grid[7]. We are interested in the behavior of the solutions in this limit since Theorem 4.1 is not valid in the case of vanishing total angular momentum.

Results for $J = \pm 1/4$

Figure 6.11 is a typical solution example for $L = 13.9539$, corresponding to $N_h = 14$ for each horizon. In Table 6.6, we show the principal quantities we computed from the numerical solutions, as in the co-rotating case.

The data presented in Table Table 6.6 corresponds to five values of L twice those in table Table 6.3 (from second to sixth row). As a reference, we add a column with the *mass per horizon*, $M/2$, as a comparison with the values obtained in the co-rotating case (although it has no physical meaning). Observe that in all the cases, the mass per horizon is less in the counter-rotating case than in the one-horizon case, but Penrose inequality still holds, having

[7] Some warnings of overflow occur when the distance between horizons is less than four grid points, due to the z-derivatives computations.

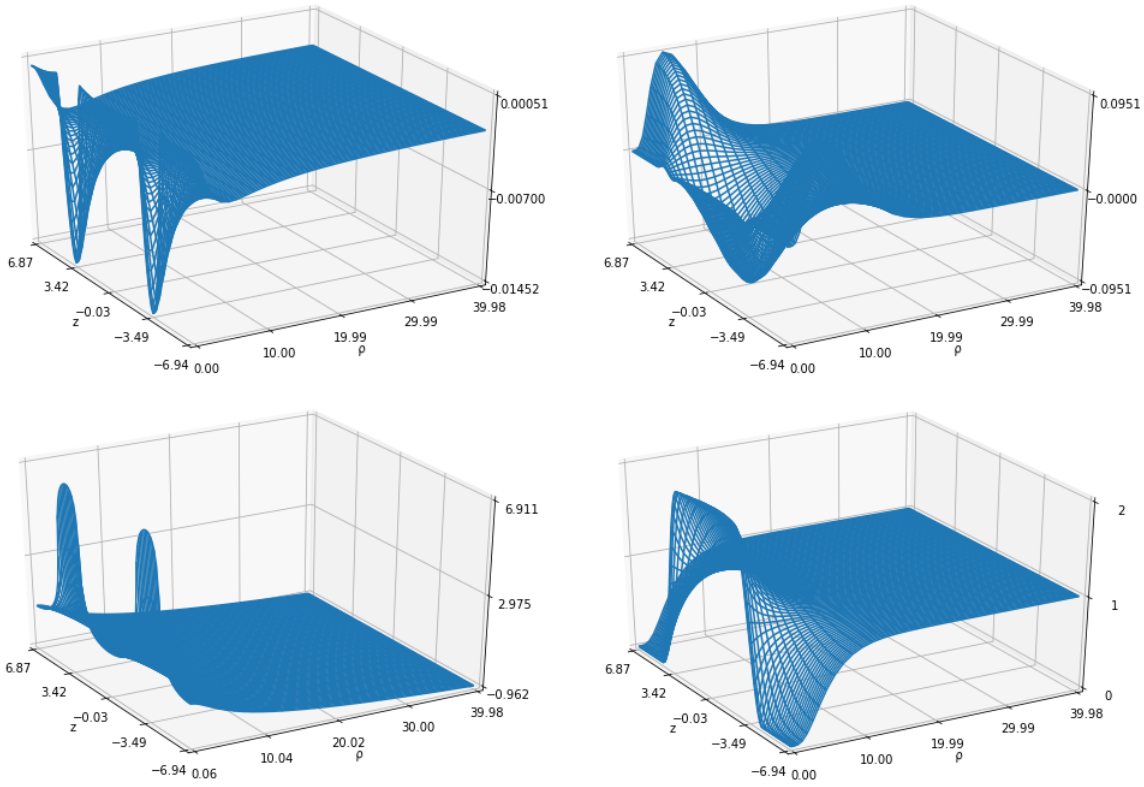

Figure 6.11: Plots of the solution corresponding to $L = 13.9539$. From left to right, from top to bottom: $\bar{\sigma}$, $\bar{\omega}$, σ, ω.

$$M \geq \sqrt{2}.$$

L	M (total mass)	$M/2$	Angular velocity ($\Omega_{\mathcal{H}}$)	α (from M)	α (from V)
13.9539	2.0165	1.0083	6.2687×10^{-2}	5.7862×10^{-1}	5.7805×10^{-1}
11.4915	2.0173	1.0086	6.3505×10^{-2}	7.0273×10^{-1}	7.0220×10^{-1}
9.7677	2.0185	1.0092	6.4737×10^{-2}	8.2684×10^{-1}	8.2661×10^{-1}
8.4937	2.0203	1.0102	6.6549×10^{-2}	9.5095×10^{-1}	9.5144×10^{-1}
7.5136	2.0229	1.0115	6.9187×10^{-2}	1.0770	1.0769

Table 6.6: Relevant quantities computed for the solutions in the series with $J = 1/4$.

In Figure 6.12, we show the final function $M(\rho)$, after a time $\tau_{end} = 500$, compared to the initial $M(\rho)$ of the seed[8]. Recall that the asymptotic behavior of the seed is a Kasner-type solution (i.e., it is not a Lewis model), with associated exponent $8M_0/L$ (M_0 the mass of one of the asymptotically flat Kerr black holes). As in the co-rotating case, checking the constancy of $M(\rho)$ at the final stages of the heat flow is an important consistency test.

For the typical solution given in Figure 6.11, a best-fitting Kasner solution can be seen in Figure 6.13.

[8]This value for τ_{end} corresponds to $\approx 2 \times 10^7$ time steps

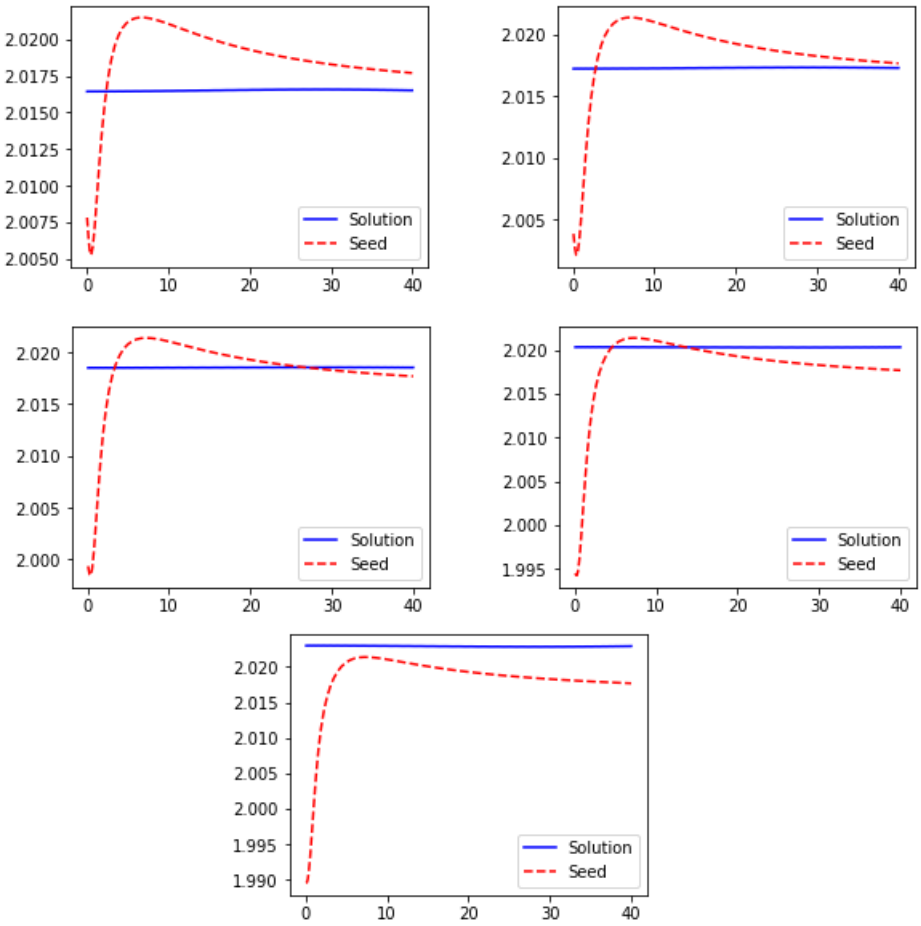

Figure 6.12: Plots of $M(\rho)$ for the seed and for the numerically computed solution compared for five runs in the series. From left to right, from top to bottom, the plots correspond to the cases with $L = 13.9539, 11.4915, 9.7677, 8.4937, 7.5136$.

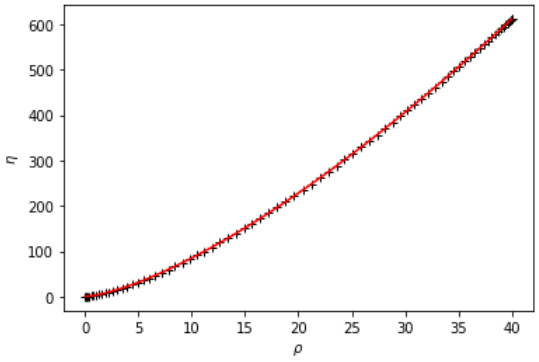

Figure 6.13: Plot of the best fitting Kasner-like asymptotic behavior for $L = 13.9539$. The Kasner exponent is given in Table 6.6.

In contrast with the co-rotating case, we have no evidence for a merging of the ergo-spheres. In Figure 6.14 we show the ergo-spheres corresponding to the solutions in Table 6.6

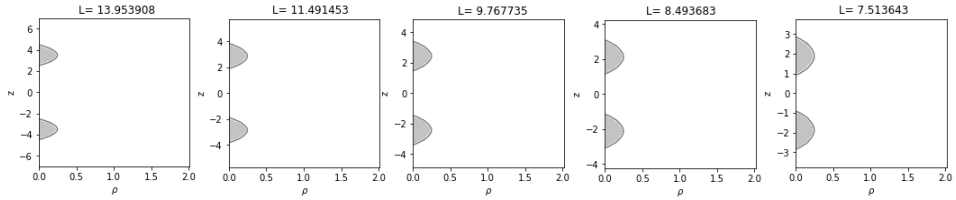

Figure 6.14: The shaded regions are the ergo-spheres of the five solutions presented in Table 6.6.

Results for $J = \pm 1/2$

In order to compare with subsection 6.4.2, we present some results regarding the counter-rotating case for $J = 1/2$. The data shown in Table 6.7 correspond to twice the periodic length as that from the second to the fourth row in Table 6.5. Also, we add a case (the fourth row) for which $\alpha > 1$. Again, the mass per horizon is less in the counter-rotating case than in the co-rotating case, but Penrose inequality still holds.

L	M (mass)	$M/2$	Angular velocity	α (from M)	α (from V)
12.9930	2.0655	1.0328	1.2269×10^{-1}	0.6366	0.6359
10.7001	2.0698	1.0349	1.2485×10^{-1}	0.7748	0.7737
9.0951	2.0762	1.0381	1.2811×10^{-1}	0.9129	0.9131
7.9088	2.0858	1.0429	1.3301×10^{-1}	1.0550	1.0548

Table 6.7: Relevant quantities computed for the solutions in the series with $J = 1/2$.

Limit $4m \to L$

The main differences between co-rotating and counter-rotating cases are when considering the ergo-region in the limit when the horizons are getting closer. Since Theorem 4.1 is not valid for counter-rotating periodic black holes, we test numerically how the solutions behaved when the horizons are closer (in Weyl-Papapetrou coordinates) than $L = 8m$.

In this run, we set $m = 0.9667$ and $J = 0.3$, so we are taking the limit $L \to 3.8667 \approx 4m$ in Weyl coordinates. Due to the discrete set of values that we can have for the space between the black holes (as explained in section 6.3), the higher N_z is the better resolution when the horizons are getting closer. We leave this careful analysis for future works while presenting here preliminary results. In Table 6.8, we show the mass for the solutions as the horizons get closer.

We want to finish this section with the following observation: as the horizons get closer, the values of α seem to converge to zero. This is unsurprising since the limiting Kasner solution for $\alpha \to 0$ is the Boost solution [46], where the horizon is the *whole* set $\{\rho = 0\}$. By definition of the asymptotic model,

$$\frac{4M}{L} = 2 - \alpha,$$

so, in principle, we should not see any divergence in the mass. However, we should see a van-

L	M (mass)	α (from η)	Angular velocity $\lvert\Omega_{\mathcal{H}}\rvert$
9.2065	2.0266	1.1131	0.0614
8.7880	2.0267	1.0690	0.0649
8.4060	2.0269	1.0270	0.0671
8.0557	2.0270	0.9850	0.0687
7.7335	2.0271	0.9429	0.0703
7.4360	2.0272	0.9009	0.0719
7.1606	2.0273	0.8589	0.0736
6.9049	2.0274	0.8148	0.0755
6.6668	2.0275	0.7728	0.0776
6.4446	2.0277	0.7328	0.0800
6.2367	2.0278	0.6907	0.0825
6.0418	2.0280	0.6487	0.0853
5.8587	2.0282	0.6066	0.0884
5.6864	2.0284	0.5646	0.0918
5.5239	2.0286	0.5246	0.0956
5.3705	2.0288	0.4825	0.0999
5.2253	2.0291	0.4425	0.1050
5.0878	2.0294	0.4005	0.1114
4.9574	2.0300	0.3584	0.1197
4.8334	2.0310	0.3164	0.1316
4.7155	2.0330	0.2723	0.1510
4.6033	2.0375	0.2263	0.1905
4.4962	2.0532	0.1703	0.3564

Table 6.8: Relevant quantities computed for the solutions in the series with $J = 0.3$, when $4m \to L$.

ishment of $\Omega_{\mathcal{H}}$. This can be deduced from Smarr identity, (3.3.3) (once again, assuming the existence of the solution). For a counter-rotating solution we have

$$\frac{(2-\alpha)L}{4} = 2m + 4J\Omega_{\mathcal{H}}.$$

Therefore

$$\Omega_{\mathcal{H}} = \frac{(2-\alpha)L}{16J} - \frac{m}{2J}.$$

Then, $\Omega_{\mathcal{H}} \to -\frac{\alpha L}{8J}$ as $L \to 4m$. If the Kasner exponent is such that $\alpha \to 0$, then the angular velocity should vanish in the limit. However, if that is the case, then $M \to 2m$.

From the numerical simulations, there appears to be a steep growth in the modulus of the angular velocity, $|\Omega_{\mathcal{H}}|$, while the mass M monotonically increases as the horizons get closer. It would be interesting to study the extent and the reason for this behavior in detail and whether there is a limiting value $L^* > 4m$ below which no solution exists.

Appendix A

Formulas and distorted Black Holes

A.1 Functions for Kerr solution on Weyl-Papapetrou coordinates

A.1.1 Prolate spheroidal coordinates

Consider the prolate spheroidal coordinates (x, y) associated with the horizon located at $[-m, m]$. The change of coordinates from (ρ, z) to (x, y)

$$\rho^2 = m^2(x^2-1)(1-y^2), \quad z = mxy.$$

where $m = \sqrt{M^2 - a^2}$, $a = J/M$. The expressions of (x, y) in terms of (ρ, z) can be deduced straightforwardly

$$\begin{aligned} \rho^2 &= -m^2x^2y^2 + m^2(x^2+y^2) - m^2, \\ \rho^2 + z^2 + m^2 &= m^2(x^2 + \frac{z^2}{m^2x^2}) = m^2(y^2 + \frac{z^2}{m^2y^2}). \end{aligned}$$

Let

$$d_+ = \sqrt{\rho^2 + (z-m)^2}, \quad d_- = \sqrt{\rho^2 + (z+m)^2}$$

be the distances from (ρ, z) to the points $(0, m)$ and $(0, -m)$, respectively. Then, we obtain a solution of the previous equations as

$$x^2, y^2 = \frac{\left(d_+^2 + d_-^2 \pm 2d_+d_-\right)^2}{4m^2}.$$

We take x with the positive sign and y the one associated with the negative sign. See Figure A.1.

The functions d_+ and d_- give us the geometrical meaning of the prolate spheroidal coordinates,

$$x = \frac{d_+ + d_-}{2m}, \quad y = \frac{d_+ - d_-}{2m}.$$

The level sets of x are ellipses with poles at $(0, m)$ and $(0, -m)$. The values of y are the *angular* parameter of the ellipses.

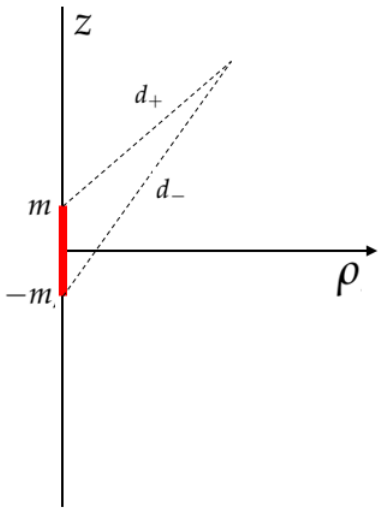

Figure A.1: Schematic representation of d_+ and d_-.

A.1.2 Kerr metric

Consider the metric given by,

$$g = -f(dt + Ad\phi)^2 + f^{-1}(\rho^2 d\phi^2 + e^{2k}(d\rho^2 + dz^2)),$$

then the Kerr metric can be written as [49,84]

$$\begin{aligned} f &= \frac{p^2x^2 + q^2y^2 - 1}{p^2x^2 + q^2y^2 + 2px + 1}, \\ A &= \frac{2mq(1-y^2)(px+1)}{p(p^2x^2 + q^2y^2 - 1)}, \\ e^{2k} &= \frac{p^2x^2 + q^2y^2 - 1}{p^2(x^2 - y^2)}, \end{aligned}$$

where

$$p = \frac{m}{M}, \quad q = \frac{a}{M}.$$

The full expressions for f and A are

$$\begin{aligned} f &= \frac{M^2(d_+^2 + d_-^2) + (m^2 - a^2)d_+d_- - 4M^2m^2}{M^2(d_+^2 + d_-^2) + (m^2 - a^2)d_+d_- + 4Mm^2(d_+ + d_-) + 4M^2m^2}, \\ A &= aM\frac{\left(4m^2 - (d_+ - d_-)^2\right)(d_+ + d_- + 2M)}{M^2(d_+^2 + d_-^2) + (m^2 - a^2)(d_+d_-) - 4M^2m^2}. \end{aligned}$$

Finally, the conformal factor k is given by

$$e^{2k} = \frac{M^2(d_+^2 + d_-^2) + (m^2 - a^2)d_+d_- - 4M^2m^2}{m^2 d_+ d_-}.$$

A.1.3 Algebraic comparison between stationary axisymmetric metric forms

Consider an axisymmetric and stationary metric in the form (3.1)

$$ds^2 = f^{-1}(e^{2k}(dx^2 + d\rho^2) + \rho^2 d\phi) - f(dt + Ad\phi)^2,$$

and also in the form (2.16),

$$ds^2 = -Vdt^2 + 2Wdtd\phi + \eta d\phi^2 + e^{2\lambda}(d\rho^2 + dz^2),$$

where $W = \eta\Omega$, $V = \eta^{-1}(\rho^2 - W^2)$ and $e^{2\lambda} = \eta^{-1}e^{2\gamma}$. A direct comparison can be established,

$$\begin{aligned} f &\rightarrow V = \eta^{-1}(\rho^2 - W^2), \\ fA &\rightarrow W = -\eta\Omega, \\ f^{-1}e^{2k} &\rightarrow e^{2\lambda}, \\ f^{-1}\rho^2 - fA^2 &\rightarrow \eta. \end{aligned}$$

Then, we have the following algebraic relations,

$$\begin{aligned} f &= e^{2k-2\lambda} \\ f &= \eta^{-1}(\rho^2 - W^2) = \eta^{-1}(\rho^2 - \eta^2\Omega^2) \\ A &= -f^{-1}X\Omega = \frac{\eta^2\Omega}{\Omega^2\eta^2 - \rho^2} \\ e^{2k} &= e^{2\lambda}\eta^{-1}(\rho^2 - \eta^2\Omega^2) = e^{2\omega}(\eta^{-2}\rho^2 - \Omega^2) \end{aligned}$$

Alternatively, we can solve for η and Ω,

$$\begin{aligned} \eta &= \frac{\rho^2}{f} - fA^2 = f^{-1}(\rho^2 - f^2A^2) \\ \Omega &= -\frac{fA}{\eta} = -\frac{fA}{\frac{\rho^2}{f} - fA^2} = \frac{f^2A}{\rho^2 - f^2A^2} \end{aligned}$$

In particular, we can compute η in terms of (x, y),

$$\eta = m^2(1-y^2)\frac{p^2(x^2-1)((px+1)^4 + q^4y^4 + 2(px+1)^2q^2y^2) - 4q^2(1-y^2)(px+1)^2}{p^2(p^2x^2 + q^2y^2 + 2px + 1)(p^2x^2 + q^2y^2 - 1)}.$$

Then,

$$e^{\sigma} = \frac{p^2(x^2-1)((px+1)^4 + q^4y^4 + 2(px+1)^2q^2y^2) - 4q^2(1-y^2)(px+1)^2}{p^2(p^2x^2 + q^2y^2 + 2px + 1)(p^2x^2 + q^2y^2 - 1)(x^2-1)}.$$

A.2 Distorted black holes and area formula

In this section, we will show the relation between the area and the value of σ at the horizon. This makes possible fixing the area (in subsection 6.2.1) by establishing the condition

$$\lim_{(\rho,z)\to(0,\pm m)} \frac{\sigma}{\sigma_0} = 1.$$

Consider (σ_0, ω_0) the Kerr solution associated with the parameters (A, J), which in Weyl-Papapetrou coordinates satisfies equations (2.26)-(2.26). The positions of the poles of the horizon are $(0, -m)$ and $(0, m)$. We will assume that the solutions are z-even or z-odd.

A *distorted Kerr black hole* is a stationary and axisymmetric black hole solution, possibly with multiple horizons, such that it has a horizon at $H = \{|z| \leq m\}$ with the same value of angular momentum J as the Kerr solution.

Such distortion can be caused by the presence of another black hole or, as in the periodic case, by the presence of infinitely many horizons.

We can write the solution as the Kerr solution plus a perturbation,

$$\sigma = \sigma_0 + \bar{\sigma}, \quad \omega = \omega_0 + \bar{\omega}.$$

Consider the function q, given by the quadrature equations, (2.22). If we define $q = q_0 + \bar{q}$, then

$$\begin{aligned} \partial_z \bar{q} &= \partial_z q_0 + \frac{\rho}{2}\left(\partial_\rho \sigma_0 \partial_z \bar{\sigma} + \partial_\rho \bar{\sigma} \partial_z \sigma_0 + \partial_\rho \bar{\sigma} \partial_z \bar{\sigma}\right) \\ &\quad + \left(\frac{1 - e^{2\bar{\sigma}}}{2\eta^2}\right) \rho \partial_\rho \omega_0 \partial_z \omega_0 + \frac{\rho}{2\eta^2}\left(\partial_\rho \omega_0 \partial_z \bar{\omega} + \partial_\rho \bar{\omega} \partial_z \omega_0 + \partial_\rho \bar{\omega} \partial_z \bar{\omega}\right) \end{aligned}$$

We will assume $\bar{\sigma}$ and its derivatives are bounded on $\mathcal{A}$ and $H = \{|z| \leq m\}$. At $\mathcal{A}$, we simply have

$$\partial_z q = \partial_z q_0,$$

and therefore $q = q_0$, where the integration constant can be taken to zero at one of the axis components. If the metric is regular, the identity holds in all the connected axis components. At the horizon, we have

$$\partial_z q \approx \partial_z q_0 - \partial_z \bar{\sigma},$$

where we use $\rho \partial_\rho \sigma_0 \to -2$ at H. Then,

$$q(0, z) - q_0(0, z) = -\bar{\sigma}(0, z) + C,$$

for some constant C. By continuity, $q(0, m) - q_0(0, m) = 0$ and the same holds at $(0, -m)$.

Therefore we have

$$C = \bar{\sigma}(0, \pm m).$$

Finally, recall $\gamma = q + \ln\rho + \sigma$. Then, at the pole $(0, m)$, we have

$$\begin{aligned}\gamma\,|_{(0,m)} &= (q + \ln\rho + \sigma_0 + \bar{\sigma})\,|_{(0,m)} \\ &= (q + \gamma_0 - q_0 + \bar{\sigma})\,|_{(0,m)} \\ &= (\gamma_0 + \bar{\sigma})\,|_{(0,m)}\,.\end{aligned}$$

Therefore, in view of (2.32), if we want that the area in terms of γ to be equal of the area in terms of γ_0, then

$$\bar{\sigma}\,|_{(0,\pm m)} = 0.$$

Due to the divergence of σ at the poles, we express this as

$$\lim_{(\rho,z)\to(0,\pm m)} \frac{\sigma}{\sigma_0} = 1.$$

Appendix **B**

Preliminary results concerning the Inverse Scattering Method

In this appendix, we explain how the Inverse Scattering Method (ISM) could be used, in principle, to construct a periodic solution *iteratively*, and present some preliminary results in this direction, obtained in collaboration with D. Korotkin and M. Bertola. We refer the reader to [23] for more details regarding the method and to [53] for studying the asymptotic behavior using ISM. A thorough introduction to the topic can be found in the book [49] and references therein.

Given a stationary and axisymmetric solution (on the same hypothesis as in chapter 2), in the form

$$g = -f(dt + Ad\phi)^2 + f^{-1}(e^{2k}(dz^2 + d\rho^2) + \rho^2 d\phi^2), \tag{B.1}$$

let $\mathcal{E}$ be the Ernst potential, defined by

$$\mathcal{E} = f + i\omega.$$

The algebraic comparison between (2.16) and (B.1) can be found in Appendix A. Ernst equations are given by

$$(\mathcal{E} + \bar{\mathcal{E}})(\mathcal{E}_{zz} + \frac{1}{\rho}\mathcal{E}_\rho + \mathcal{E}_{\rho\rho}) = 2(\mathcal{E}_z^2 + \mathcal{E}_\rho^2), \tag{B.2}$$

which is equivalent to (2.26) and (2.27).

The Inverse Scattering Method consists of solving an associated linear system to (B.2), such that, after certain normalization conditions, the Ernst potential is obtained. Specifically, let $\xi = z + i\rho$, then the following quadrature equations

$$\partial_{\bar{\xi}}\Psi = \left(\begin{pmatrix} E & 0 \\ 0 & F \end{pmatrix} + \sqrt{\frac{\lambda - \bar{\xi}}{\lambda - \xi}}\begin{pmatrix} 0 & E \\ F & 0 \end{pmatrix}\right)\Psi,$$
$$\partial_{\bar{\xi}}\Psi = \left(\begin{pmatrix} \bar{F} & 0 \\ 0 & \bar{E} \end{pmatrix} + \sqrt{\frac{\lambda - \bar{\xi}}{\lambda - \xi}}\begin{pmatrix} 0 & \bar{F} \\ \bar{E} & 0 \end{pmatrix}\right)\Psi,$$

where

$$E = \frac{\partial_{\tilde{\zeta}}\mathcal{E}}{\mathcal{E}+\bar{\mathcal{E}}}, \quad F = \frac{\partial_{\tilde{\zeta}}\bar{\mathcal{E}}}{\mathcal{E}+\bar{\mathcal{E}}},$$

and λ is the *spectral parameter*. The normalization and reality condition for Ψ are

$$\Psi(\lambda = +\infty) = \begin{pmatrix} 1+\mathcal{E} & -1+\mathcal{E} \\ -1+\bar{\mathcal{E}} & 1+\bar{\mathcal{E}} \end{pmatrix},$$

and

$$\Psi(\iota(\lambda)) = \begin{pmatrix} 1 & 0 \\ 0 & -1 \end{pmatrix} \Psi(\lambda) \begin{pmatrix} 1 & 0 \\ 0 & -1 \end{pmatrix}, \quad \bar{\Psi}(\bar{\lambda}) = \begin{pmatrix} 0 & 1 \\ 1 & 0 \end{pmatrix} \Psi(\lambda) \begin{pmatrix} 0 & 1 \\ 1 & 0 \end{pmatrix},$$

with ι the involution that changes the sign of the square root in $\sqrt{\frac{\lambda-\bar{\zeta}}{\lambda-\zeta}}$.

Given N black holes, the associated linear system can be solved via $2N$ *solitons*, where the positions of the poles of each connected horizon component represent each soliton. For example, Kerr solution subsection 2.4.1 can be obtained by inserting two solitons at $-m$ and m and solving the linear equation. Details of how this is done can be found in [49].

The main advantage of the ISM is that it gives us an exact expression for a sequence of N black holes, i.e., if we fix N to be the number of horizons on the axis, then we compute the solution to Einstein's Equations using the ISM, and we obtain an *exact* expression. On the downside, the physical parameters are difficult to control, especially the area of the black holes.

B.1 Numerical implementation

The implementation on a finite domain is the same as we previously discussed for the harmonic map heat flow: we work in Weyl-Papapetrou coordinates and use a uniform grid along z and a Chebyshev grid along ρ. This choice is for an easier comparison between the methods.

The numerical domain is the rectangle determined by $[\epsilon_\rho, \rho_{\text{MAX}}] \times [-L/2, L/2]$. Since some expressions are singular at the axis and horizons, we avoid this by shifting the grid ϵ_ρ. The input parameters are

- m, the semi-length of the horizons,
- L, the periodic length,
- $\alpha \in \mathbb{C}$, a modulus one complex number related to the angular momentum via the formula

$$J = m^2 \frac{\text{Re}(\alpha)}{\text{Im}(\alpha)^2}. \tag{B.3}$$

The steps for our code are the following:

1. We fix the number of solitons to be added, N_s. In general, $N_s = 4k+2$, so we have $2k$ solitons above and below, besides the central pair between the lines $z = -L/2$ and $z = +L/2$. located at $-m$ and m.

2. We initialize the empty background matrix Ψ_0 and add the first two solitons at the lowest position, in the strip located between $z = -(k-1/2)L$ and $z = -(k+1/2)L$. This gives a Kerr black hole whose horizon is represented by the interval $[-kL-m, -kL+m]$.

3. Telescopically, we add each pair of new solitons, from low to high z's. At each step, we solve the transition matrix T_n such that

$$\Psi_n = T_n \Psi_{n-1},$$

via the equations

$$\Psi_n(-nL \pm m) \begin{pmatrix} 1 \\ \beta_{-nL\pm m} \end{pmatrix} = 0,$$

where $\beta_{-nL\pm m}$ is the rotation parameter at the pole $-nL \pm m$. Observe that we are not only solving T_n but also finding the β's.

4. Once Ψ_{N_s} is found, we obtain the Ernst potential $\mathcal{E}$ via the normalization

$$\Psi_{N_s}(+\infty) = \begin{pmatrix} 1+\mathcal{E} & -1+\mathcal{E} \\ -1+\bar{\mathcal{E}} & 1+\bar{\mathcal{E}} \end{pmatrix}.$$

The final function, $\mathcal{E}$, satisfies the Ernst equation, (B.2). To measure the error within which equation (B.2) is satisfied, we compute the quotient between the L_2 norms of the operator

$$\mathfrak{E}(\mathcal{E}) := (\mathcal{E}+\bar{\mathcal{E}})(\mathcal{E}_{zz} + \frac{1}{\rho}\mathcal{E}_\rho + \mathcal{E}_{\rho\rho}) - 2(\mathcal{E}_z^2 + \mathcal{E}_\rho^2),$$

and the function $\mathcal{E}$, that is, the relative error in the Ernst equation,

$$\epsilon_{\mathfrak{E}} := \frac{\|\mathfrak{E}(\mathcal{E})\|}{\|\mathcal{E}\|}. \tag{B.4}$$

For the comparison with the harmonic map heat flow, it is necessary to compute only the real part of the Ernst potential

$$\mathrm{Re}(\mathcal{E}) = V,$$

and comparing it with the results obtained in section 6.4.

B.2 Results

First, we want to check that the method converges to a solution of the Ernst equation (B.2). Using the relative error, (B.4), we can have an estimate, given a sequence of iterative steps $\{\mathcal{E}_i\}_{i>0}$, how far away from an *actual* solution we are. In figure B.1, we plot the relative error $\epsilon_{\mathfrak{E}}$ for a wide number of steps, ranging from 102 up to 6.4×10^4 solitons.

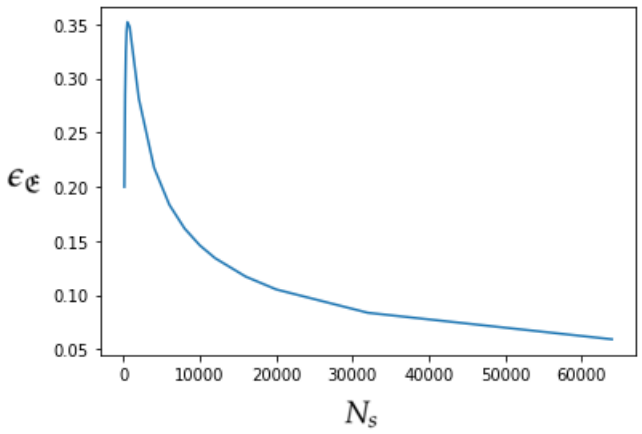

Figure B.1: Plot of the relative error, (B.4), for several values of N_s: $10^2, 2\times10^2, ..., 6.4\times10^4$.

We also studied the convergence of the sequence $\{\mathcal{E}_i\}_{i>0}$, to know whether

$$\lim_{i\to+\infty} \mathcal{E}_i = \mathcal{E}_\infty,$$

is a good approximation of the *periodic* solution. In this context, a good starting point is to plot the real part of $\mathcal{E}_i$ at one point at the ρ_{max} end. We chose this coordinate value because it is where the values of $\mathcal{E}$ are higher. We show in Figure B.2 the results.

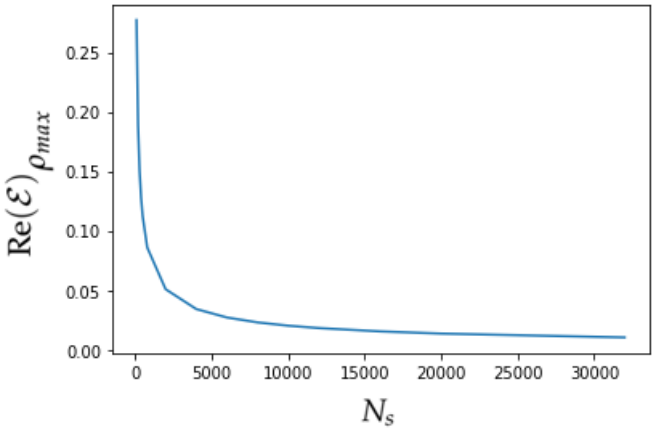

Figure B.2: Plot of the value of $\mathrm{Re}(\mathcal{E})$ at one point in the numerical domain, corresponding to $\{\rho = \rho_{max}\}$, for N_s: $10^2, 2\times10^2, ..., 3.2\times10^4$.

B.3 Comparison with the harmonic map heat flow method

When imposing the boundary conditions for the initial value problem in the harmonic map heat flow, we consider the parameters $(m/L, A, J)$. In the ISM case, we are *fixing* (m, L) and the initial rotation parameter α. Since m and L are not independent, we are missing one parameter!

Given a domain, a periodic length and an angular momentum, $(m/L, J)$, we constructed a solution with each method. First, we have to translate the parameters.

- Harmonic map heat flow: we take $A = 16\pi$ as usual for the harmonic heat map heat flow and compute its corresponding m. In this way, we have also the value of L.
- We use the values of m and L computed for the Harmonic map heat flow, and compute α from the given value of J (B.3).

We run the ISM code with (m, L, α) as inputs. We find that the quotient of both solutions obtained is *almost a constant*, within 10^{-3} in relative error. In Figure B.3, we show a typical example of two solutions.

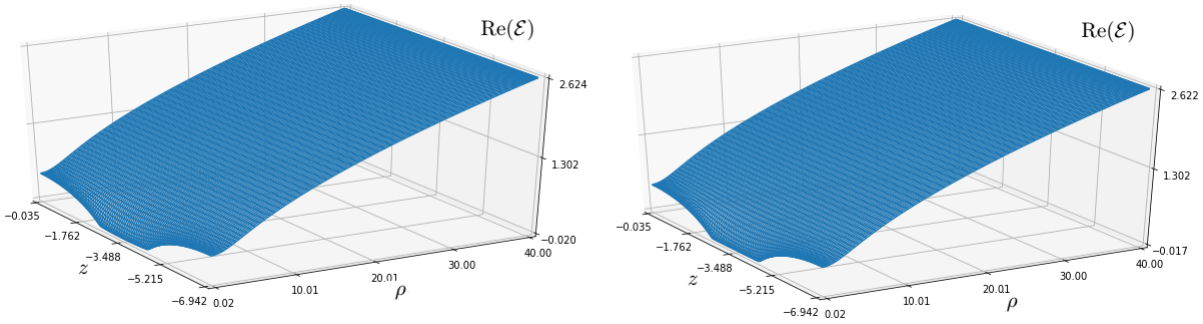

Figure B.3: Plot of two solutions on the same domain, Re($\mathcal{E}$), with two different numerical methods: harmonic map heat flow (left) and soliton iterative method (right) with $N_s = 20002$. The function on the right has been multiplied by a scale factor. The period and the angular momentum values are $L = 6.9770$ and $J = 1/4$.

Let us call $\mathcal{E}_{HMHF}$ the Ernst potential derived numerically via the harmonic map heat flow method. The numerical constant C obtained such that

$$\mathcal{E}_{HMHF} = C\mathcal{E}_{\infty},$$

should be computed independently, either by fixing the area of the black hole or the value of a multiplicative factor in the metric, (2.24).

The difference in a global factor is consistent with the fact that a scaling in the metric translates as a sum by a constant in σ, cf. (2.24) and below. The idea of fixing the area in the harmonic map heat flow accounts for the fixing of the scale, which in turn is a fixing of the norm of the stationary Killing vector. In the ISM, we have no a priori way to ensure a fixed value for the area unless an *iterative* correction is imposed. In fact, by taking the condition

$$\lim_{(\rho,z)\to(0,\pm m)} \frac{\sigma}{\sigma_0} = 1,$$

on each iterative loop of the ISM code, the numerical constant $C \approx 1$. This is an important check for the validity of the methods used and the consistency of the results presented.

Bibliography

[1] R. C. Myers. Higher-dimensional black holes in compactified space-times. *Phys. Rev. D*, 35:455–466, Jan 1987.

[2] D. Korotkin and H. Nicolai. A Periodic Analog of the Schwarzschild Solution, arxiv:gr-qc/9403029. March 1994.

[3] Werner Israel. Event horizons in static electrovac space-times. *Comm. Math. Phys.*, 8:245–260, 1968.

[4] H. Mueller Zum Hagen, David. C. Robinson, and H. J. Seifert. Black holes in static vacuum space-times. *Gen. Rel. Grav.*, 4:53–78, 1973.

[5] G. L. Bunting and A. K. M. Masood-ul Alam. Nonexistence of multiple black holes in asymptotically Euclidean static vacuum space-time. *Gen. Rel. Grav.*, 19:147–154, 1987.

[6] Roy P. Kerr. Gravitational field of a spinning mass as an example of algebraically special metrics. *Phys. Rev. Lett.*, 11:237–238, 1963.

[7] H. Weyl. The theory of gravitation. *Annalen Phys.*, 54:117–145, 1917.

[8] Rudolf Bach and H. Wevl. Neue lösungen der einsteinschen gravitationsgleichungen. *Mathematische Zeitschrift*, 13:134–145.

[9] Robert C. Myers. Superstring Gravity and Black Holes. *Nucl. Phys. B*, 289:701–716, 1987.

[10] Ashoke Sen. Black hole solutions in heterotic string theory on a torus. *Nucl. Phys. B*, 440:421–440, 1995.

[11] Ramzi R. Khuri. Black holes and solitons in string theory. *Helv. Phys. Acta*, 67:884–922, 1994.

[12] Valeri P. Frolov. Black holes and cosmic strings. In World Scientific Publishing Company, editor, *6th APCTP Winter School on Black Hole Astrophysics 2002*, pages 39–58, 1 2002.

[13] G. W. Gibbons and D. L. Wiltshire. Black Holes in Kaluza-Klein Theory. *Annals Phys.*, 167:201–223, 1986. [Erratum: Annals Phys. 176, 393 (1987)].

[14] Finn Larsen. Kaluza-Klein black holes in string theory. In World Scientific Publishing Company, editor, *7th International Symposium on Particles, Strings and Cosmology*, pages 57–66, 12 1999.

[15] Finn Larsen. Rotating Kaluza-Klein black holes. *Nucl. Phys. B*, 575:211–230, 2000.

[16] Jaemo Park. Black hole solutions of Kaluza-Klein supergravity theories and string theory. *Class. Quant. Grav.*, 15:775–785, 1998.

[17] Roberto Emparan and Harvey S. Reall. A Rotating black ring solution in five-dimensions. *Phys. Rev. Lett.*, 88:101101, 2002.

[18] Henriette Elvang and Pau Figueras. Black Saturn. *JHEP*, 05:050, 2007.

[19] Marcus Khuri, Gilbert Weinstein, and Sumio Yamada. 5-Dimensional Space-Periodic Solutions of the Static Vacuum Einstein Equations. *JHEP*, 12:002, 2020.

[20] Marcus Khuri, Gilbert Weinstein, and Sumio Yamada. Balancing Static Vacuum Black Holes with Signed Masses in 4 and 5 Dimensions. *Phys. Rev. D*, 104:044063, 2021.

[21] Edward Kasner. Geometrical theorems on Einstein's cosmological equations. *Am. J. Math.*, 43:217–221, 1921.

[22] Tulio Levi-Civita. Meccanica–ds 2 einsteiniani in campi newtoniani. viii. soluzioni binarie di weyl. *Rendiconti della Reale Accademia dei Lincei*, 28:3–13, 1919.

[23] D. Korotkin and H. Nicolai. The Ernst equation on a Riemann surface. *Nucl. Phys. B*, 429:229–254, 1994.

[24] Stephen W. Hawking and George F. R. Ellis. *The Large Scale Structure of Space-Time*. Cambridge Monographs on Mathematical Physics. Cambridge University Press, 2 2023.

[25] R.M. Wald. *General Relativity*. University of Chicago Press, 1984.

[26] Alexandru Ionescu and Sergiu Klainerman. Rigidity Results in General Relativity: a Review, arxiv:gr-qc/1501.01587. 1 2015.

[27] Ted Jacobson and Gungwon Kang. Conformal invariance of black hole temperature. *Class. Quant. Grav.*, 10:L201–L206, 1993.

[28] V. P. Frolov and I. D. Novikov, editors. *Black hole physics: Basic concepts and new developments, DOI: 10.1007/978-94-011-5139-9*. 1998.

[29] Achille Papapetrou. Eine rotationssymmetrische losung in der allgemeinen relativitatstheorie. *Annals Phys.*, 12:309–315, 1953.

[30] Achille Papapetrou. Champs gravitationnels stationnaires a symetrie axiale. *Ann. Inst. H. Poincare Phys. Theor.*, 4:83–105, 1966.

[31] Gilbert Weinstein. On rotating black holes in equilibrium in general relativity. *Communications on Pure and Applied Mathematics*, 43(7):903–948, 1990.

[32] Frederick J. Ernst. New formulation of the axially symmetric gravitational field problem. *Phys. Rev.*, 167:1175–1179, 1968.

[33] Brandon Carter. Killing horizons and orthogonally transitive groups in space-time. *J. Math. Phys.*, 10:70–81, 1969.

[34] Thomas Thiemann. *Modern Canonical Quantum General Relativity*. Cambridge Monographs on Mathematical Physics. Cambridge University Press, 2007.

[35] Karl Schwarzschild. On the gravitational field of a mass point according to Einstein's theory. *Sitzungsber. Preuss. Akad. Wiss. Berlin Math. Phys.*, 1916:189–196, 1916.

[36] Albert Einstein. The Field Equations of Gravitation. *Sitzungsber. Preuss. Akad. Wiss. Berlin Math. Phys.*, 1915:844–847, 1915.

[37] James B. Hartle and Kip S. Thorne. Slowly Rotating Relativistic Stars. II. Models for Neutron Stars and Supermassive Stars. *Astrophys. J.*, 153:807, 1968.

[38] Arthur Komar. Positive-definite energy density and global consequences for general relativity. *Phys. Rev.*, 129:1873–1876, Feb 1963.

[39] Larry Smarr. Mass formula for Kerr black holes. *Phys. Rev. Lett.*, 30:71–73, 1973. [Erratum: Phys.Rev.Lett. 30, 521–521 (1973)].

[40] James M. Bardeen, B. Carter, and S. W. Hawking. The Four laws of black hole mechanics. *Comm. Math. Phys.*, 31:161–170, 1973.

[41] Anne Ashtekar, Abhay; Magnon-Ashtekar. On conserved quantities in general relativity. *J. Math. Phys.*, 20:793–800, 1978.

[42] Andrei V. Frolov and Valeri P. Frolov. Black holes in a compactified space-time. *Phys. Rev. D*, 67:124025, 2003.

[43] Gregory J. Galloway and Richard Schoen. A Generalization of Hawking's black hole topology theorem to higher dimensions. *Comm. Math. Phys.*, 266:571–576, 2006.

[44] Gregory J. Galloway. On the Topology of Balck Holes. *Comm. Math. Phys.*, 51(2):53–66, 8 1993.

[45] Gregory J. Galloway. Rigidity of outer horizons and the topology of black holes, arxiv:gr-qc/0608118. 8 2006.

[46] Martín Reiris Ithurralde. A classification theorem for static vacuum black holes. Part I: the study of the lapse, arxiv:gr-qc/1806.00818. 6 2018.

[47] Martín Reiris Ithurralde. A classification theorem for static vacuum black holes. Part II: the study of the asymptotic, arxiv:gr-qc/1806.00819. 6 2018.

[48] Martín Reiris and Javier Peraza. A complete classification of S1-symmetric static vacuum black holes. *Class. Quant. Grav.*, 36(22):225012, 2019.

[49] Hans Stephani, Dietrich Kramer, Malcolm MacCallum, Cornelius Hoenselaers, and Eduard Herlt. *Exact Solutions of Einstein's Field Equations*. Cambridge Monographs on Mathematical Physics. Cambridge University Press, 2 edition, 2003.

[50] D. Gilbarg and N.S. Trudinger. *Elliptic Partial Differential Equations of Second Order*. Classics in Mathematics. Springer Berlin Heidelberg, 2001.

[51] Thomas Lewis. Some special solutions of the equations of axially symmetric gravitational fields. *Proc. Roy. Soc. Lond.*, 57:135–154, 1932.

[52] Willem Jacob van Stockum. The gravitational feild of a distribution of particles rotating about an axis of symmetry. *Proc. Roy. Soc. Edinburgh*, 57:135–154, 1937.

[53] B. Mavrin. *The Search for the Compactified Kerr Solution*. Concordia University, 2015.

[54] Sergio Dain and Omar E. Ortiz. Numerical evidences for the angular momentum-mass inequality for multiple axially symmetric black holes. *Phys. Rev. D*, 80:024045, Jul 2009.

[55] Javier Peraza, Martin Reiris, and Omar E Ortiz. Periodic analogues of the kerr solutions: a numerical study. *Class. Quant. Grav.*, 2023.

[56] Michael T. Anderson. On stationary vacuum solutions to the Einstein equations. *Annales Henri Poincare*, 1:977, 2000.

[57] Martin Reiris. On static solutions of the Einstein-Scalar Field equations. *Gen. Rel. Grav.*, 49(3):46, 2017.

[58] Marcus Khuri, Benjamin Sokolowsky, and Gilbert Weinstein. A Penrose-type inequality with angular momentum and charge for axisymmetric initial data. *Gen. Rel. Grav.*, 51(9):118, 2019.

[59] Marcus Khuri, Martin Reiris, Gilbert Weinstein, and Sumio Yamada. Gravitational Solitons and Complete Ricci Flat Riemannian Manifolds of Infinite Topological Type, arxiv:math.DG/2204.08048. 4 2022.

[60] Vishnu Kakkat, Marcus Khuri, Jordan Rainone, and Gilbert Weinstein. The geometry and topology of stationary multiaxisymmetric vacuum black holes in higher dimensions. *Pacific J. Math.*, 322(1):59–97, 2023.

[61] P. Petersen. *Riemannian Geometry*. Graduate Texts in Mathematics. Springer New York, 2006.

[62] Marc Mars, Tim-Torben Paetz, and José M. M. Senovilla. Multiple Killing Horizons and Near Horizon Geometries. *Class. Quant. Grav.*, 35(24):245007, 2018.

[63] Th. Kaluza. Zum Unitätsproblem der Physik. *Sitzungsber. Preuss. Akad. Wiss. Berlin Math. Phys.*, 1921:966–972, 1921.

[64] Oskar Klein. Quantum Theory and Five-Dimensional Theory of Relativity. (In German and English). *Z. Phys.*, 37:895–906, 1926.

[65] Vivek Iyer and Robert M. Wald. Some properties of Noether charge and a proposal for dynamical black hole entropy. *Phys. Rev. D*, 50:846–864, 1994.

[66] Sergio Dain. Proof of the angular momentum-mass inequality for axisymmetric black holes. *J. Diff. Geom.*, 79(1):33–67, 2008.

[67] Sergio Dain and Martin Reiris. Area - Angular momentum inequality for axisymmetric black holes. *Phys. Rev. Lett.*, 107:051101, 2011.

[68] Qun Chen and Hongbing Qiu. Existence and liouville theorems for v -harmonic maps from complete manifolds. *Annals of Global Analysis and Geometry*, 42:565–584, 04 2012.

[69] Martin Reiris. On the existence of charged electrostatic black holes in arbitrary topology - to be released.

[70] Jeffrey Case. The nonexistence of quasi-einstein metrics. *Pacific J. Math.*, 248, 02 2009.

[71] Andreas Dieckmann. Collection of infinite products and series, 2024.

[72] S. Labrosse and A. Morison. dmsuite: A collection of spectral collocation differentiation matrices, url: https://github.com/labrosse/dmsuite, 2018.

[73] Elsayed M.E. Elbarbary and Salah M. El-Sayed. Higher order pseudospectral differentiation matrices. *Applied Numerical Mathematics*, 55(4):425–438, 2005.

[74] L. N. Trefethen. *Spectral Methods in MATLAB*. SIAM, 2000.

[75] I. Cabrera-Munguia and Claus Lammerzahl. Exact solution for two unequal counter-rotating black holes. *AIP Conf. Proc.*, 1548(1):156, 2013.

[76] I. Cabrera-Munguia, Claus Lämmerzahl, and Alfredo Macías. Exact solution for a binary system of unequal counter-rotating black holes. *Class. Quant. Grav.*, 30:175020, 2013.

[77] I. Cabrera-Munguia, V. E. Ceron, L. A. López, and Omar Pedraza. Corotating two-body system of identical Kerr sources. *Phys. Lett. B*, 772:10–15, 2017.

[78] Miguel S. Costa, Carlos A. R. Herdeiro, and Carmen Rebelo. Dynamical and thermodynamical aspects of interacting kerr black holes. *Phys. Rev. D*, 79:123508, Jun 2009.

[79] Vladimir Manko, E. Rodchenko, E. Ruiz, and Boris Sadovnikov. Exact solutions for a system of two counter-rotating black holes. *Phys. Rev. D*, 78, 12 2008.

[80] V.S. Manko and E. Ruiz. On a Simple Representation of the Kinnersley-Chitre Metric. *Prog. Theor. Phys.*, 125:1241–1254, 2011.

[81] Vladimir Manko and E. Ruiz. Metric for two equal kerr black holes. *Phys. Rev. D*, 96, 02 2017.

[82] Akira Tomimatsu. On the soliton solutions of stationary, axisymmetric gravitational fields. *Prog. Theor. Phys.*, 63:1054–1057, 1980.

[83] A. Tomimatsu and H. Sato. Mulit-soliton solutions of the Einstein Equation and the Tomimatsu-Sato metric. *Prog. Theor. Phys. Suppl.*, 70:215–237, 1981.

[84] Hideo Kodama. Lecture on Black Holes, url: https://inspirehep.net/literature/1601944. 2011.